TRC1603

Deep Shear Wave Velocity Profiling in Northeastern Arkansas

Clinton M. Wood
Ethan Baker
Micheal Deschenes
Ashraf Kamal Himel

University of Arkansas

Final Report

March 2019

TRC1603

Deep Shear Wave Velocity Profiling in Northeastern Arkansas

Clinton M. Wood
Ethan Baker
Micheal Deschenes
Ashraf Kamal Himel

University of Arkansas

Final Report

March 2019

DISCLAIMER

The contents of this report reflect the view of the author(s), who is (are) responsible for the facts and the accuracy of the data presented herein. The contents do not necessarily reflect the official views or policies of the Arkansas Department of Transportation or the Federal Highway Administration. This report does not constitute a standard, specification, or regulation.

.

Final Report:

Deep Shear Wave Velocity Profiling in Northeastern Arkansas
(Research Project No. TRC1603)

for:

Joseph Jabo, Ph.D.
Arkansas Department of Transportation
P.O. Box 2261
Little Rock, AR 72703
(501) 569-2195

prepared by:

Clinton M. Wood, Ph.D., P.E.
Assistant Professor
The University of Arkansas
E-mail: cmwood@uark.edu
Phone: (479) 575-6084

and

Ethan Baker, Micheal Deschenes, & Ashraf Kamal Himel
Graduate Research Assistants
The University of Arkansas

March 2019

Technical Report Documentation Form

1. Report No.	2. Government Accession No.	3. Recipient's Catalog No.
TRC1603		

4. Title and Subtitle	5. Report Date
Deep Shear Wave Velocity Profiling in Northeastern Arkansas	March 2019
	6. Performing Organization Code

7. Author(s)	8. Performing Organization Report No.
Clinton M. Wood, Ph.D, P.E., Ethan Baker, Michael Deschenes, and Ashraf Kamal Himel	

9. Performing Organization Name and Address	10. Work Unit No. (TRAIS)
1 University of Arkansas University of Arkansas Fayetteville, AR 72701	11. Contract or Grant No. TRC1603

12. Sponsoring Agency Name and Address	13. Type of Report and Period Covered
Arkansas Department of Transportation 10324 Interstate 30 Little Rock, AR 72209	Final Report Feb 2016-Mar 2018
	14. Sponsoring Agency Code ARDOT

15. Supplementary Notes

16. Abstract

Deep dynamic site characterization was conducted at fifteen ARDOT bridge sites in northeast Arkansas with the goal of developing shear wave velocity profiles to bedrock. A combination of active and passive surface wave methods along with horizontal to vertical spectral ratio measurements were used to develop the Vs profiles. These Vs profiles along with the methodology used to develop the Vs profiles are discussed. These Vs profiles were then utilized to develop an updated 3D velocity model (UA_MEVM) of the region for the purpose of conducting future site-specific ground motion response analysis (SSGMRA) for future ARDOT bridge projects.

For one location in Monette, Arkansas, a full SSGMRA in accordance with the American Association of State Highway and Transportation Officials (AASHTO) guidelines was conducted using the Vs profile developed to bedrock. A combination of equivalent linear and non-linear site response analysis was utilized. Both analysis demonstrated attenuation of short period seismic waves and amplification of long period waves. The attenuation in the short period range led to a reduction in the design acceleration response spectrum for the bridge of 1/3 for period less than ~1.0 second. Using the updated design response spectrum from the SSGMRA, seismic aspects of the bridge were redesigned including retaining blocks, bent/columns, piles and pile lengths, and approach embankment. A cost comparison between the original bridge designed using the AASHTO general seismic procedure and the updated bridge designed using the results from the SSGMRA indicated a potential gross cost-savings of $205,000 or approximately 7% of the original bid price was possible as a result of conducting the SSGMRA.

17. Key Words	18. Distribution Statement
Mississippi Embayment, New Madrid Seismic Zone, Surface Wave Method, Site Specific Ground Motion Response Analysis, Short Period Bridges.	No Restrioction.

19. Security Classification (of this report)	20. Security Classification (of this page)	21. No. of Pages	22. Price
Unclassified	Unclassified	125	$287,043

Form DOT F 1700.7 (8-72) **Reproduction of completed page authorized**

EXECUTIVE SUMMARY

E.1 Introduction

This report details the findings of research project TRC1603, a two year study to develop shear wave velocity profiles down to bedrock in the Mississippi Embayment and to assess the cost-savings potential of performing SSGMRA for design of Northeast Arkansas bridges. Background on this project is provided in Chapter 1 of this report. Chapter 2 discusses dynamic site characterization which was conducted at 15 sites in Northeast Arkansas. Chapter 3 discusses data processing of collected information from the dynamic site characterization efforts. Chapter 4 discusses the results from the dynamic site characterization efforts and the development of UA_MEVM. Chapter 5 discusses site-response at the Monette bridge site including background, methodology, results, and implementation. Chapter 6 summarizes seismic bridge design using SSGMRA results. Chapter 7 details the cost-savings benefits of performing SSGMRA for a case-study ARDOT bridge in Monette, Arkansas. Chapter 8 is a summary of conclusions. Electronic appendices are also provided that contain supplemental information such as design calculations.

E.2 Dynamic Site Characterization

Dynamic site characterization testing was conducted at 15 sites located throughout Northeast Arkansas (see Figure E.1). These sites were chosen based first on the location of current or potential ARDOT bridge job locations. However, if the area near or around the job site could not accommodate testing (i.e. too urban, poor soil conditions, no landowner permission) or there was another job site within close proximity, other locations were explored. An attempt was also made to distribute the sites across Northeast Arkansas as much possible to understand the distribution of dynamic soil properties across in the region and aid in the development of the 3D velocity model of the area. In Table E.1, the site names and locations where testing was conducted are tabulated along with the nearest ARDOT Job. From the sites tested, only the Mounds and Harrisburg sites were not located in close proximity to an ARDOT job. These sites were tested to provide a more consistent distribution across the Northeast Arkansas area.

Testing at the sites was conducted using a number of methods including P-wave refraction, active source MASW, and passive source MAM. P-wave refraction was conducted at each of the testing locations to help locate the water table (i.e., line of saturation) below the surface. Active source MASW utilizing both Rayleigh and Love type surfaces waves was conducted at each site using a sledgehammer source to understand the dynamic properties of the very near surface materials. The use of both Rayleigh and Love type surface waves increases the robustness of the testing and helps ensure the correct mode assignments are made during the analysis process (Wood *et al.,* 2014). At select sites, Rayleigh wave MASW was conducted using a Vibroseis source in order to develop deeper active source dispersion data for comparison with passive source dispersion data.

Passive source testing (MAM) was conducted at each of the sites to understand the dynamic properties of the soil and rock layers at deeper depths. At each site, 2D circular arrays of 10 broadband seismometers with diameters of 50, 200, and 500 meters were used to measure microtremors (i.e., background noise). At select sites, 1000 meter diameter circular arrays were

used for comparison with the smaller diameter arrays. For some sites, an L-array of geophones were used for passive surface wave testing in addition to the circular arrays. A typical testing site layout is shown in Figure E.2. For each site, a common center point for the circular arrays was maintained where possible. The P-wave refraction, active MASW (Rayleigh and Love) using a sledgehammer source, and passive L-array testing were conducted near the center point of the circular array where possible. Testing around a common midpoint helps reduce the influence of lateral variability on surface wave measurements and ensure each method is measuring similar soil and rock properties. The active MASW testing using a Vibroseis source was often conducted away from the center of the array due to site constraints (i.e., the vibroseis truck could not access locations away from roads). Therefore, testing was often conducted on the nearest farm or public road to the center of the array.

Table E.1: Dynamic site characterization testing locations in Northeast Arkansas and corresponding ARDOT job number

Site Name	**Nearest ARDOT Job Number**	**Latitude**	**Longitude**
McDougal	100842	36.398583	-90.388175
Mounds	-	36.118611	-90.313083
Fontaine	100841	36.017175	-90.799475
Bay	100833/100657/100824x1/100824x2	35.761622	-90.594256
Monette	CA1001	35.885581	-90.335186
Manila	CA1002x1/ CA1002x2/ CA1002x3	35.852500	-90.147089
Athelstan	100760x2	35.704214	-90.217497
Amagon	050272x1/ 050272x2/ 050272x3/ 050272x4	35.567572	-91.155928
Harrisburg	-	35.565781	-90.730197
Marked Tree	100782	35.520050	-90.435811
Wynne	110574	35.188317	-90.789519
Earle	CA0103x1/ CA0103x2	35.258642	-90.422603
Palestine	110586	34.986725	-90.911181
Greasy Corner	110617	35.015908	-90.403436
Aubrey	110616x1/ 110616x2	34.711003	-90.943864

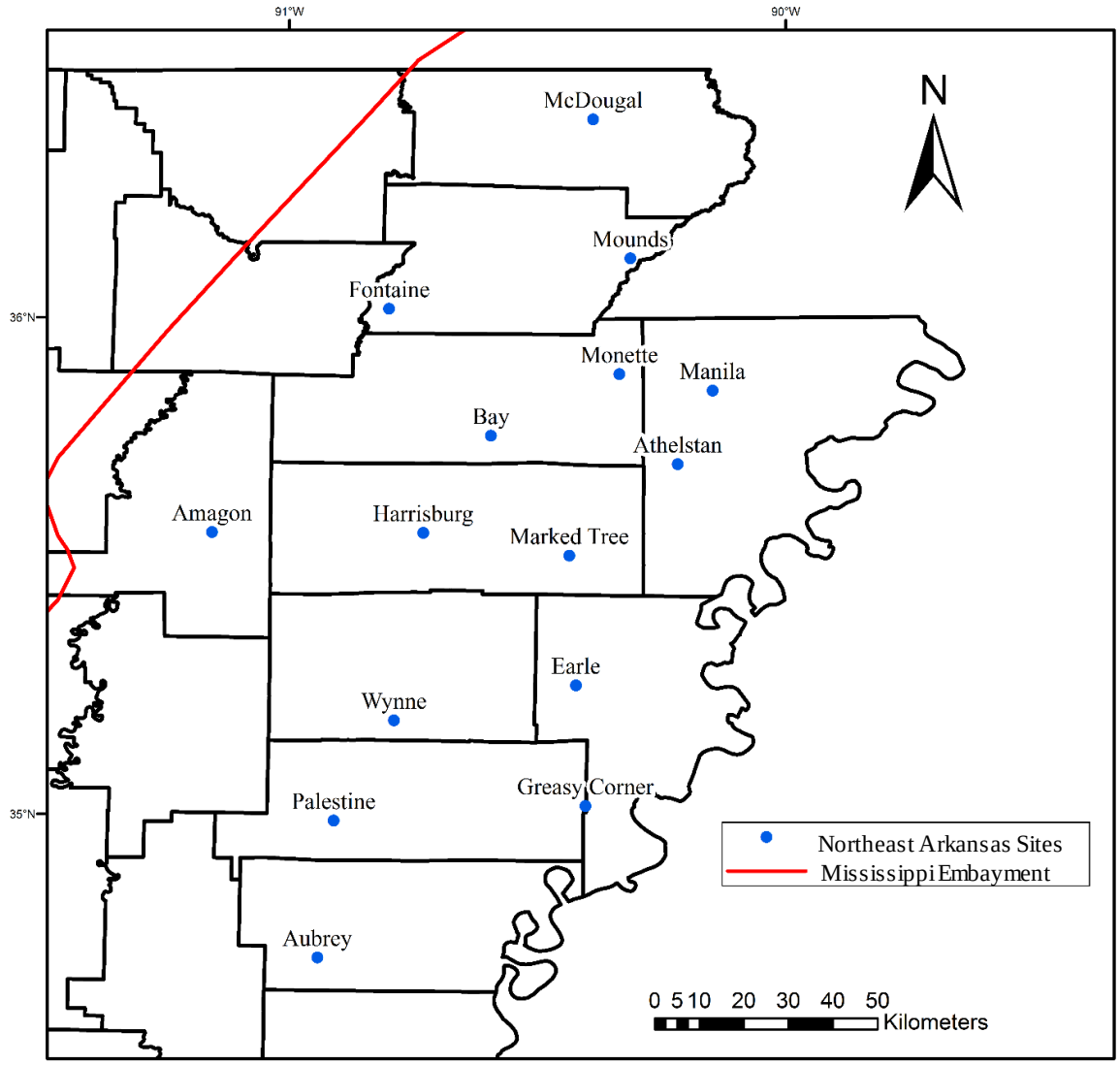

Figure E.1: Dynamic site characterization testing locations in Northeast Arkansas.

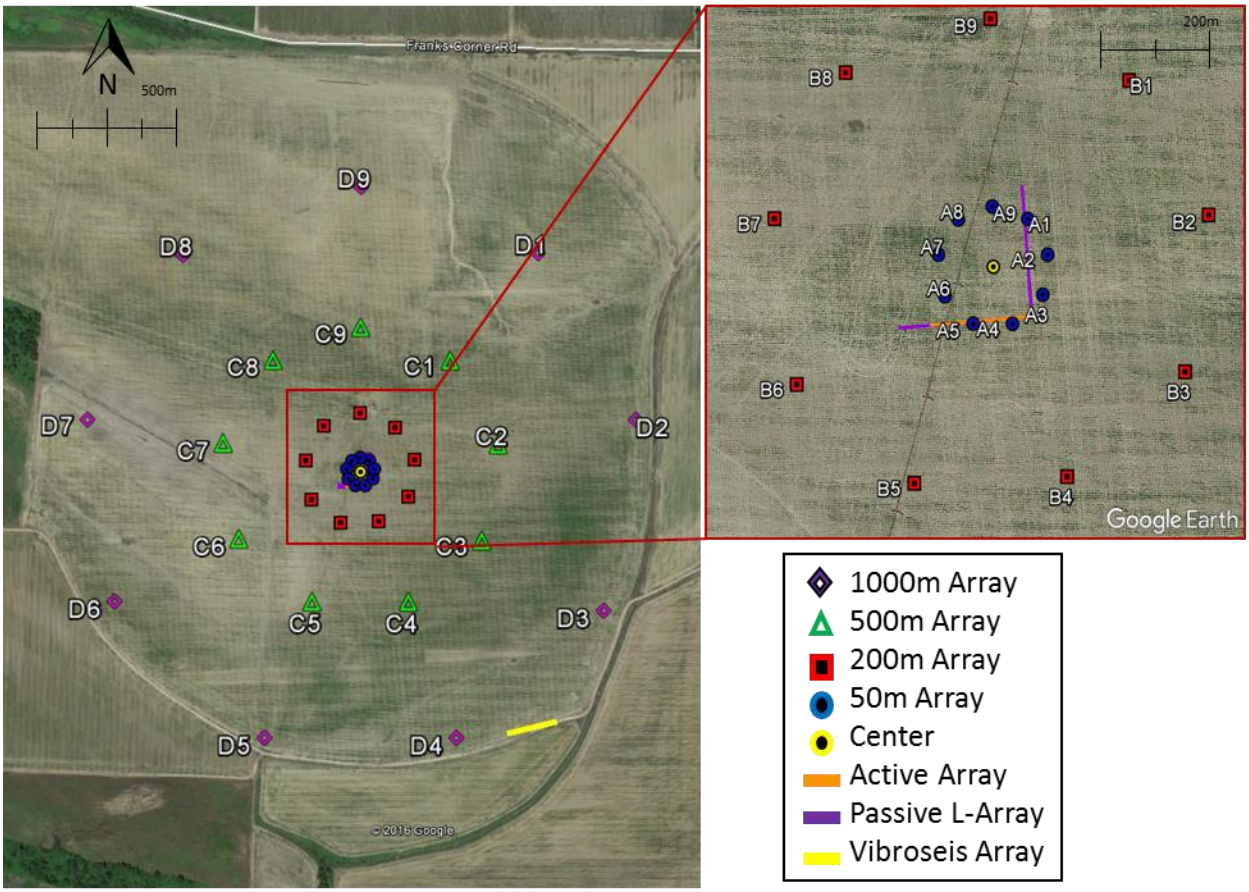

Figure E.2: A typical testing site setup. All testing site maps are included in Appendix A.

E.3 Data Processing

Shear wave velocity profiles were developed at each site in Northeast Arkansas. Processing methods to develop the V_s profiles generally consist of developing experimental dispersion curves and HVSR from raw data collected in the field at each site. This dispersion and HVSR information is used to conduct a joint inversion to solve for the V_s profile at each site. The five different data processing steps used in this investigation are as follows:

- Active-source surface wave processing.
- Passive-source surface wave processing.
- Horizontal-to-vertical spectral ratio processing.
- Dispersion comparison.
- Inversion.

E.4 Dynamic Site Characterization Results and 3D Velocity Model

V_s profiles were generated at fifteen sites in Northeast Arkansas using the CUSVM geologic boundaries to define a parameterization. Bedrock depth at sites in this study ranged from 250 meters to over 1100 meters with the shallow sites located toward the western portion of the Embayment and the deeper sites located toward the Mississippi River on the eastern side of the state. The Vs profiles developed at the 15 sites showed a general consistency with depth. However, there was some variation especially between 50-150 meters deep. These differences are believed to be caused by differences in geologic layering at each site. A velocity model for estimating the deep (>30 meter) V_s characterization within the Northeast Arkansas portion of the Mississippi Embayment was created from the velocity profiles generated in the inversion. In total 15,000 V_s profiles consisting of the 1000 lowest misfit profiles from each site were utilized to provide a robust data set for creating the model and to evaluate the uncertainty in the model. An example of the GUI for the UA_MEVM is provided in Figure E.3. A discussion is provided for performing shallow (<30 meter) V_s characterization and combining this shallow V_s profile with the deep V_s profiles generated in the model for SSGMRA.

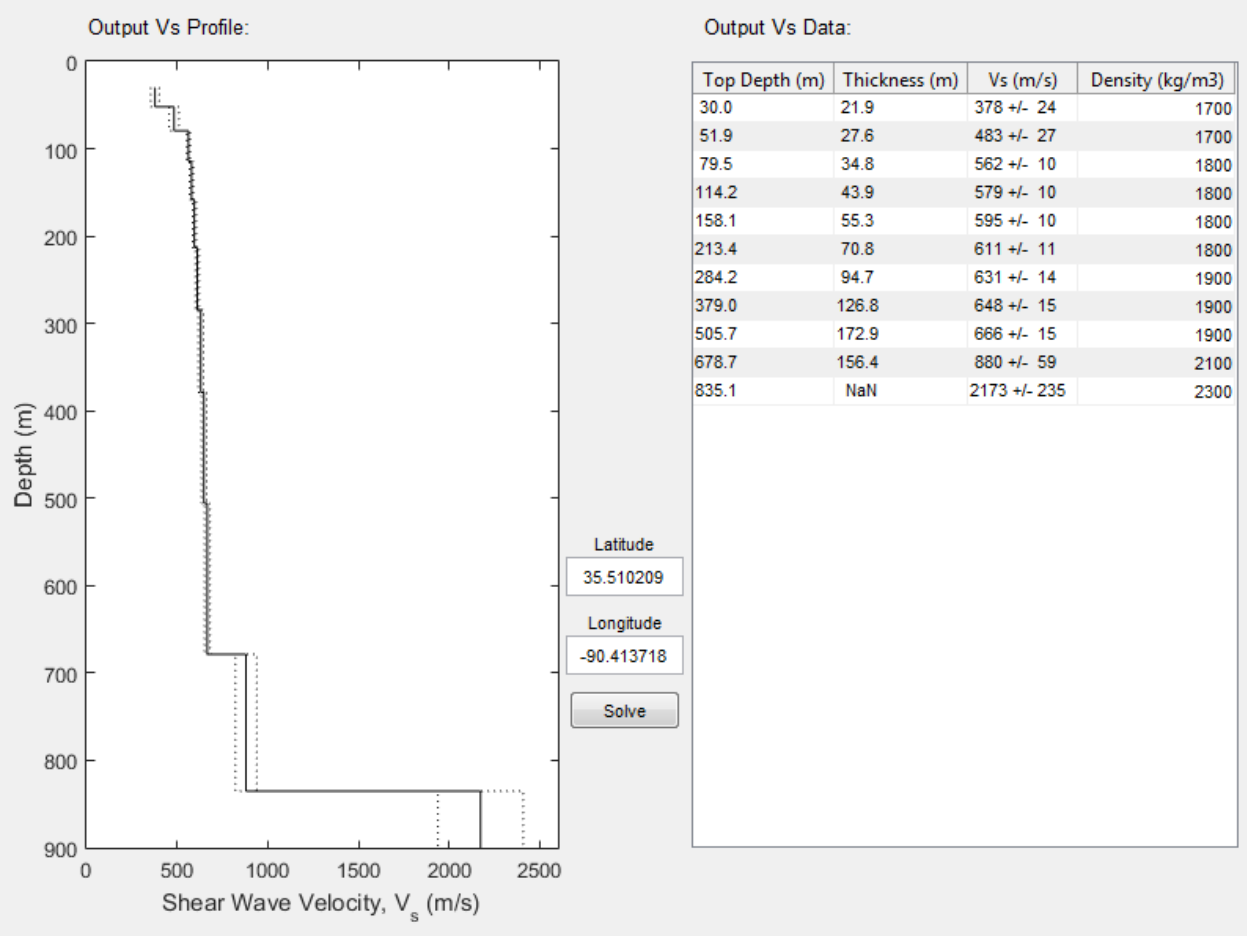

Figure E.3: An example of output data from the UA_MEVM velocity model.

E.5 Site-Response Analysis

A site SSGMRA was conducted at the Monette bridge site as a case study on the use of SSGMRA for bridge projects. The site-response analysis results indicated that the seismic accelerations determined by the AASHTO general procedure could be reduced by 33% from the PGA (i.e., 0 seconds to approximately 0.8 seconds). From 0.8 seconds to approximately 1.3 seconds, the site-response spectrum transitions between the 2/3 AASHTO general procedure response spectrum and the regular AASHTO general procedure response spectrum. From 1.3 to 2.3 seconds, the spectrum is considered to be greater than the regular AASHTO general procedure response spectrum. Figure E.4 highlights important design acceleration values from the SSGMRA. Because the seismic accelerations were lowered in the short period range, and the Monette bridge is considered to be short period, a cost-savings benefit is expected.

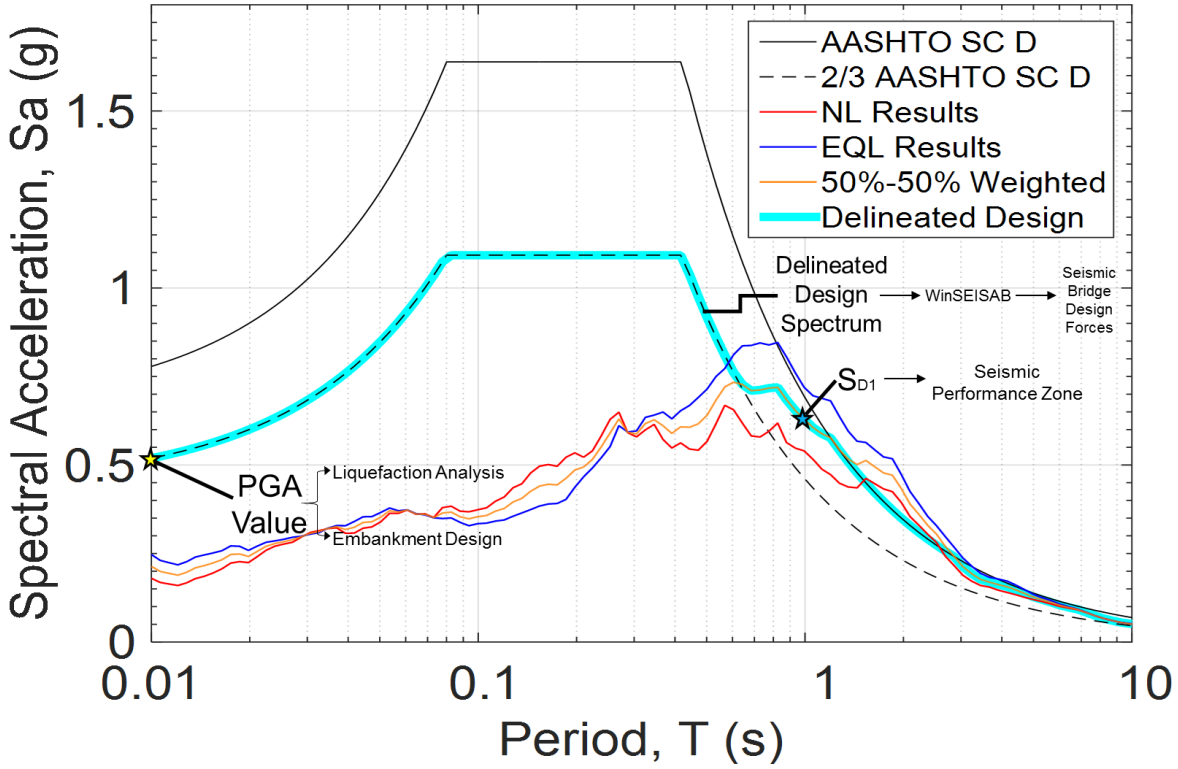

Figure E.4: Example updated design acceleration response spectrum determined from SSGMRA with important values highlighted.

E.6 Bridge Redesign based on SSGMRA

By using the reduced seismic accelerations in the short period range from SSGMRA, several bridge components were reduced in size and length. It was determined that the bridge pilings could be reduced from 24 inches in diameter to 18 inches in diameter. The lengths of the intermediate piles could be reduced by 4 feet each, and the lengths of the bent 6 piles could be reduced by 23 feet each compared to the original design. Restrainer block sizes could also be reduced due to a lower transverse force on the structure. Embankment reinforcement was reduced from 8 layers of 9000 lb/ft Geogrid on 1 foot vertical spacing to 4 layers of 2000 lb/ft Geogrid on 1foot vertical spacing. Little benefit was observed in liquefaction analysis due to the soil conditions at the site.

E.7 Cost-Savings Analysis

From the findings of a cost savings analysis for the Monette bridge project, a gross cost savings of approximately $200,000 was estimated as a result of performing the SSGMRA at the site. For future projects, this number is expected to vary from project to project as the original design details such as the relationship of S_{D1} to performance zone boundaries, location of liquefiable layers, original factor of safety of liquefiable layers, embankment requirements, and site specific soil conditions all play a role in the potential cost savings associated with conducting a SSGMRA. Savings based on each SSGMRA benefit area are shown in Table E.2. Further research is needed to determine these spatial boundaries based on site classification, seismic hazard, soil conditions, liquefaction hazard, embankment requirements, specific bridge details, and many other aspects of a particular project.

To determine the yearly cost savings, which could be possible, we assume an average savings of $200,000 per bridge and assume an average of 20 bridges built per year in Arkansas seismic regions (based on ARDOT data from January 2005-December 2014 for bridges in Districts 1,2,5,6, and 10). By these assumptions, performing SSGMRA could potentially result in a $4,000,000 per year savings for ARDOT.

Table E.2: Cost savings associated with each bridge design categorized by SSGMRA benefits.

	Cost Savings for Monette Bridge	
SSGMRA Benefits	24" Column Structure	18" Column Structure
AASHTO Site Classification	-	-
AASHTO Seismic Performance Zone	-	-
Liquefaction Analysis	$0	$0
Bridge Design	$49,489.65	$92,392.39
Embankment Design	$114,600.00	$114,600.00
TOTAL	**$164,089.65**	**$206,992.39**

TABLE OF CONTENTS

List of Figures

List of Tables

Appendices[1]

Appendix A: Testing site maps

Appendix B: Site soil borings and geotechnical recommendations

Appendix C: ARDOT design calculations

Appendix D: 18-inch column structure redesign calculations (MathCAD)

Appendix E: 24-inch column structure redesign calculations (MathCAD)

Appendix F: Liquefaction calculations (Old and New PGA)

Appendix G: Pile capacities redesign calculations (Driven)

Appendix H: Cost-Savings Tables

[1]Appendices are provided separately as electronic copies

List of Symbols and Abbreviations

AASHTO	American Association of State Highway and Transportation Officials
ARDOT	Arkansas Department of Transportation
A_S	Shear wave velocity of soil corresponding to 1 atm mean effective stress
CPT	Cone Penetration Test
CUSSO	Central US Seismic Observatory
CUSVM	Central US Velocity Model
DRIVEN	Computer program for determining pile capacity
EQL	Equivalent Linear
ERS	Earthquake Resisting Systems
f_0	Fundamental frequency
f-k	Frequency-Wavenumber method
g	Gravitational acceleration (9.81 m/sec^2)
G_{max}	Small strain shear modulus of soil
GUI	Graphical User Interface
h	Bedrock depth in meter
HRFK	High Resolution Frequency-Wavenumber method
HVSR	Horizontal to Vertical Spectral Ratio
LRFD	Load and Resistance Factor Design
MAM	Microtremor Array Measurement
MASW	Multichannel Analysis of Surface Wave
MRDF-UIUC	Modulus Reduction and Damping curve Fitting procedure developed at University of Illinois at Urbana-Champaign
MSPAC	Modified Spatial Auto-Correlation
M_w	Moment magnitude of an earthquake
NL	Non-Linear
NMSZ	New Madrid Seismic Zone
n_s	Empirical normalized mean effective stress exponent

P_a	Atmospheric pressure
PGA	Peak Ground Acceleration
ReMi	Refraction Microtremor
SASW	Spectral Analysis of Surface Wave
SCPT	Seismic Cone Penetration Test
SPT	Standard Penetration Test
SPAC	Spatial Auto Correlation
SSGMRA	Site Specific Ground Motion Response Analysis
T_n	Site Period
UA_MEVM	University of Arkansas Mississippi Embayment Velocity Model
UHS	Unified Hazard Spectrum
USGS	United States Geological Survey
V_R	Rayleigh wave velocity in m/sec
V_S	Shear wave velocity in m/sec
V_{S30}	Average shear wave velocity upper 30 depth
WinSEISAB	Computer program for seismic bridge design analysis
λ	Wavelength
ρ	Density of soil
σ'_0	Mean effective stress of soil
σln(Vs)	Standard deviation of the natural logarithm of Vs

CHAPTER 1
INTRODUCTION

1.1 Introduction

Chapter 1 of this report discusses the background and seismicity of Northeast Arkansas as well as the significance of the Mississippi Embayment and the NMSZ. Background information on dynamic site characterization methods, geology of Northeast Arkansas, site-response analysis, and seismic bridge design are also discussed. Finally, an outline of the report is presented.

1.2 Problem Statement

Northeast Arkansas is located in the heart of the NMSZ, an area of the U.S. that has some of the highest design ground motions in the nation. This large seismic hazard is the result of past large magnitude earthquakes occurring within the NMSZ, noted in Figure 1.1. In addition to the high seismic threat in Northeast Arkansas, the region is located within the upper Mississippi Embayment. This geologic area, illustrated in Figure 1.2, is characterized by deep, unconsolidated sedimentary deposits, which form a plunging syncline with an axis that closely traces the course of the Mississippi River (Mento *et al.,* 1986). The thickness of these deposits range from approximately 477 m at New Madrid, Missouri to 987 m below Memphis, Tennessee (Van Arsdale and TenBrink 2000, Rosenblad *et al.,* 2010).

These two regional characteristics significantly increase the seismic design costs of bridge abutments, deep foundations, and ERS in Northeast Arkansas. Currently, the ARDOT typically uses the general procedure outlined in the AASHTO LRFD Bridge Design Specifications to estimate the seismic demand for highway bridges. Although this methodology usually provides a conservative design, the AASHTO LRFD specifications clearly warn that short-period structures may be over-designed at a significant cost, and long-period structures may be under-designed at a significant risk. This is because the amplification/deamplification implied by immense sediment thicknesses is far different than that implied by the AASHTO site classification considering only the top 30 m of soil (Malekmohammadi and Pezeshk 2015). Therefore, to better estimate the design ground motions at bridge sites and ensure safe and cost efficient designs, AASHTO recommends conducting a site-specific ground motion response analysis (SSGMRA) for areas such as the Mississippi Embayment. AASHTO specifications directly mention that sites with deep, soft deposits, like those in the Mississippi Embayment, are locations where SSGMRA should be performed. Recognizing the value these types of site specific analysis can add when complex conditions exist, AASHTO allows seismic design forces obtained from general, code based procedures to be reduced by up to 33% if the SSGMRA indicates this is appropriate. Cox *et al.,* (2012) concluded that this reduction could be achieved for short period ranges (<1.0 seconds) at bridge sites in Northeast Arkansas, which is where the natural period of most Northeast Arkansas bridges designed by ARDOT fall.

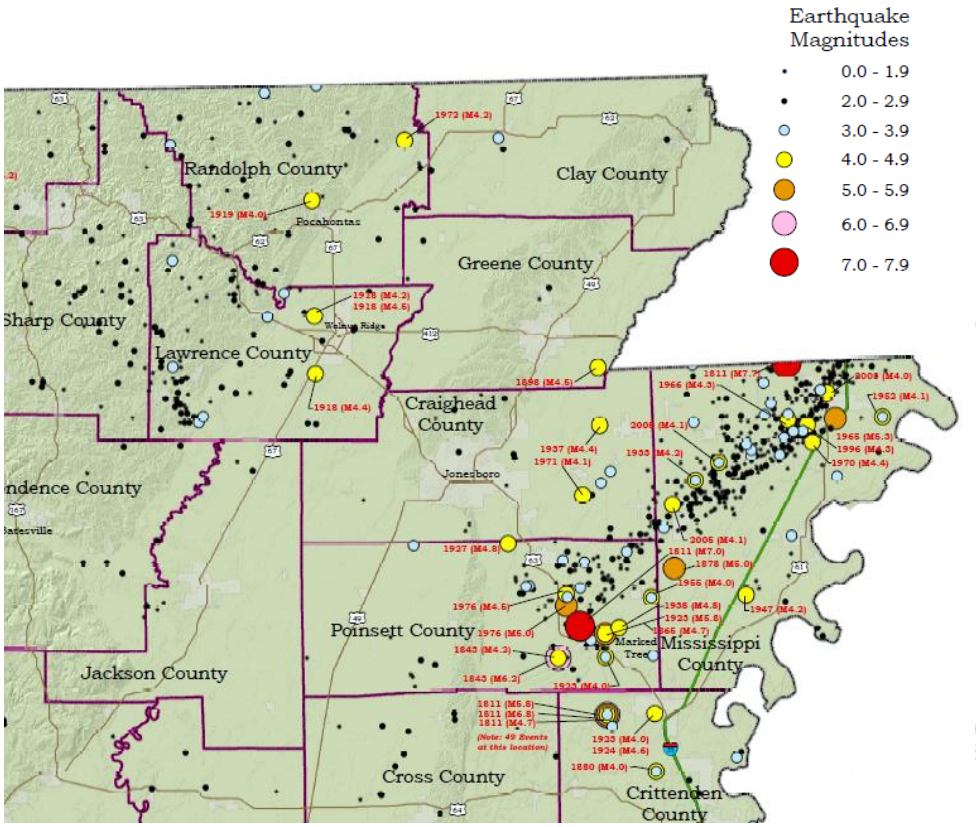

Figure 1. 1: Three centuries of earthquakes in Northeast Arkansas (Arkansas Geological Survey 2017).

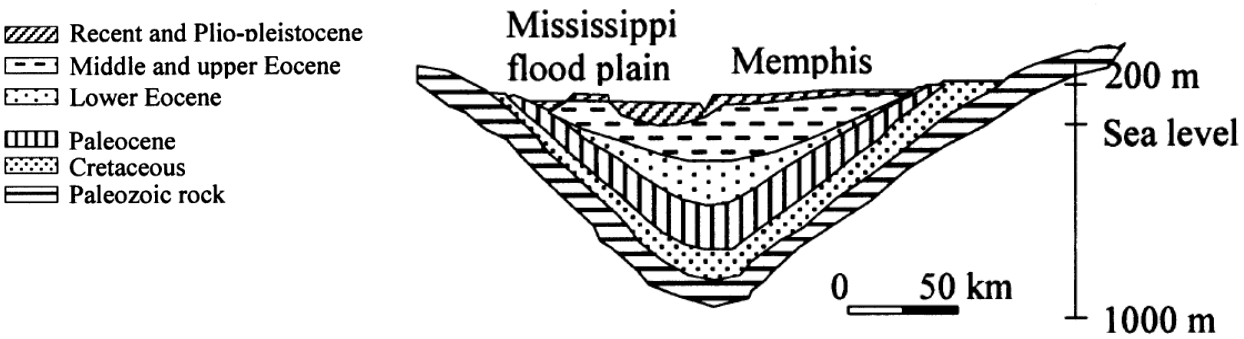

Figure 1. 2: Idealized cross section of the Mississippi Embayment (Hashash and Park 2001).

One of the primary inputs into the SSGMRA are shear wave velocity (V_s) profiles at the site down to bedrock. Although this can be relatively straight forward for some sites, the Mississippi Embayment consists of very deep sediments to a great depth (>1000 m in some locations) before bedrock is encountered. These V_s profiles to bedrock have been shown to be critical to properly estimate the ground motions for a site (Cramer *et al.*, 2004; Hashash and Park 2001). Many researchers, particularly Rix *et al.*, (2001) and Rosenblad and Li (2009), have attempted to profile soils in the Mississippi Embayment. However, they were only successful at developing V_s profiles to less than 300 m in depth, which would not reach bedrock in much of Northeast Arkansas. To insure accurate estimates of the ground motion demand using SSGMRA, a methodology to

measure V_s to bedrock in the Mississippi Embayment needs to be established and a set of V_s profiles in the Mississippi Embayment need to be collected to further understand the subsurface condition in the Embayment.

Other research has been conducted to understand the implications of conducting site-response at NMSZ bridge sites. Rogers *et al.,* (2007) performed site-response analyses at three Missouri River highway bridge sites using artificial acceleration time histories, which predicted site amplification between six and nine times for a large magnitude earthquake. They also concluded that serious foundation failure could occur for earthquakes over M_w 6.5 to 6.6 (Rogers *et al.,* 2007). However, the bedrock depths for these bridge sites are between 30 m and 40 m, which is much shallower than bedrock depths at bridge sites within the Mississippi Embayment. The deep Mississippi Embayment sedimentary deposits have a very large impact on the transfer of bedrock motions to surface ground motions during a large earthquake (Romero and Rix 2001, Hashash *et al.,* 2010). The thick sedimentary deposits in Northeast Arkansas are expected to damp out high frequency seismic waves, posing little threat for amplification like that seen in the Missouri River Flood Plain (Cox *et al.,* 2012). Liu and Stephenson (2004) conducted site-response for two bridge sites in the Missouri Bootheel where subsurface soils are more than 600 m thick. They demonstrated the importance of using both EQL and NL analyses and the effects of deep soil deposits that cause period migration from short to long periods. This resulted in a broad short period range where site-response predicted accelerations less than typical design accelerations. Other Mississippi Embayment site-response research also predicts deamplificaiton of short period motions for sites in western Tennessee and Kentucky due to deep unconsolidated sediments (Wang *et al.,* 1996, Harris *et al.,* 1994).

Ketchum *et al.,* (2004) demonstrated the potential cost savings of conducting SSGMRA for post-tensioned box-girder and I-girder bridges, which the California Department of Transportation (CalTrans) typically prefers. Their results show that for typically low overhead bridges, a 5% cost savings can be obtained for each 10% reduction in PGA above a baseline of 0.3 g to 0.4 g. Since AASHTO (2014) allows up to a 33% reduction in the simplified code based design response spectra (including the PGA), based on these results, conducting an SSGMRA could result in a cost reduction on the order of 15% of the total cost of the bridge. This cost savings would be significant when considered for Arkansas bridges within the Mississippi Embayment. Figure 1.3 illustrates Arkansas state owned bridges within AASHTO seismic performance zones when AASHTO site class D is assumed. Cost savings associated with conducting SSGMRA would be even more significant when the AASHTO seismic performance zone could be lowered from IV or III to II or I where design requirements are less stringent.

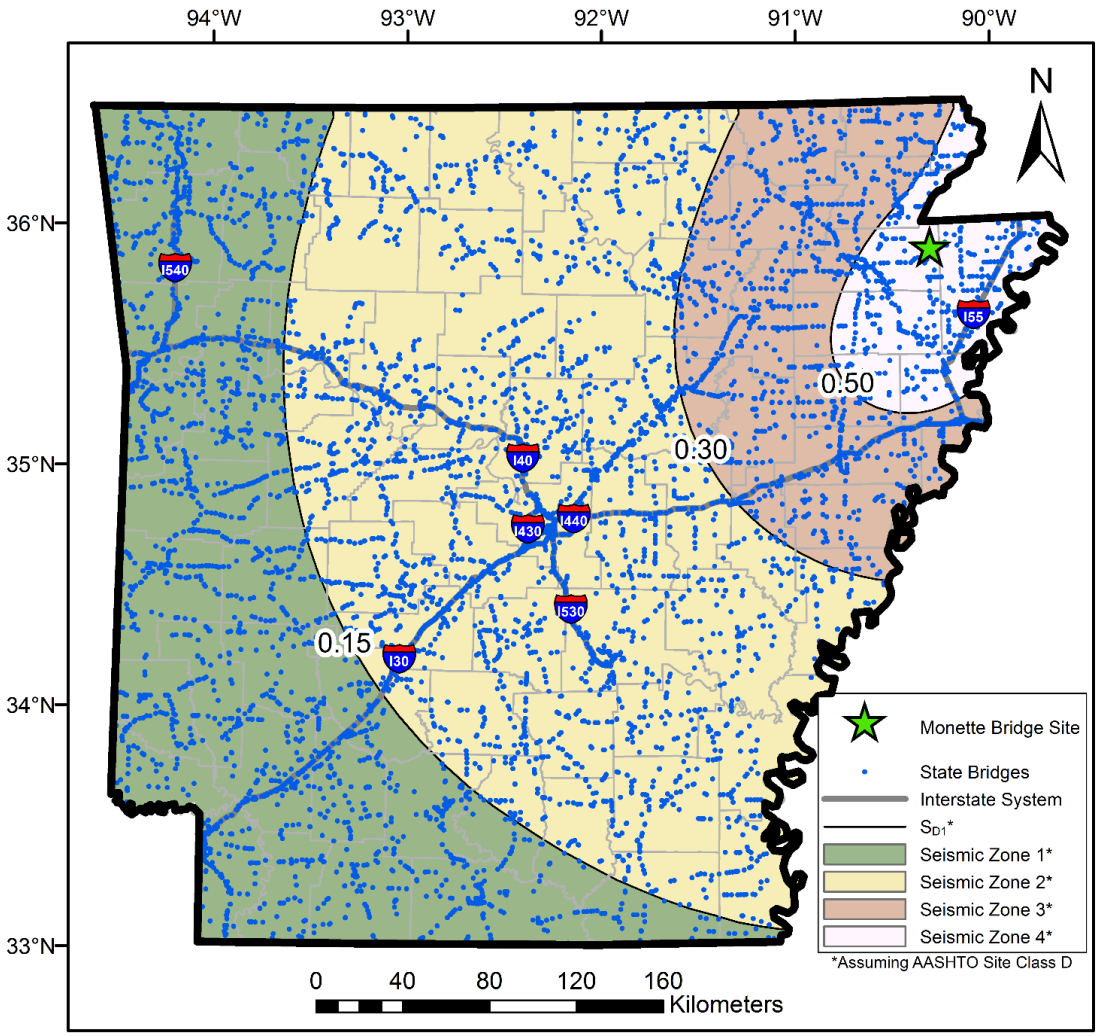

Figure 1. 3: Arkansas State owned bridges within respective AASHTO Seismic Performance Zones assuming site classification D. The Monette bridge used for the study is highlighted.

1.3 Dynamic Site Characterization Testing

Methods to obtain the in-situ small strain V_s measurements for a site typically fall into one of two categories: invasive and non-invasive. Invasive methods such as Crosshole, Downhole, P-S logging, and SCPT measure the layering and V_s of a site directly by placing sensors or both sensors and source below the surface in a borehole or CPT cone. V_s is directly measured by dividing the known distance between source and receiver by the measured travel time between source and receiver. These methods are proven to provide accurate results in a variety of conditions. However, the cost of drilling boreholes and conducting tests is often far more expensive than non-invasive methods. This is especially true for sites in the Mississippi Embayment, which would require boreholes or soundings to 1000 m in some cases.

Non-invasive methods have the advantage of only requiring sensors and source to be placed on the ground surface. This often significantly reduces the cost of developing V_s profiles for deeper

sites. Non-invasive methods for determining in-situ V_s are spilt into two main categories: body wave methods and surface wave methods. Body wave methods include seismic refraction and seismic reflection methods, while surface wave methods include the SASW, MASW, ReMi, MAM, and HVSR. The methods used in this study were P-wave refraction, MASW, MAM, and HVSR.

1.3.1 P-wave Refraction

The seismic refraction method (Redpath 1973) is a body wave method which consists of measuring (at known points along the surface) the travel times of compression or shear waves generated by an impulsive energy source. The energy source is typically a sledgehammer or explosives. The energy is detected by a linear array of receivers (geophones) placed along the ground surface in equal spacings between the receivers (i.e. 2 m) and recorded via a seismograph. The instant of the source pulse (e.g., the sledgehammer hitting the ground), "zero time," is recorded by the seismograph and the time to the first wave arrival at each geophone is identified. The raw data is then displayed as the travel time to each receiver (first wave arrival) versus receiver distance from the source. The slopes of the arrival times to each geophone are used to determine the velocity of subsurface layers, while an application of Snell's law of refraction of waves is used to determine the depth-to-layer interfaces. The method is often used for mapping strong velocity contrasts below the surface such as bedrock or the water table. Although seismic refraction is effective at mapping large velocity contrasts below the surface, it suffers from several serious drawbacks. The first of which requires that all layers below the ground surface must increase in velocity (or stiffness) with depth. While this is typically a good assumption, it is not true for some sites and significant errors will result if velocity reversals exist in the subsurface. Second, the method is most effective when developing compression wave velocity, which is not the wave velocity of interest in most geotechnical surveys (Redpath 1973). The use of shear waves in a refraction survey make detection and picking of wave arrivals more difficult, leading to additional ambiguity. Given the short falls of seismic refraction it is typically not used as a primary survey method, rather it is used to identify the water table to constrain other analyses.

1.3.2 Surface Wave methods

Surface wave methods rely on the dispersive nature of Rayleigh or Love waves to determine changes in subsurface stiffness. Rayleigh waves have traditionally been the wave of choice for surface wave methods, because Rayleigh waves are simpler to generate and sample in the field. However, Love wave use has increased significantly in the past decade. Love waves have been shown to provide more coherent data at difficult (soft-over-stiff) sites and provide additional constraint to the inversion problem (Wood *et al.,* 2014). Surface wave methods can broadly be split into two categories: (1) active source methods and (2) passive source methods. Active source methods generally use a linear array of sensors to measure the phase velocity of waves emanating from a known source (typically located in-line with the array) and propagating past the receivers. Traditionally, passive source methods have employed two-dimensional (2D) sensor arrays to measure the phase velocity of microtremors (passive environmental noise) emanating from an ambient source(s) (Tokimatsu *et al.,* 1992). 2D arrays are used because it is impossible to determine the propagation direction of waves emanating from an unknown source with a linear array of sensors, and in a dispersive material, knowledge of the direction of wave propagation and

the true velocity of its propagation are mutually dependent – one cannot be calculated without knowledge of the other (Zywicki 2007).

Active source surface wave methods are generally capable of resolving shorter wavelengths (higher frequencies) than passive methods because the source and receiver spacing/array length can be tailored to the desired frequency range needed to resolve near-surface layers. On the other hand, passive methods can generally resolve longer wavelengths because microtremors typically contain significant low frequency energy, while a specialized active source is required to actively generate low frequency (< 3 Hz) waves with significant energy. As such, researchers and practitioners have attempted to combine active and passive methods to exploit the strengths of both techniques and accurately resolve a wider range of frequencies/wavelengths (Yoon and Rix 2004, Park *et al.*, 2005, Wood *et al.*, 2014). Regardless of the method used to develop the experimental dispersion curve, an inversion process must be used to develop the V_s profile of the site. This inversion process uses a numerical solution, which propagates Rayleigh or Love type surface waves over a layered half space with each layer being assigned properties such as shear wave velocity, thickness, unit weight, and compression wave velocity. The numerical model solves for the theoretical dispersion of surface waves over this layered half space. The theoretical dispersion curve is then compared to the experimental dispersion curve. Model parameters are updated until the theoretical dispersion curve matches the experimental dispersion curve for the site. A diagram of the process of surface wave testing is shown in Figure 1.4. Additional information regarding general surface wave testing can be found in Foti *et al.*, (2014).

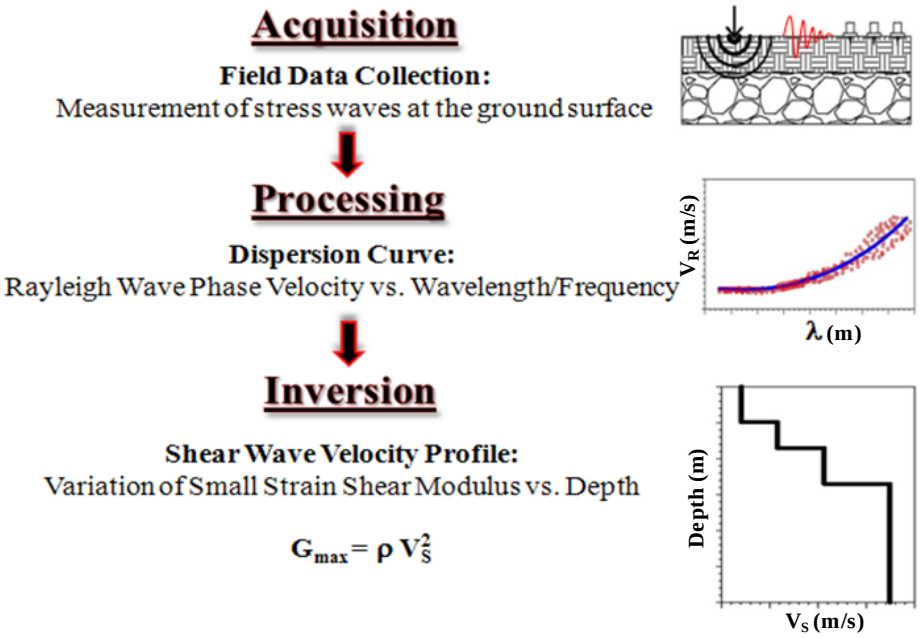

Figure 1. 4: Diagram of the process of surface wave testing from acquisition to final shear wave velocity profile.

1.3.3 Multi-Channel Surface Wave Analysis

The Multi-Channel Analysis of Surface Waves (MASW) method (Park *et al.*, 1999) is an active source technique that uses a linear array of typically 24-48 receivers to measure surface wave phase velocities in the field. A diagram of the MASW method is shown in Figure 1.5. Typically, a constant spacing between receivers is used (Zywicki 1999). One of the greatest advantages of the MASW method is its capacity to separate higher mode surface waves from fundamental mode propagation in the experimental dispersion analysis. However, most analyses only use the fundamental mode in subsequent inversion calculations. The ability to separate higher modes allows for the direct calculation of the fundamental mode dispersion curve primarily by automation, which speed up the data processing significantly compared to previous methods. Several different dispersion analysis techniques (f-k, f-p, Park transform, beamformer) have been developed to process the raw signals recorded in the field. While all of these options provide viable results, it has been shown that the beamformer analysis (Zywicki 1999) may provide the highest resolution of the four methods (Tran and Hiltunen 2008). Despite the method used to generate the experimental dispersion curve, a single fundamental mode or multimodal fundamental and higher mode inversion analysis can be used to match the experimental data and obtain a V_s profile.

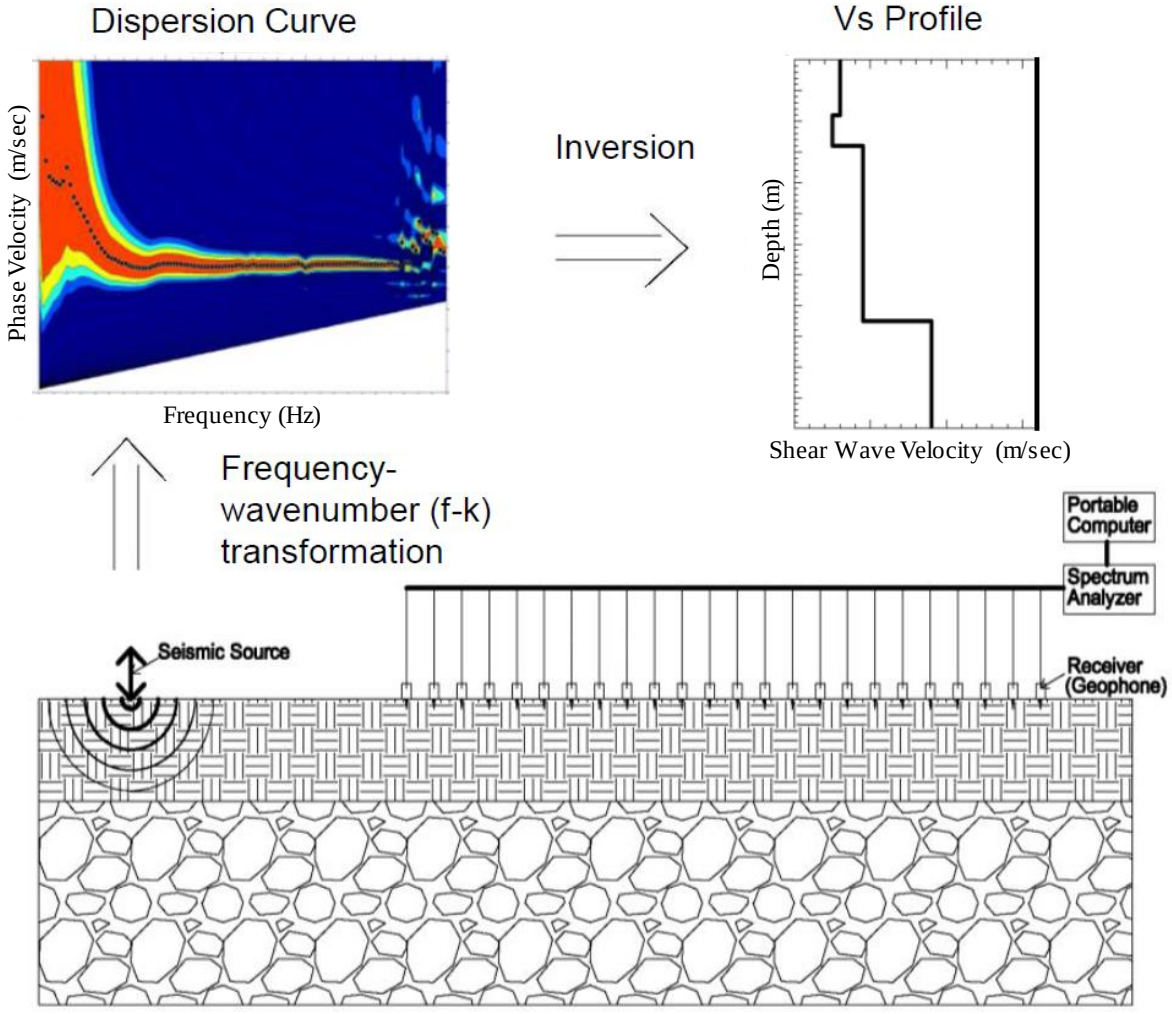

Figure 1. 5: Diagram of the process of MASW testing from field acquisition to final shear wave velocity profile.

1.3.4 Microtremor Array Methods (MAM)

Microtremor Array Methods (MAM) were first introduced and refined by Japanese researchers as a way to use passive microtremor energy to assess subsurface V_s profiles using 2D arrays of receivers (Aki 1957, Tokimatsu 1997). A diagram of MAM is shown in Figure 1.6. Arrays are typically configured in circular, nested triangular, L shapes, or other 2D geometric patterns. The 2D arrays are capable of resolving both the propagation direction of the surface waves and the true velocity of those surface waves regardless of the direction of propagation. This is particularly important given the unknown direction of the propagation of ambient microtremors. The arrays are typically formed using between 5-10 receivers, but can utilize many receivers. Multiple arrays setups with increasing array apertures (diameters) are typically employed to estimate the spectral curves over a wider frequency band (Wathelet *et al.*, 2008). Arrays are allowed to record microtremor noise for 30 minutes to several hours to improve spectral estimates (Wood *et al.*, 2014). As profiles are developed to greater depths increasingly large wavelengths (or small frequencies) are required for the spectral estimates. To properly record these very low frequencies, broadband seismometers are typically used because traditional 4.5 Hz geophones have difficulty measuring frequencies below approximately 2.5 Hz, while broadband seismometers are capable of measuring frequencies below 0.05 Hz (SESAME 2004). The collected MAM data is typically processed using one of three methods: (1) f-k, (2) HRFK, and (3) MSPAC. Each method has shown reliable results in many conditions. However, each method has advantages and disadvantages based on the subsurface and wavefield conditions at a particular site (Wathelet *et al.*, 2008). Therefore, it is best if raw data is processed using each of the methods and results compared to determine the best spectral estimate. Once spectral estimates are made the data is typically fit with a multi-mode algorithm to obtain the V_s profile.

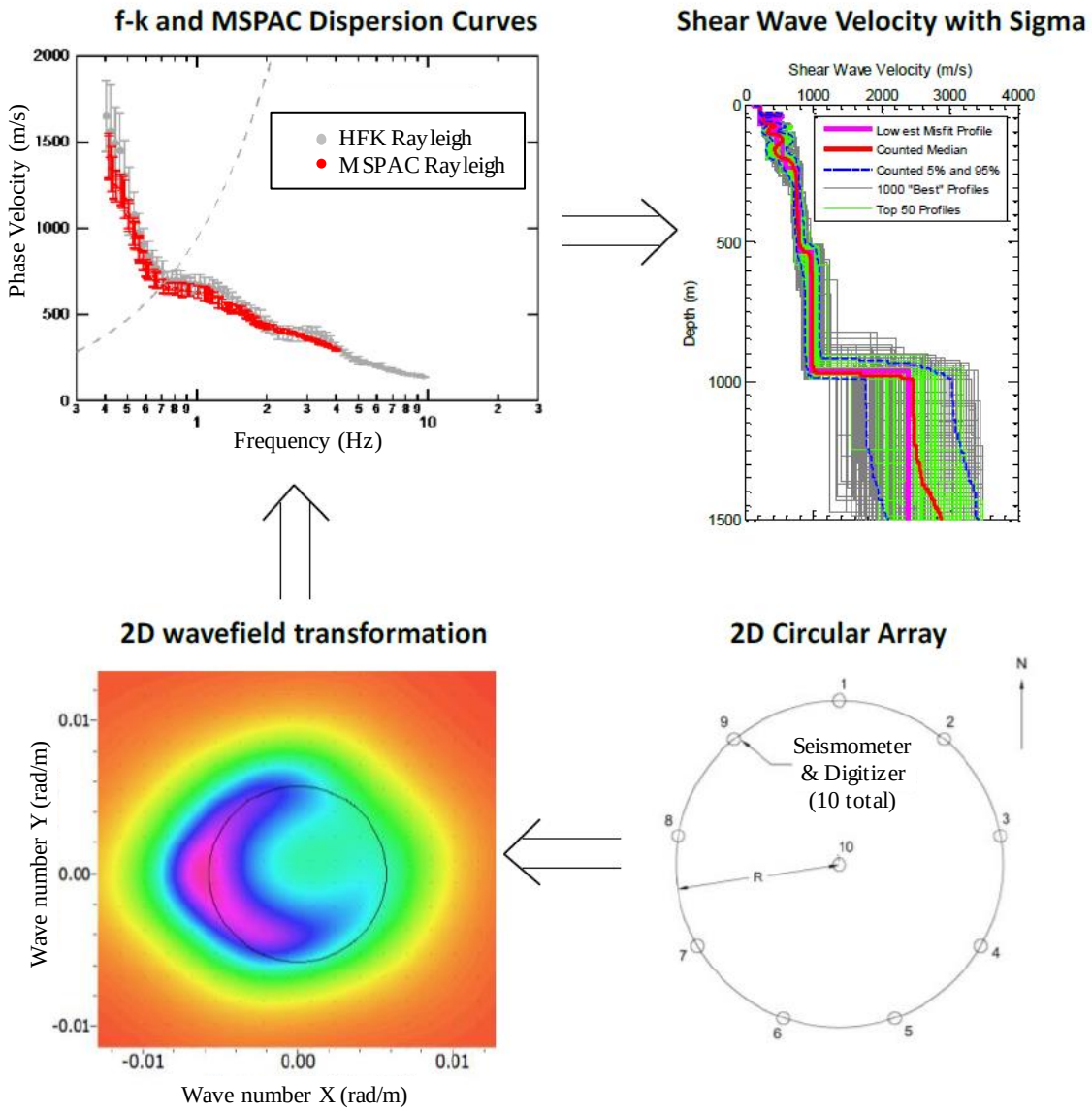

Figure 1. 6: Diagram of the process of MAM testing from field acquisition to final shear wave velocity profile.

1.3.5 Horizontal-to-Vertical Spectral Ratio

In addition to traditional site characterization methods, the horizontal-to-vertical spectral ratio (HVSR) method can be used to determine a sites fundamental vibration frequency. The fundamental frequency of a site can be used to constrain the V_s profile development and specifically provide additional knowledge of the location of bedrock or other strong impedance contrast below the surface (SESAME 2004). The method is also useful for conducting microzonation studies and mapping bedrock locations across a large area. Here, microzonation is defined as subdividing seismic prone area into zones with respect to geological and geophysical characteristics. The HSVR method, also called Nakamura technique, was first introduced by Nogoshi and Igarashi (1971). HVSR utilizes a single 3 component (usually broadband)

seismometer to record microtremors from the surface. For processing, the time records are transformed to the frequency domain and smoothed; then the geometric mean of the horizontal components are divided by the vertical components. If there are strong velocity contrasts in the subsurface (e.g., an impedance ratio greater than approximately 2), a spectral peak will form. This method can be used to identify the fundamental site period.

1.3.6 Combined use of Multiple Methods

Each of the methods mentioned above can be used individually to develop a V_s profile at a particular site. However, to reduce the uncertainty of the analysis and develop a more accurate estimate of V_s over a broad depth range multiple methods should be combined together. The combination of active source methods such as MASW with passive source methods such as MAM and utilization of both Rayleigh and Love wave dispersion estimates along with HVSR estimates provides additional constraint to the inversion problem needed to develop the V_s profile (Wood *et al.,* 2014). To solve the inversion problem while providing constraint to the problem, a joint inversion using a multi-mode solution should be performed, where the dispersion estimate or fundamental period from each method is given a weight in the analysis and the data is inverted together so that the theoretical model fits all data well (Wathelet 2008). Using a multi-mode solution with a joint inversion is particularly important when developing deep V_s profiles because higher modes tend to dominate around the fundamental site period and at longer wavelengths (SESAME 2004). Failure to identify these higher mode shifts in the dispersion data can lead to overestimates in the V_s by over 50% (Cox *et al.,* 2014).

1.4 Geology of Northeast Arkansas

Northeast Arkansas lies within the Mississippi Embayment, which is characterized by very deep sedimentary deposits. The Mississippi Embayment is generally described as a southward plunging syncline with an axis that closely traces the Mississippi River, as shown in Figure 1.7 (Mento *et al.,*, 1986). It sits between the Ozark Uplift on its west and the Nashville Dome on its east. The depth of bedrock in Northeast Arkansas can extend from depths of approximately 150 m in Jackson County to approximately 1100 m in Lee County (Dart 1995). There are several unique geological layers within Northeast Arkansas. The following layers are grouped according to the Central United States Velocity Model (Ramírez-Guzmán *et al.,* 2012):

The uppermost layer is the Quaternary layer. This layer consists of alluvium and Loess deposits of sand, gravel, silt, and clay from the Holocene and Pleistocene series (Brahana *et al.,* 1987). These two different series are the typical classifications of surface deposits in the Mississippi Embayment. The Holocene deposits are found within the alluvial plains of the Embayment and particularly in the Mississippi River floodplain. The Pleistocene deposits are older deposits located inland. The bluffs along the eastern edge of the Mississippi River are a geological boundary which separates the Holocene and Pleistocene deposits (Romero and Rix 2005).

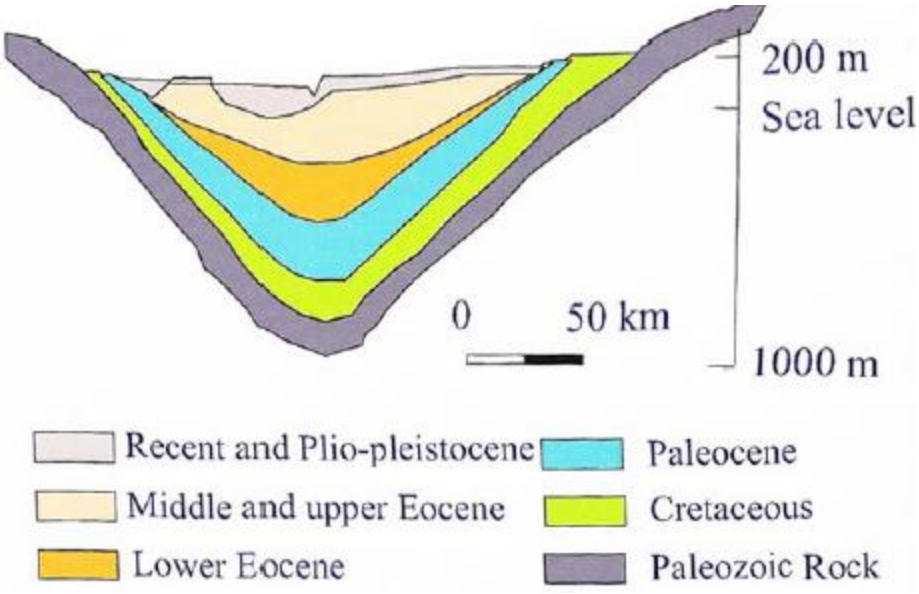

Figure 1. 7: Idealized cross section of the Mississippi Embayment (Hashash and Park 2001).

One significant geological feature in Northeast Arkansas is Crowley's Ridge. Crowley's Ridge separates the St. Francis Basin and the Western Lowlands. It rises an average of 60m above the alluvial plain. The origin of Crowley's Ridge is uncertain, but has been assumed to be either an erosional remnant or tectonic feature (Van Arsdale *et al.,* 1995).

Below the Quaternary layer is the Upper Tertiary layer, which consists of the Jackson Formation and part of the Claiborne group. The Jackson Formation consists of clays, silts, sands, and lignite (Brahana *et al.,* 1987). Approximately 14 m of the Jackson Formation is exposed in the base of the Mississippi River Valley bluffs (Hardeman 1996). The upper portion of the Claiborne group contains several formations including the Cockfield and Cook Mountain formations, which are characterized by light-gray to light-brown slits and clay (Van Arsdale and TenBrink 2000).

Below the Upper Tertiary layer is the Lower to Middle Claiborne layer, which contains the Memphis Sand layer. Memphis sand is a fluvial, very fine to coarse grained, and light gray-white sand (Van Arsdale and TenBrink 2000). It is the principle aquifer for the Memphis area. This layer is about 164-292 m thick and about 300m deep (Brahana *et al.,* 1987).

Next is the Paleocene layer, which contains the Wilcox and Midway groups. Several formations make up each of these groups. The Wilcox group contains the Flour Island Formation, Fort Pillow Sand, and Old Breastworks Formation. The Flour Island Formation consists of alternating layers of silt, clay, and medium to light-gray sand. The Fort Pillow Sand is thick, fine to coarse grained, marine sand and is 64 m thick in Shelby County, Tennessee (Van Arsdale and TenBrink 2000). The Old Breastworks Formation is 95 m thick clayey silt beneath Shelby County, Tennessee (Hosman, 1996). The Midway group contains the Porters Creek Clay Formation (thick body clay) and Clayton Formation (clay, sand, and minor limestone) (Brahana *et al.,* 1987). The Midway group is composed primarily of marine clay and thins from 160m near Memphis to 100 m near New Madrid, Missouri (Van Arsdale and TenBrink 2000).

Just above the bedrock layer is the Cretaceous and Mesocenozoic layer. These layers contain several forms of clays and sands, and consist of the McNairy Sand layer, the Demopolis Formation, and the Coffee Formation. The McNairy Sand layer indicated the top of the layer. It is composed of thick calcareous marine sand. It thins from 130 m thick at Shelby County to 95m thick at New Madrid. The Demopolis Formation lies below the McNairy Sand. It is a calcareous marine clay (Van Arsdale and TenBrink 2000). Below the Demopolis Formation is the Coffee Formation, which contains a well-sorted, loose-to-friable sand and that is interbedded with thin carbonaceous clays (Russell *et al.*, 1982). The Paleozoic bedrock layer signifies the basement of the Mississippi Embayment deposits and is primarily made up of white to dark-gray, fine to coarse crystalline dolomite (Van Arsdale and TenBrink 2000).

1.5 Site-Response Analysis Background

Design of transportation infrastructure is primarily governed by the AASHTO LRFD Bridge Design Specifications (AASHTO 2012). Additionally, guidelines for seismic consideration are contained in the AASHTO Guide Specifications for LRFD Seismic Bridge Design (AASHTO 2009). When determining the seismic design under the AASHTO provisions, one can choose to use the simplified approach or do a more detailed SSGMRA.

For the simplified code based approach, construction sites within any seismic zone must be grouped into one of five possible generalized site classifications (i.e., Site Class A-E). These site classifications are based solely on the material in the upper 30 m of the subsurface. For this study, AASHTO site classification method was followed. While these simplified procedures are generally conservative and work well for many seismic areas with shallow soil deposits, their applicability to geologic conditions in the Mississippi Embayment, where soil thicknesses can range up to 1000 m, is uncertain. AASHTO (2012) directly mentions deep, soft deposits (like those in the Mississippi Embayment) as location where SSGMRA should be performed. Otherwise, longer-period (i.e., long span, relatively flexible) bridges may be under-designed at a significant risk and shorter period (i.e., short span, relatively stiff) bridges may be over-designed at a significant cost.

Recognizing the value these types of site specific analysis can add when complex conditions exist, AASHTO (2012) allows seismic design forces obtained from general, code based procedures to be reduced by up to 33% if the SSGMRA indicates this is appropriate. This potential benefit would allow structural seismic loads used in bridge design and peak ground accelerations used in soil liquefaction analyses and embankment designs to be decreased substantially.

To conduct a SSGMRA, there are three main steps: (1) characterize the small-strain V_s of the soil profile down to bedrock, (2) collect and adjust appropriate input earthquake acceleration time histories, and (3) simulate the propagation of input ground motions from bedrock to the ground surface using appropriate numerical analyses. Each of these steps has its own challenges that can contribute to the overall uncertainty in surface ground motion estimates.

1.6 Seismic Bridge Design

Bridge components such as piles, columns, bents, abutments, restrainer blocks, and embankments are typically the main systems designed to resist and withstand seismic loads. This

can significantly increase the cost of the bridge project due to long pile lengths, oversized abutments, and large, difficult to construct earthquake resisting systems. A reduction in the sizes of these elements could be justified by a reduced seismic demand if the SSGMRA deems this appropriate. However, other factors such as soil conditions, bridge period, and other AASHTO limit states can also govern the design of these components rather than seismic demand.

1.7 Outline of Report

Background on this project is provided in Chapter 1 of this report. Chapter 2 discusses dynamic site characterization which was conducted at 15 sites in Northeast Arkansas. Chapter 3 discusses data processing of collected information from the dynamic site characterization efforts. Chapter 4 discusses the results from the dynamic site characterization efforts and the development of University of Arkansas Mississippi Embayment Velocity Model (UA_MEVM). Chapter 5 discusses site-response at the Monette bridge site including background, methodology, results, and implementation. Chapter 6 summarizes seismic bridge design using SSGMRA results. Chapter 7 details the cost-savings benefits of performing SSGMRA for a case-study ARDOT bridge in Monette, Arkansas. Chapter 8 is a summary of conclusions. Electronic appendices are also provided that contain supplemental information such as design calculations.

CHAPTER 2
SITE INVESTIGATION

2.1 Introduction

Dynamic site characterization testing was conducted at 15 sites located throughout Northeast Arkansas (see Figure 2.1). These sites were chosen based on their proximity to the location of current or potential ARDOT bridge job sites. However, if the area near or around the job site could not accommodate testing (i.e. too urban, poor soil conditions, no landowner permission) or there was another job site within close proximity, other locations were explored. An attempt was also made to distribute the sites across Northeast Arkansas as much possible to understand the distribution of dynamic soil properties across the region and to aid in the development of the 3D velocity model of the area. In Table 2.1, the site names and locations where testing was conducted are tabulated along with the nearest ARDOT job. Testing site maps are included in Appendix A. From the sites tested, only the Mounds and Harrisburg sites were not located in close proximity to an ARDOT job. Since several ARDOT jobs were 5-6 miles away from the Bay site, it was selected to fill a gap in the testing region. These sites were tested to provide a more consistent distribution

across the Northeast Arkansas area.

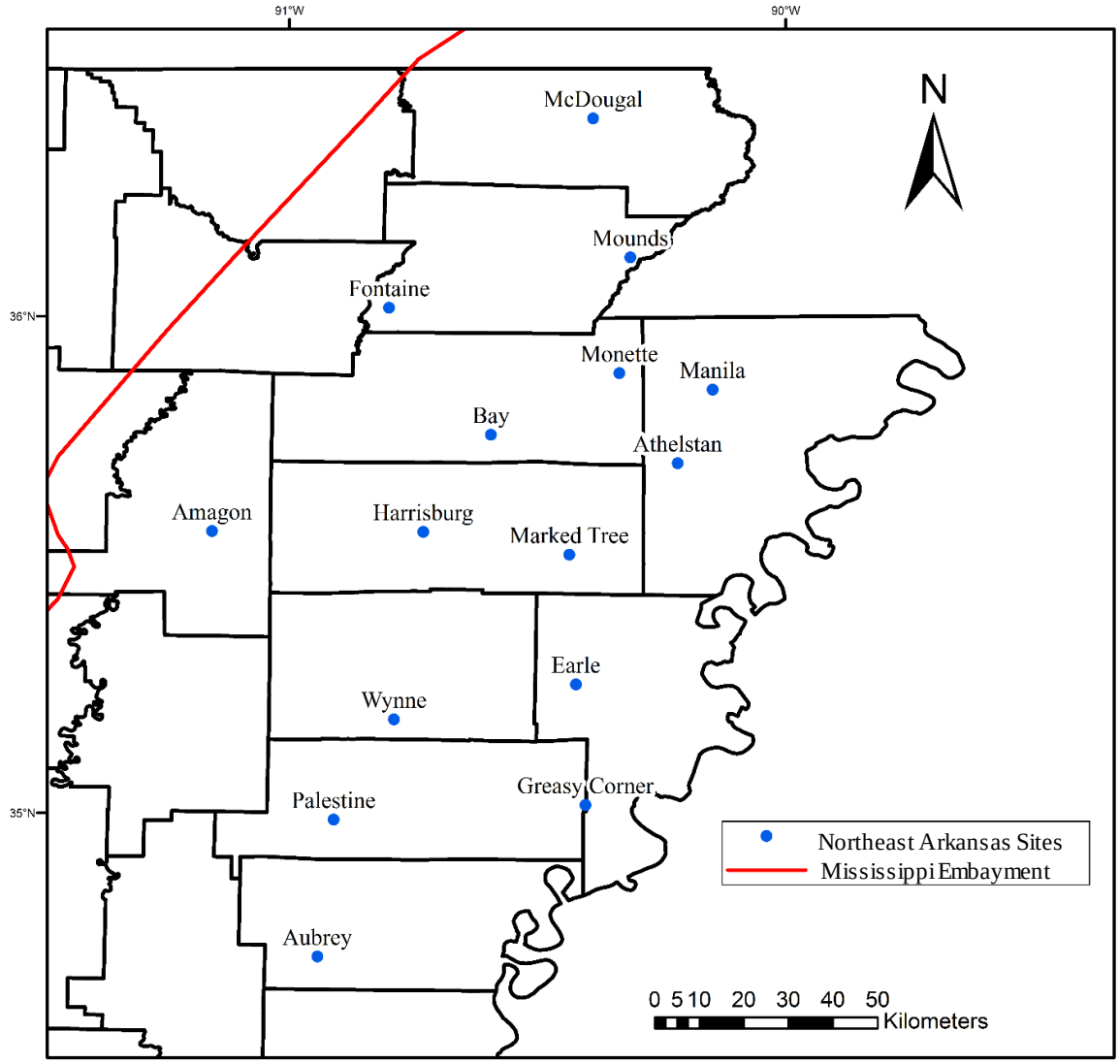

Figure 2. 1: Dynamic site characterization testing locations in Northeast Arkansas.

Table 2. 1: Dynamic site characterization testing locations in Northeast Arkansas and corresponding ARDOT job number

Site Name	**Nearest ARDOT Job Number**	**Latitude**	**Longitude**
McDougal	100842	36.398583	-90.388175
Mounds	-	36.118611	-90.313083
Fontaine	100841	36.017175	-90.799475
Bay	100833/100657/100824x1/100824x2	35.761622	-90.594256
Monette	CA1001	35.885581	-90.335186
Manila	CA1002x1/ CA1002x2/ CA1002x3	35.852500	-90.147089
Athelstan	100760x2	35.704214	-90.217497
Amagon	050272x1/ 050272x2/ 050272x3/ 050272x4	35.567572	-91.155928
Harrisburg	-	35.565781	-90.730197
Marked Tree	100782	35.520050	-90.435811
Wynne	110574	35.188317	-90.789519
Earle	CA0103x1/ CA0103x2	35.258642	-90.422603
Palestine	110586	34.986725	-90.911181
Greasy Corner	110617	35.015908	-90.403436
Aubrey	110616x1/ 110616x2	34.711003	-90.943864

Dynamic site characterization in Northeast Arkansas included a combination of p-wave refraction, active and passive source surface wave testing, and HVSR. The actual tests conducted at each site are identified in Table 2.2. P-wave refraction was conducted at each of the testing locations to help locate the water table (i.e., line of saturation) below the surface. Active source MASW utilizing both Rayleigh and Love type surfaces waves was also conducted at each site using a sledgehammer source to understand the dynamic properties of the very near surface materials. The use of both Rayleigh and Love type surface waves increases the robustness of the testing and helps ensure the correct mode assignments are made during the analysis process (Wood *et al.*, 2014). At select sites (see Table 2.2), Rayleigh wave MASW was conducted using a Vibroseis source in order to develop deeper active source dispersion data for comparison with passive source dispersion data.

Table 2. 2**:** Types of testing conducted at each site.

Site Name	Active Source Testing				Passive Source Testing				
	P-Wave	**Rayleigh**	**Love**	**Vibroseis**	**50m**	**200m**	**500m**	**1000m**	**L array[2]**
McDougal	Y	Y	Y	Y	Y	Y	Y	N	48
Mounds	Y	Y	Y	Y[1]	Y	Y	Y	N	48
Fontaine	Y	Y	Y	N	Y	Y	Y	N	48
Bay	Y	Y	Y	Y	N	Y	Y	Y	N
Monette	Y	Y	Y	N	Y	Y	Y	N	N
Manila	Y	Y	Y	N	Y	Y	Y	N	N
Athelstan	Y	Y	Y	N	Y	Y	Y	N	N
Amagon	Y	Y	Y	Y	Y	Y	Y	N	24
Harrisburg	Y	Y	Y	N	Y	Y	Y	N	48
Marked Tree	Y	Y	Y	N	Y	Y	Y	Y	24
Wynne	Y	Y	Y	Y	Y	Y	Y	N	24
Earle	Y	Y	Y	Y	Y	Y	Y	Y	24
Palestine	Y	Y	Y	N	Y	Y	Y	N	N
Greasy Corner	Y	Y	Y	Y	Y	Y	Y	Y	24
Aubrey	Y	Y	Y	N	Y	Y	Y	N	N

[1]Conducted on stiffer road soil

[2]24/48 denotes number of geophones used

[3]Y indicates the test was conducted at the site, N indicates the test was not conducted at the site

Passive source testing (microtremor array methods) was conducted at each of the test sites to understand the dynamic properties of the soil and rock layers at deeper depths. At each site, 2D circular arrays of broadband sensors with diameters of 50, 200, and 500 meters were used to measure microtremors (i.e., background noise). At select sites (see Table 2.2), 1000 meter diameter circular arrays were used for comparison with the smaller diameter arrays. Also at select sites, an

L-array of geophones were used for passive testing in addition to the circular arrays at applicable sites.

A typical testing site layout is shown in Figure 2.2. For each site, a common center point for the circular arrays was maintained where possible (although it was not possible at all sites due to obstructions or site constraints). The P-wave refraction, active MASW (Rayleigh and Love) using a sledgehammer source, and L-array passive testing were conducted near the center point of the circular array where possible. Testing around a common midpoint helps reduce the influence of lateral variability on surface wave measurements and ensure each method is measuring similar soil and rock properties. The active MASW testing using a Vibroseis source was often conducted away from the center of the array due to site constraints (i.e., the vibroseis truck could not access locations away from roads). Therefore, testing was often conducted on the nearest farm or public road to the center of the array. Each testing method utilized in the research is explained in detail below.

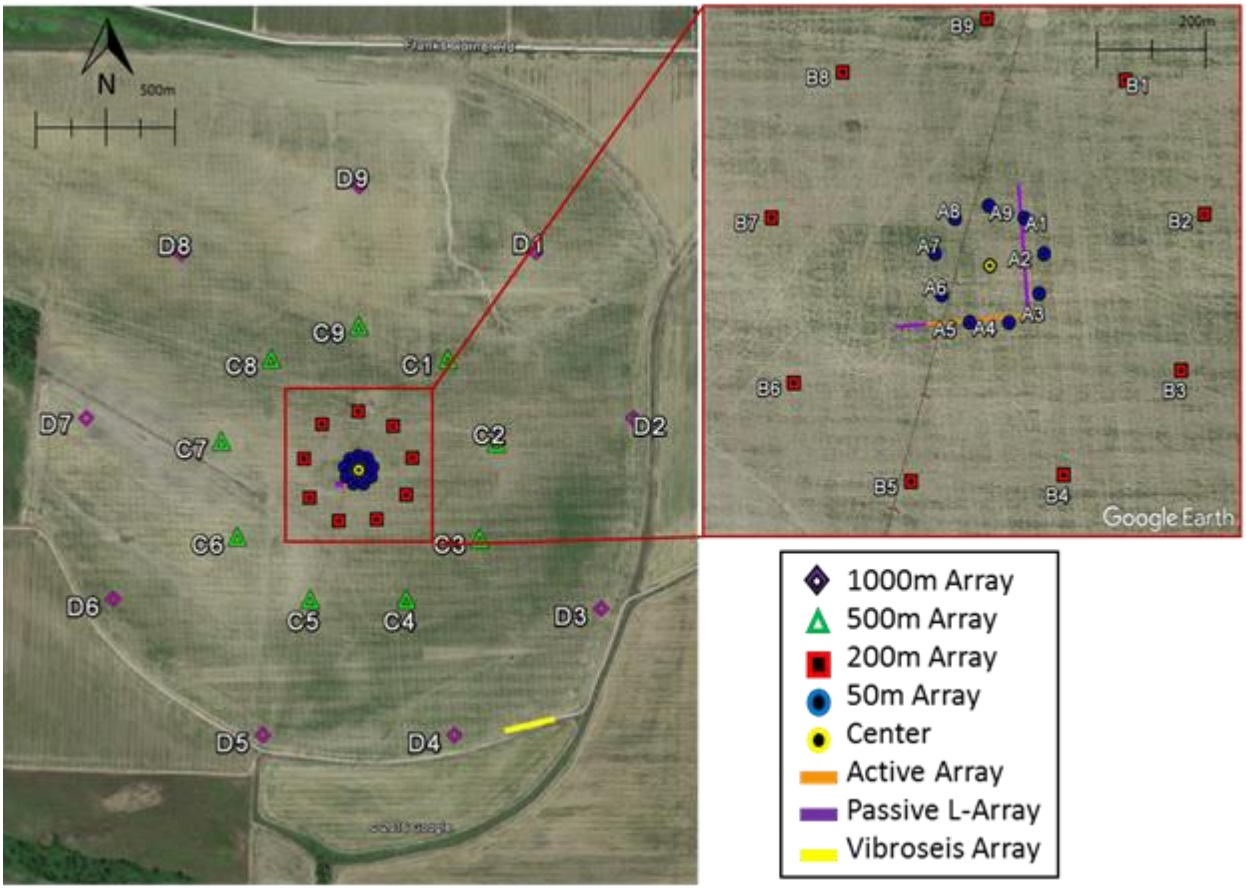

Figure 2. 2: A typical testing site setup.

2.2 Active Source Testing

Active source testing was conducted using four arrangements: (1) Rayleigh wave surface wave testing utilizing a sledgehammer source, (2) P-wave refraction testing utilizing a sledgehammer source, (3) Love wave surface wave testing utilizing a sledgehammer source, and (4) Rayleigh wave surface wave testing utilizing a vibroseis source.

2.2.1 Rayleigh wave surface wave testing utilizing a sledgehammer source

Rayleigh wave surface wave testing utilizing a sledgehammer source was conducted using a linear array of 24, 4.5 Hz vertical geophones with uniform spacing between each geophone of 2 meters (total array length of 46 meters). The array setup in the field is shown in Figure 2.3. Geophones used for testing were Geospace GS-11D, 4.5 Hz geophones with coil resistance of 4000 Ohms and shunt damping of 70%. Geophones are housed in a PC-21 land case with 7.5 centimeter spike. Geophones were installed flush with the ground surface to ensure proper coupling with the ground. Geophones were attached to a refraction cable via a KCL-4 connector. The refraction cable was connected to a Geometrics Geode seismograph to record the geophone output. The Geode seismograph has 24 channels per unit, multiple units can be connected together to form systems of up to 1000 channels. Specifications of the geodes include 24 bit, ultra-high resolution, 24 kHz bandwidth (8 to 0.02 millisecond sampling rates), low distortion (0.0005%), low noise (0.2uV), and a high stacking accuracy (1/32 sample interval) (Geometrics 2017). The Geode is controlled by a standard laptop computer via Geometrics Seismodule Controller software where signals are viewed and recorded via the laptop. The Geode along with the laptop computer is shown in Figure 2.4.

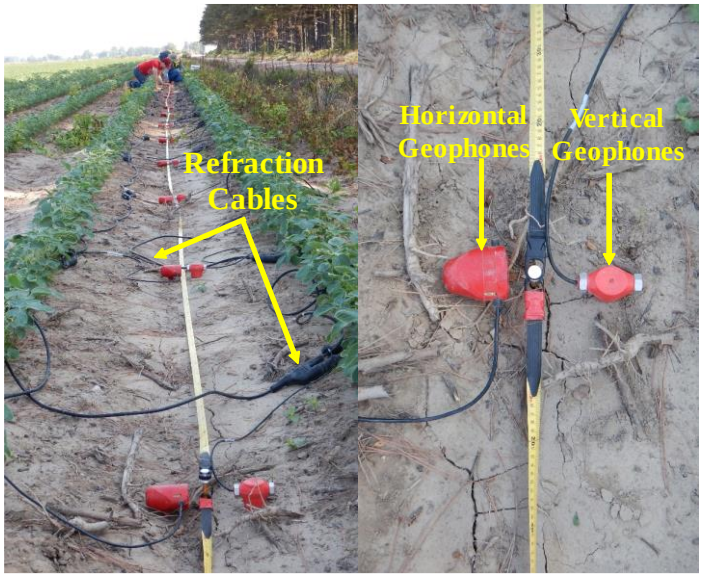

Figure 2. 3: Left - Active sledgehammer source surface wave testing array. Right - a horizontal geophone for measuring Love waves to the left of the tape and a vertical geophone measuring Rayleigh waves to the right of the tape.

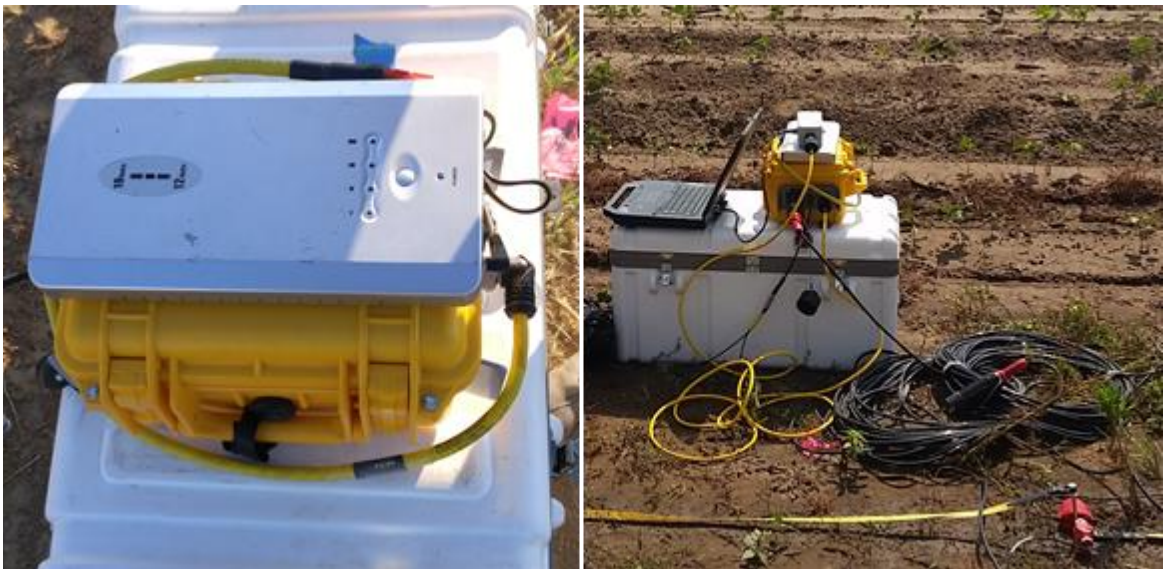

Figure 2. 4: Left - A Geometrics Geode Seismograph with portable battery attached to the top. Right: A geode linking the geophone refraction cable and field laptop.

For data collection, Rayleigh waves were generated using a 5.4 kg sledgehammer striking an aluminum plate overlain by a rubber damping pad. Source locations of 5m, 10 m, 20 m, and 40 m from the first geophone in the array were used at each site. Multiple source offsets were used to ensure high quality data, allow uncertainty to be estimated, and ensure near-field effects do not corrupt the data. At each source location, 10 vertical blows of the sledgehammer were stacked, using the Geode, to increase the signal-to-noise ratio of the measured waveform (see Figure 2.5). A 4 ms sampling rate and 4 second record length were used to record the waveforms.

2.2.2 P-wave refraction testing utilizing a sledgehammer source

P-wave refraction testing utilizing a sledgehammer source used the same array of vertical 4.5 Hz geophones as the Rayleigh wave surface wave testing. For data collection, the same sledgehammer was used at a source location 2 meters from the first receiver and 10 blows were stacked similar to the Rayleigh wave MASW. A 0.125 ms sampling rate, 2 second record length, and 0.25 second delay were used to record the waveforms.

2.2.3 Love wave surface wave testing utilizing a sledgehammer source

Love wave surface wave testing utilizing a sledgehammer source was conducted using a linear array of 24, 4.5 Hz horizontal geophones with uniform spacing between each geophone of 2 meters (total array length of 46 meters). The array setup in the field is shown in Figure 2.3. Similar horizontal Geospace GS-11D geophones encased in a PC803H land case were used and installed in the same way as in the Rayleigh wave surface wave testing. However, these geophones did

require leveling and orientation cross line to the array orientation (See Figure 2.3). The same 5.4 kg sledgehammer was used for Love wave generation. However, it was used to strike a wooden beam with aluminum ends horizontally cross line to the array to generate Loves waves (see Figure 2.5). Source locations of 5m, 10 m, 20 m, and 40 m from the first geophone in the array were used at each site. To increase the signal-to-noise ratio of the measured waveform, 10 horizontal blows of the sledgehammer were stacked using the Geode. A 4 ms sampling rate and 4 second record length were used to record the waveforms.

Figure 2. 5: Left - A sledgehammer impacted vertically being used to generate Rayleigh waves. Right - A sledgehammer impacted horizontally being used to generated Love waves.

2.2.4 Rayleigh wave surface wave testing utilizing a vibroseis source

Rayleigh wave surface wave testing utilizing a vibroseis source was conducted using a linear array of 24, 4.5 Hz vertical geophones with uniform spacing between each geophone of 4 meters (total array length of 92 meters). The longer array length was used to profile deeper below the surface. The geophones used for testing were the same as used for the previous Rayleigh wave testing. The vibroseis source, shown in Figure 2.6, is an Industrial Vehicles International (IVI) T-15000 minivib mounted to an International DuraStar 4300 Crew Cab truck. The minivib has a peak force output of 26.7 KN between frequencies of 14 Hz and 225 Hz, with lower output at frequencies higher and lower than this range.

Figure 2. 6: A vibroseis truck being used as a source of excitation for surface wave testing.

For testing, vibroseis source positions were located at 5m, 10m, 20m, and 40m offsets from the beginning of the linear array. A stepped sine sweep was used for testing, which started at a frequency of 60 Hz and cycled downward frequency by frequency to 2 Hz. Individual frequencies used for testing were divided into three frequency bands: (1) 60 Hz to 20.5 Hz, where a 0.5 Hz frequency spacing with 50 cycles at each frequency was used, (2) 20 Hz to 10.25 Hz, where a 0.25 frequency spacing with 50 cycles at each frequency was used, and (3) 10 Hz to 2 Hz, where a 0.25 Hz frequency spacing with 100 cycles at each frequency was used. A Data Physics Mobilyzer dynamic signal analyzer was used to control the source vibration as well as record the waveforms measured by each geophone. The Mobilyzer has a 49 kHz bandwidth, 32 channel inputs and 2 channel outputs for simultaneous sampling, 105 kHz simultaneous sampling rate, 120 GB internal hard drive, 24-bit ADC, 120 dB dynamic range, and 110 dB anti-alias filters. An adapter was used to convert the live end of the refraction cable to 24 separate BNC output cables, which were then connected to the separate input channels of the Mobilyzer. The system uses a windows interface and connects to a laptop via a standard Ethernet cable (Data Physics Corporation 2016) (Wood 2009). The Mobilyzer is shown in Figure 2.7.

Figure 2. 7: Data Physics Mobilyzer with a 32 channel dynamic signal analyzer.

2.3 Passive Testing

Two different forms of 2D MAM testing were utilized in Northeast Arkansas: L-array and circular array. L-array testing was primarily used for dispersion comparison purposes, while the circular arrays were the primary testing method utilized to measure the dynamic properties of materials at deeper depths. The two-dimensional geometry of the arrays allows for the determination of the orientation of wave propagation from unknown sources utilized in passive surface wave testing.

2.3.1 L-Array

L-Array MAM testing utilized an array of 24 or 48, 4.5 Hz vertical geophones in a near equal length L-shaped array. (see Figure 2.8) These geophones are the same as utilized for active Rayleigh wave testing. The geophones, arranged in an L-shape were positioned at an equal spacing of 5 m between each geophone. This resulted in an L-array with one leg having a length of 115 m and the other leg with length of 120 m when 48 geophones were used or 55 meters and 60 meters when 24 geophones were used. Microtremors (i.e., background noise) were recorded for approximately 1 hour at each site using the Geodes used for active testing. A sampling rate of 8 ms with a record length of 60 or 120 seconds were used to record the waveforms.

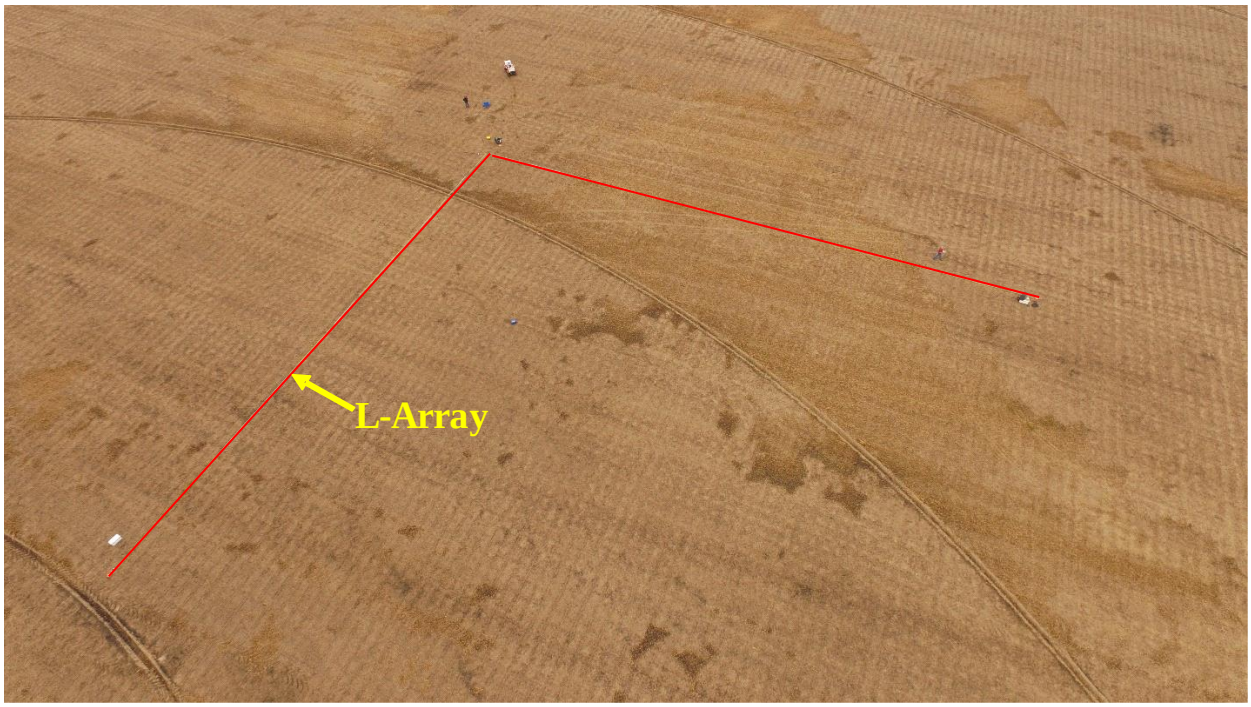

Figure 2. 8: L-Array testing setup using 24 geophones.

2.3.2 Circular Array (MAM)

Circular array MAM testing utilized circular arrays of 10 three component broadband seismometers. Nine of these seismometers were arranged along the outside edge of the circle, while one seismometer was placed in the center of the array. Array diameters of 500 meter, 200 meter, and 50 meter were used at all sites. For some sites a 1000 meter diameter array was also used. Seismometers used for testing were Nanometrics Trillium Compact Broadband Seismometers. The Trillium Compact seismometers are a broadband seismometer with a flat frequency response from 0.05 Hz to 100 Hz, and have a tilt tolerance of 10 degrees (Nanometrics 2017). Each sensor is recorded using a Nanometrics Centaur Digitizer. The Centaur digitizer is a high resolution 3 channel, 24-bit data acquisition system capable of recording at sample rates up to 5000 samples per second. The Centaur uses a GPS timing system to time stamp waveforms to ensure waveforms records are synced between stations (Nanometrics 2017). Both the Trillium Compact, Centaur Digitizer, battery, and GPS unit are housed in a Nanometrics rapid deployment case for easy deployment in the field, as shown in Figure 2.9.

During field deployment, each station was initially placed in the circular arrays using standard handheld Garmin GPS units based on maps generated pre-trip. Each sensor was buried approximately 15-30 centimeters below the ground surface to reduce uncorrelated noise from wind. In Figure 2.10, a typically sensor placement is shown. Once all seismometers were set, the arrays were left to record microtremors. The 1000 meter and 500 meter arrays were allowed to record for approximately 2 hours, while the 200 meter and 50 meter arrays were allowed to record

for 1 hour. After placement of the stations, a Trimble Geo 7x centimeter GPS unit with a Zephyr 2 external antenna was used to survey the precise location of each sensor. The Trimble GPS unit is shown in Figure 2.11. The external antenna of the Trimble GPS unit brings the accuracy of the unit to below ± 2 centimeters.

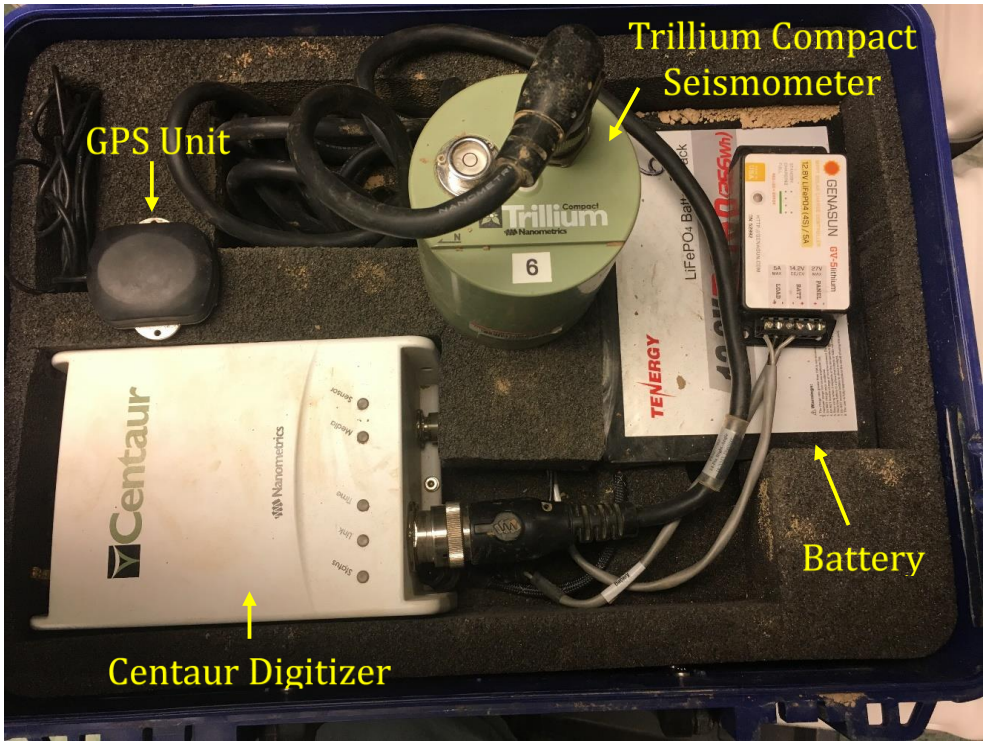

Figure 2. 9: Nanometrics Trillium compact and Centaur placed in a rapid deployment case.

Figure 2. 10: (1) A 15 centimeter diameter hole is dug to a depth of approximately 15-30 centimeters. (2) A Trillium Compact seismometer is placed in the hole, oriented toward magnetic North, and leveled. (3) The soil is replaced around the sensor and compacted to ensure sufficient coupling. (4) The station is allowed to record data for 1-2 hours.

Figure 2. 11: Trimble GPS with external antenna.

2.4 Horizontal-to-Vertical Spectral Ratio

Data for the horizontal-to-vertical spectral ratio (HVSR) method were recorded using the 3 component, Trillium Compacts Seismometers during the circular array passive testing.

CHAPTER 3
DATA PROCESSING

3.1 Introduction

Shear wave velocity (Vs) profiles were developed for each site in Northeast Arkansas. Processing methods to develop the V_s profiles are explained in detail below and generally consist of developing experimental dispersion curves and horizontal-to-vertical spectral ratios (HVSR) from raw data collected in the field at each site. This dispersion and HVSR information is used to conduct a joint inversion to solve for the V_s profile at each site. The five different data processing steps used in this investigation, which will be discussed in detail below, are as follows:

- Active-source surface wave processing.
- Passive-source surface wave processing
- Horizontal-to-vertical spectral ratio processing.
- Dispersion comparison.
- Inversion.

3.2 Active-Source Dispersion Data Processing.

The active-source data collected using the sledgehammer and vibroseis sources were analyzed for the four testing arrangements: (1) Rayleigh wave data collected utilizing a sledgehammer source, (2) P-Wave refraction data collected using a sledgehammer source, (3) Love wave surface wave testing utilizing a sledgehammer source, and (4) Rayleigh wave surface wave testing utilizing a vibroseis source.

3.2.1 Rayleigh wave surface wave processing utilizing a sledgehammer source

The Rayleigh wave sledgehammer data was processed using the frequency domain beamformer (FDBF) method (Zywicki 1999) combined with the multiple source-offset technique for identifying near-field contamination and quantifying dispersion uncertainty (Cox and Wood 2011). For each source offset (5, 10, 20 and 40 meter), dispersion data were generated. The maximum spectral peak was automatically picked from the 3D contour plots (Figure 3.1) for each frequency. All the 3D contour plots are based on a probability distribution scheme that compares the fit between a theoretical wavenumber at each frequency to the experimentally measured data, i.e., the plot can be considered a topographic map where the red color represents the best match (maximum spectral peak) similar to the top of a ridge, whereas the blue represents the poorest match (a valley). This shifting of a data color from red towards the blue indicates a lower probability of that velocity representing the maximum spectral peak at that point. This color code explanation is applicable for all the 3D dispersion curve contour plots presented in this report. The

individual dispersion data from each offset were combined to form a composite dispersion curve (see Figure 3.2).

For the composite curve, all identifiable near-field data for the active-source testing (below approximately 5-7 Hz depending on the site) were eliminated. Additionally, all identifiable effective mode data were eliminated, prior to creating the mean experimental dispersion curve. To develop an experimental dispersion curve with mean velocity and associated uncertainty, the remaining composite experimental dispersion curve was divided into 50 frequency bins distributed evenly on a log scale between 1 to 100 Hz. For each bin, the mean phase velocity and standard deviation were calculated. The fundamental mode and at several sites some higher mode data were resolved from the Rayleigh wave sledgehammer data.

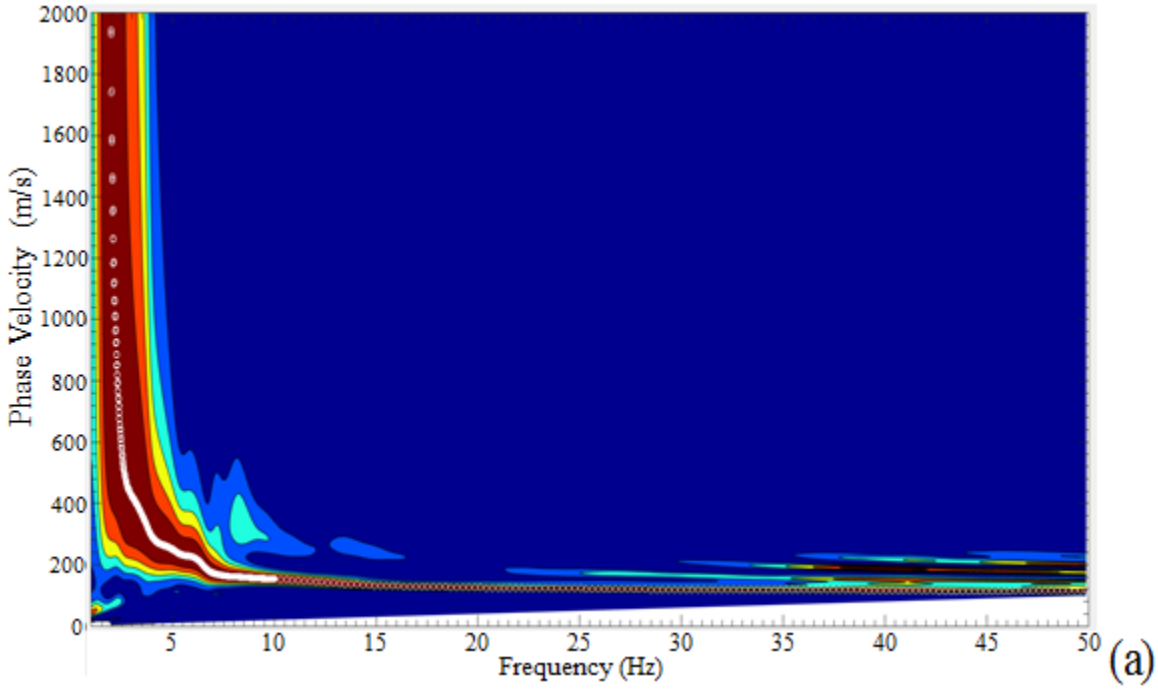

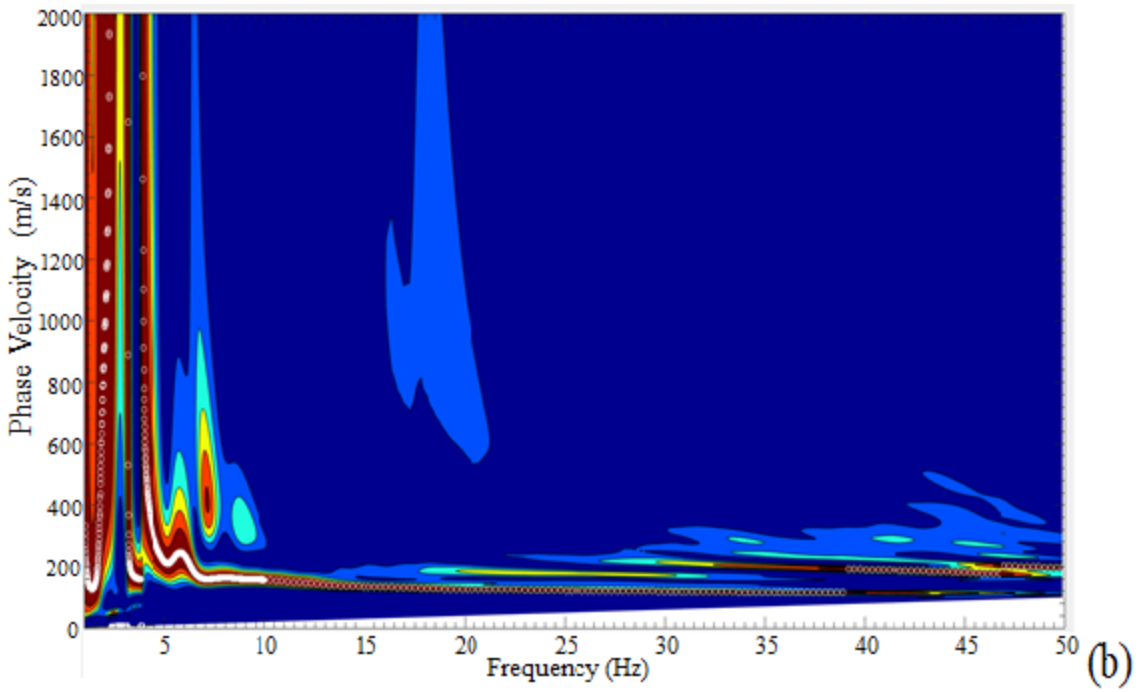
Phase Velocity (m/s)
2000
1800
1600
1400
1200
1000
800
600
400
200
0
5
10
15
20
25
30
35
40
45
50
Frequency (Hz)

(b)

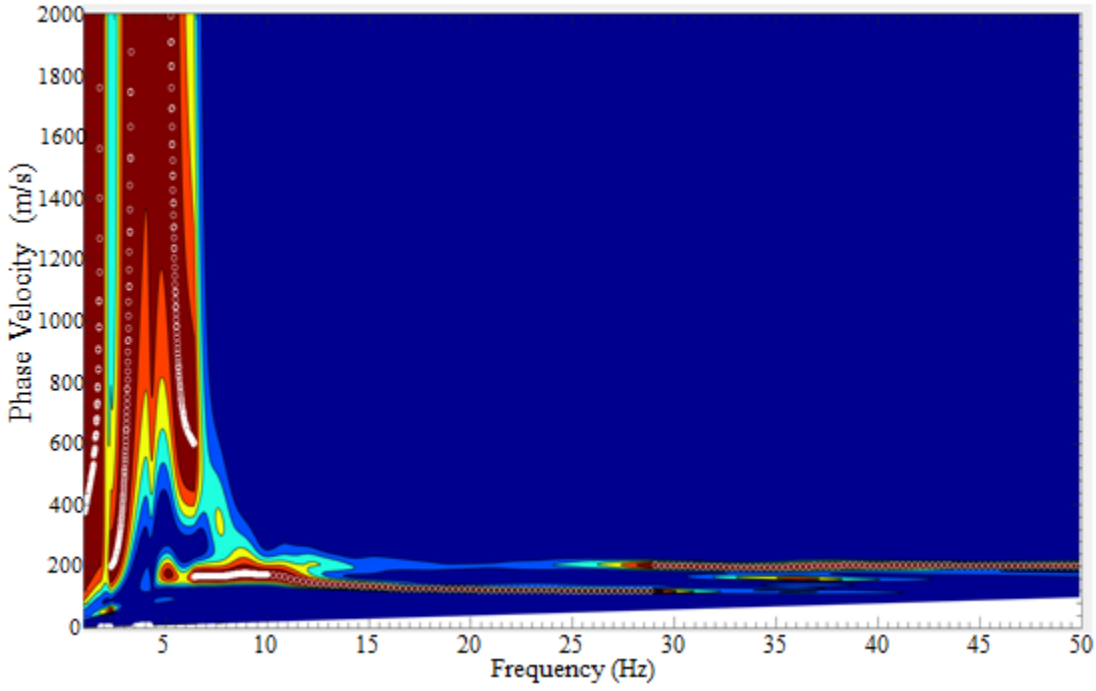
Phase Velocity (m/s)
2000
1800
1600
1400
1200
1000
800
600
400
200
0
5
10
15
20
25
30
35
40
45
50
Frequency (Hz)

(c)

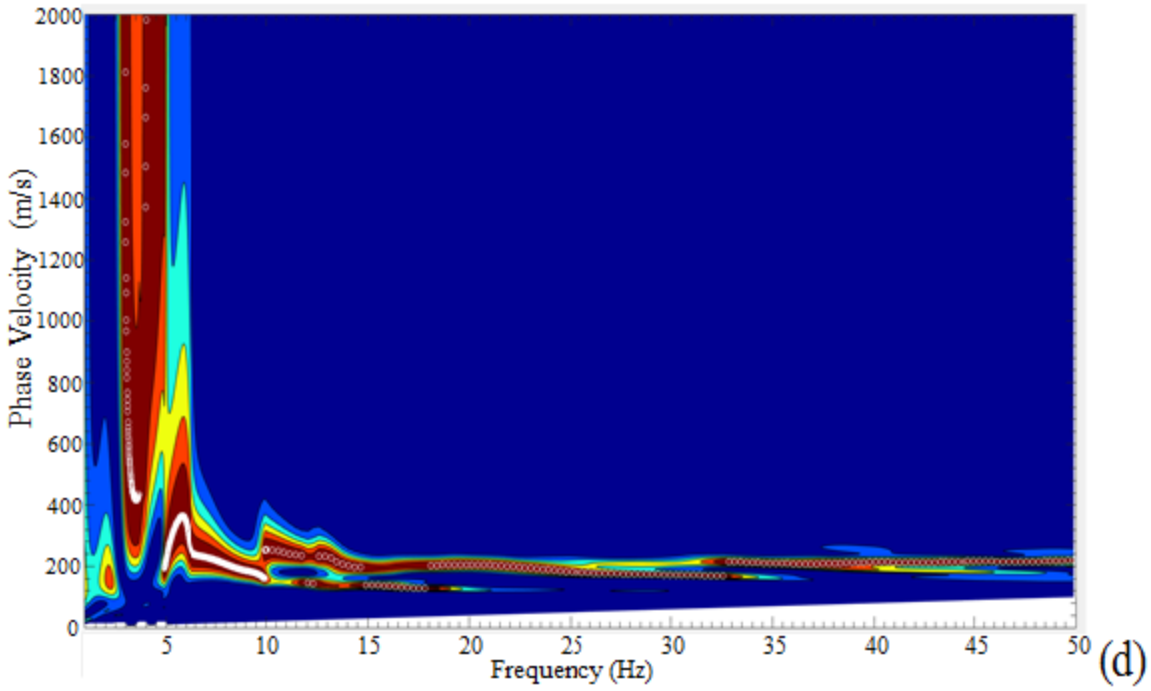

Figure 3. 1: An example of the 3D contour plots with the maximum spectral peak picked at each frequency forming the Rayleigh wave dispersion curve for each source offset: 5 m (a), 10 m (b), 20 m (c), and 40 m (d).

In Figure 3.2, an example of the composite dispersion curve for the active-source sledgehammer Rayleigh wave data is shown. The vertical black line in the figure indicates where the uncertainty in the dispersion data increases significantly below 6.5 Hz, which is likely due to low signal-to-noise ratio. Therefore, all dispersion data less than 6.5 Hz were eliminated from the composite dispersion curve prior to binning and averaging the data into a mean dispersion curve. The dispersion data that plots above the lower line of dispersion data is expected to be first higher mode data, whereas, the lower data is expected to be fundamental mode Rayleigh wave dispersion data.

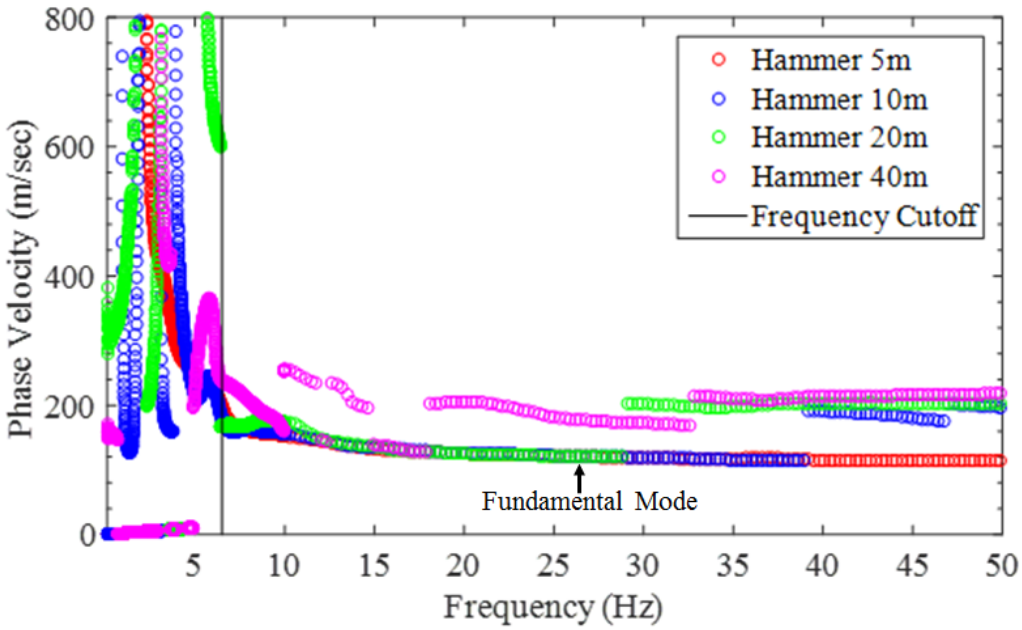

Figure 3. 2: Active-source Rayleigh wave dispersion data from an example site. Dispersion data less than approximately 6 Hz were eliminated (left to the vertical black line). The dispersion data at the lower line, ranging from 10-50 Hz are expected to be the fundamental mode Rayleigh wave dispersion data. The dispersion data above the fundamental mode data are expected to be the higher mode.

3.2.2 P-Wave refraction data processing collected using a sledgehammer source

The P-wave refraction data was processed following the Redpath (1973) method. Time series averaged from 10 blows with the sledgehammer at a 2 meter source-offset were processed to identify the P-wave arrival, at each receiver offset, as a function of time. These time records were analyzed in a 'waterfall' plot as shown in Figure 3.3, which was used to identify the arrival time at each receiver. The red circles show the picks of the P-wave arrivals and the black lines are linear fits through the points at what appear to be layers with the intersection of these lines representing the location of the layer interface. The slopes of the lines are equivalent to the P-wave velocity (V_p) of the layers (e.g., upper soil layer and the water table). The critical distance and intercept time methods are used to estimate the depth to the water table (line of saturation), which is approximately 6.5 meters deep at this site.

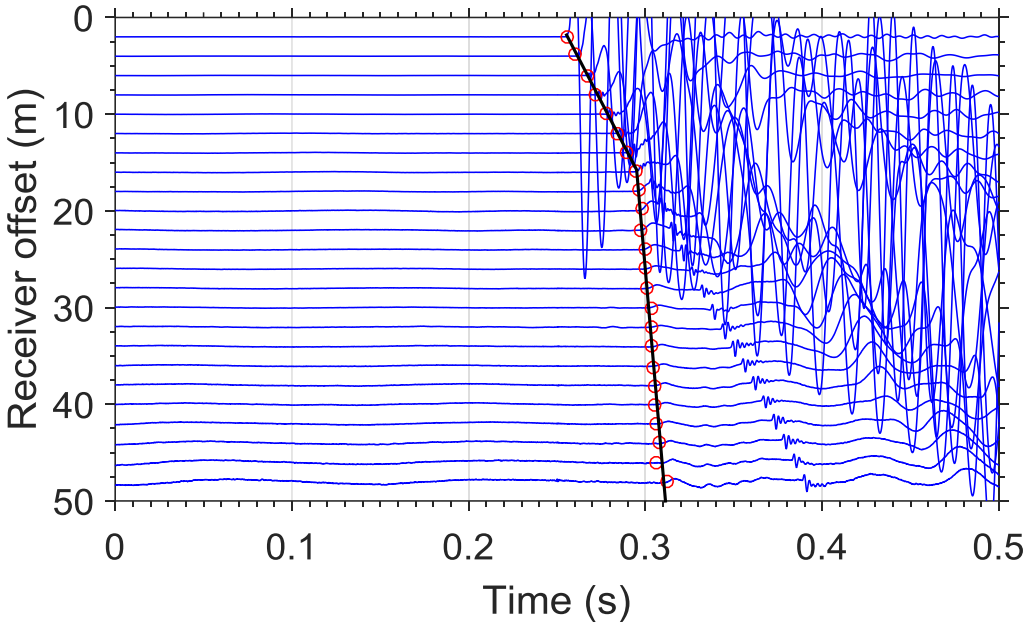

Figure 3. 3: An example of a waterfall plot of P-wave arrivals at each receiver. The red circles show the picks of the P-wave arrivals and the black lines are linear fits through the points at what appear to be layers with the intersection of these lines representing the location of the layer interface.

3.2.3 Love wave surface wave processing utilizing a sledgehammer source

The Love wave sledgehammer data was processed using the same methods as the Rayleigh wave sledgehammer data processing (FDBF). However, the Love wave data was used to develop a separate dispersion curve. An example of the 3D plots for each source offset are provided in Figure 3.4. In Figure 3.5 an example of the composite dispersion curve for the active-source sledgehammer Love wave data is shown. The vertical black line in the figure shows where the uncertainty in the dispersion data, less than approximately 6 Hz, increased significantly at this location likely due to low signal-to-noise ratio.

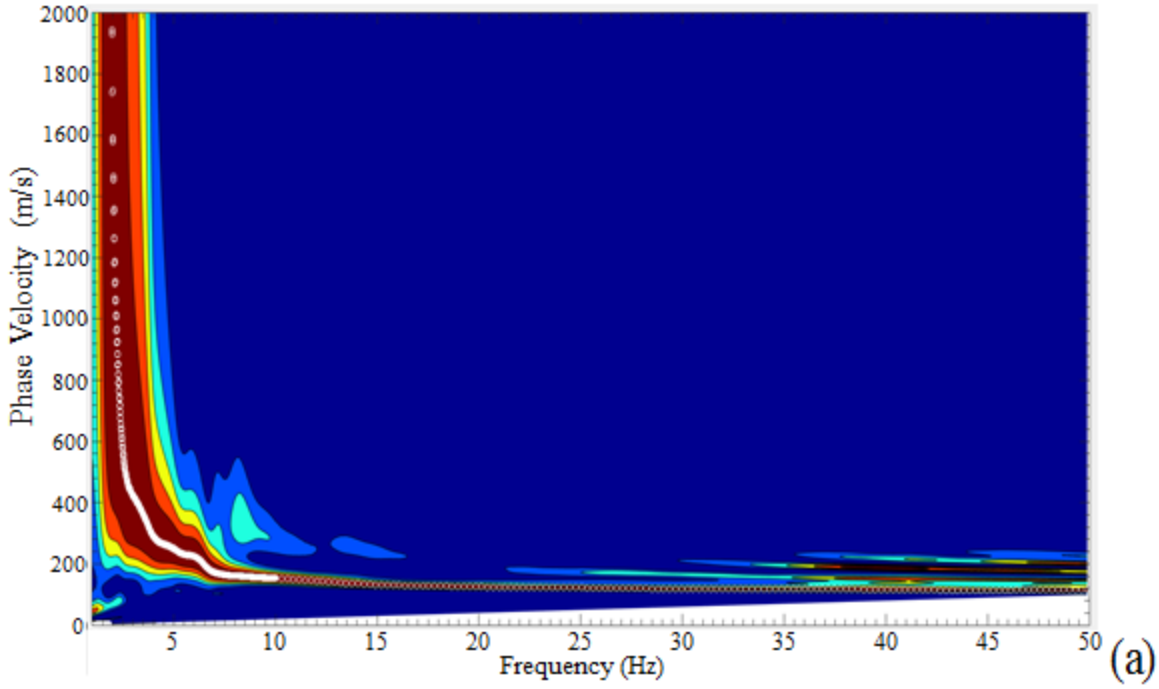
Phase Velocity (m/s)
2000
1800
1600
1400
1200
1000
800
600
400
200
0
5
10
15
20
25
30
35
40
45
50
Frequency (Hz)

(a)

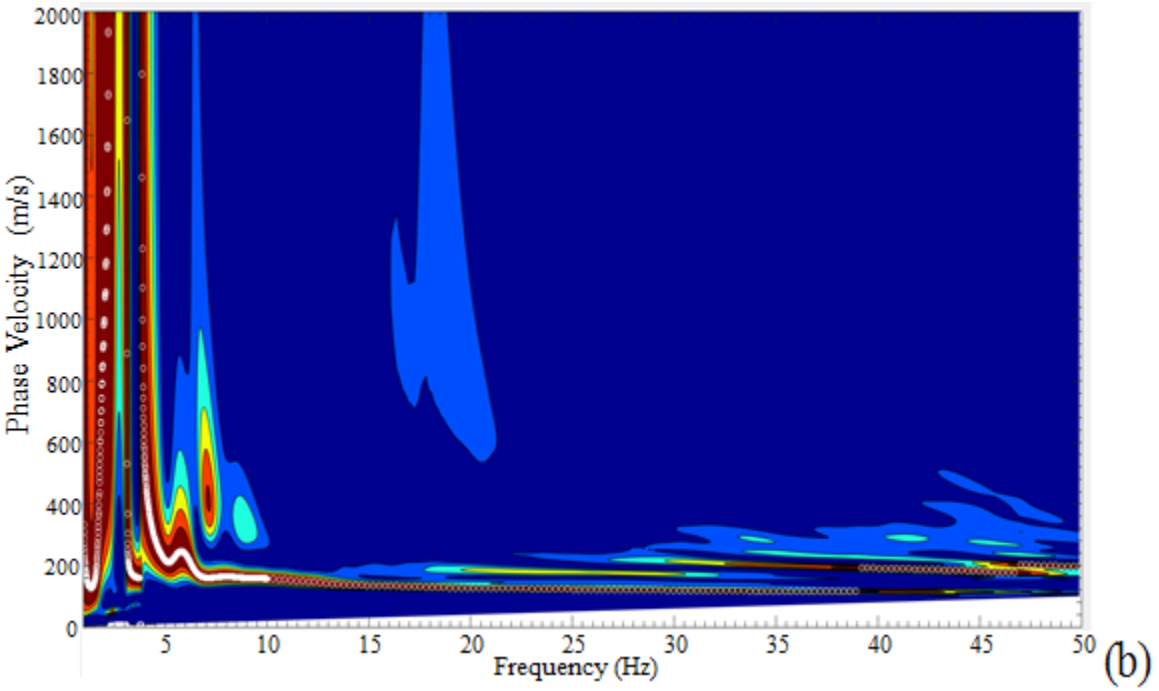
Phase Velocity (m/s)
2000
1800
1600
1400
1200
1000
800
600
400
200
0
5
10
15
20
25
30
35
40
45
50
Frequency (Hz)

(b)

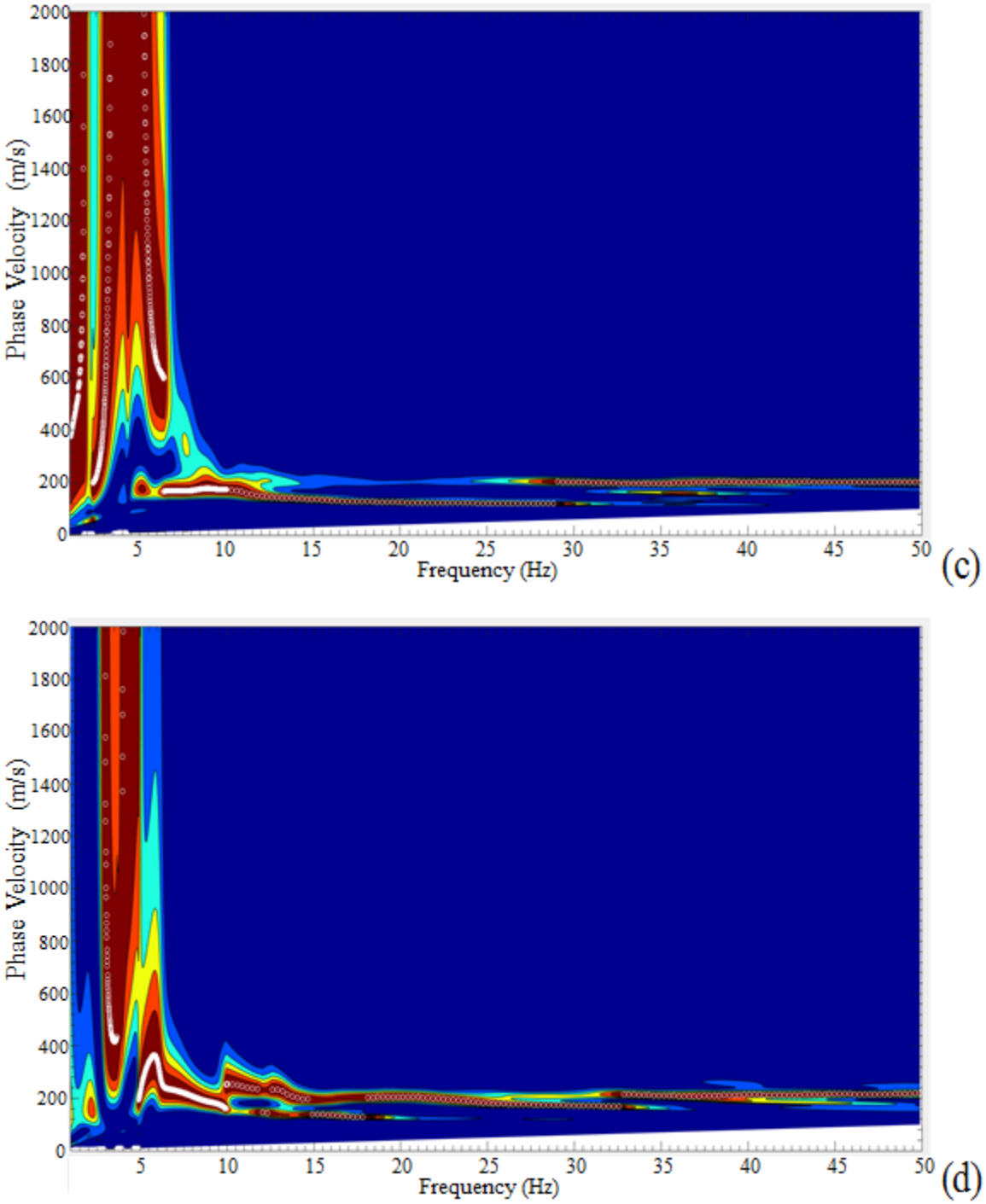

Figure 3. 4: An example of the 3D contour plots with the maximum spectral peak picked at each frequency forming the Love wave dispersion curve for each source offset: 5 m (a), 10 m (b), 20 m (c), and 40 m (d).

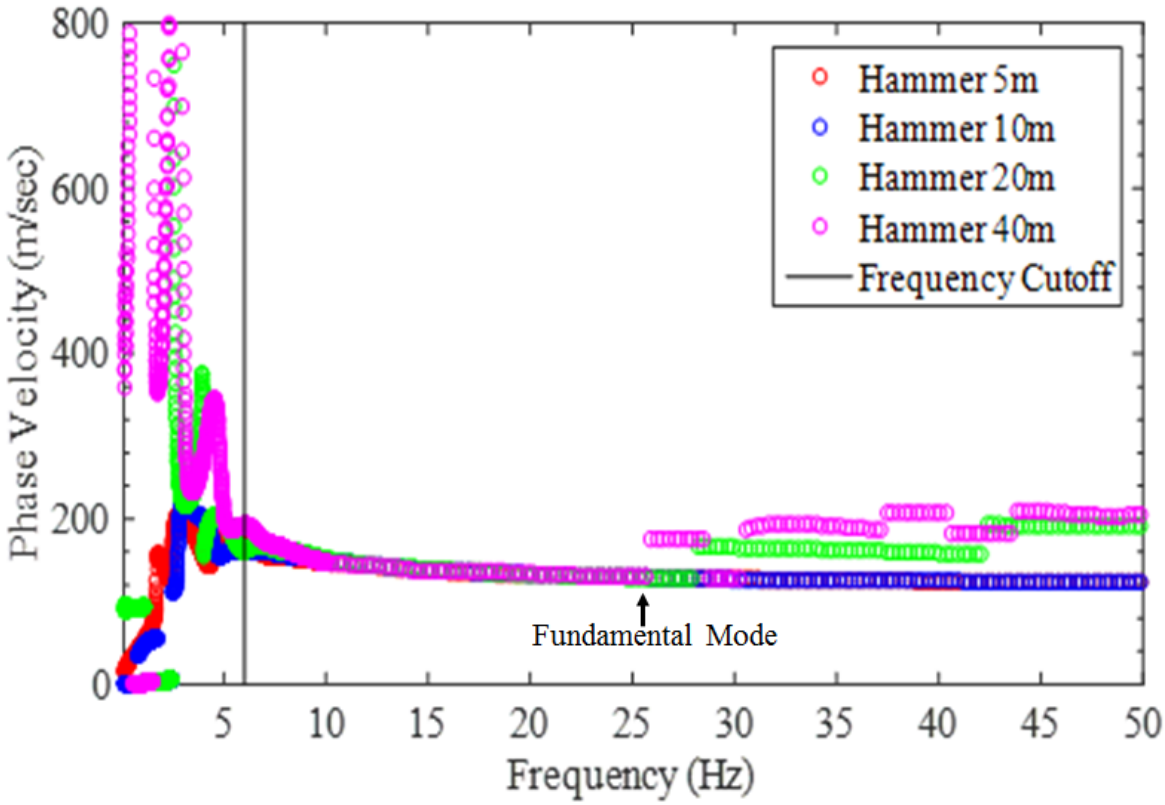

Figure 3. 5: Active-source Love wave dispersion data from an example site. Dispersion data less than approximately 6 Hz were eliminated (to the left of vertical black line). The dispersion data at the lowest line, ranging from 6-50 Hz are expected to be fundamental mode Love wave data. The dispersion data above the fundamental mode are expected to be the higher mode Love wave dispersion data.

3.2.4 Rayleigh wave surface wave processing utilizing a Vibroseis source

The Rayleigh wave Vibroseis data were processed using the FDBF method (Zywicki 1999) combined with the multiple source-offset technique for identifying near-field contamination and quantifying dispersion uncertainty (Cox and Wood 2011). For each source offset (5, 10, 20 and 40 m), dispersion data were generated for the vibroseis source. The maximum spectral peak was automatically picked from the 3D contour plots (Figure 3.6) for each frequency. The individual dispersion data from each offset were combined to form a composite dispersion curve.

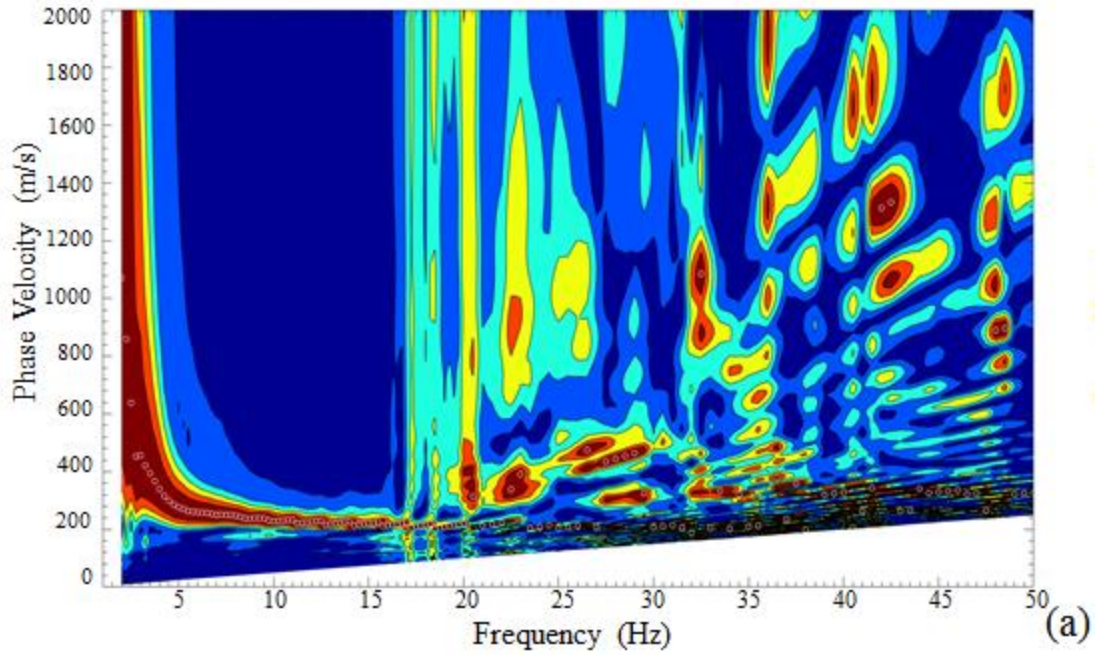
Phase Velocity (m/s)
2000
1800
1600
1400
1200
1000
800
600
400
200
0
5
10
15
20
25
30
35
40
45
50
Frequency (Hz)

(a)

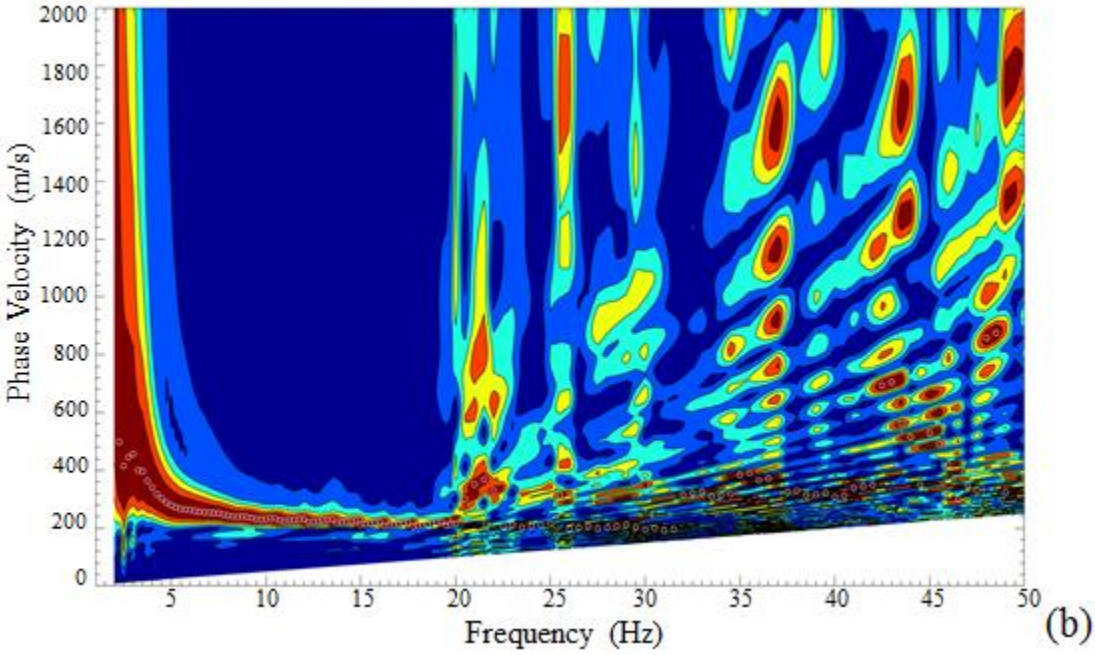
Phase Velocity (m/s)
2000
1800
1600
1400
1200
1000
800
600
400
200
0
5
10
15
20
25
30
35
40
45
50
Frequency (Hz)

(b)

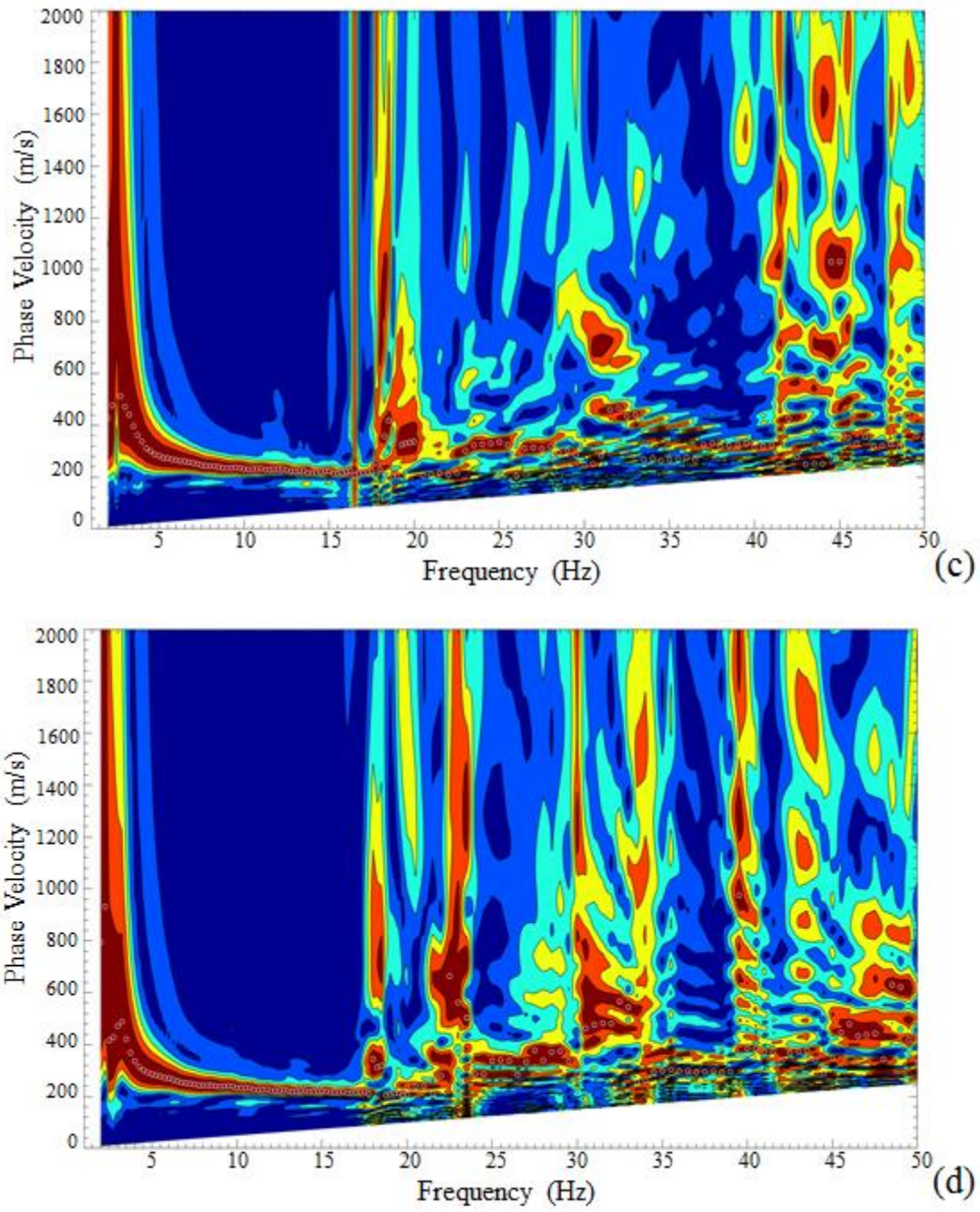

Figure 3. 6: An example of 3D contour plots with the maximum spectral peak picked at each frequency forming the Rayleigh wave dispersion curve for each source offset: 5 m (a), 10 m (b), 20 m (c), and 40 m (d) of the Vibroseis data.

For the composite curve, unlike the sledgehammer data, near field effects did not impact the resulting composite dispersion curve significantly. In other words, the uncertainty in the low

frequency data range below 5-7 Hz was lower than the sledgehammer data. In fact, for some sites there were no data that had to be eliminated in the low frequency range. The sledgehammer data were used to clearly identify the fundamental mode to approximately 50 Hz and in some cases identify first higher mode energy to 50 Hz. However, for the vibroseis data, as can be seen in Figure 3.7, there was significant variation in the data. The energy being input at these frequencies was not very consistent and resulted in waves at some higher frequencies propagating at higher modes. Figure 3.7 is the composite dispersion curve from the vibroseis data. As shown, the dispersion data from 30 to 50 Hz were clouded with the higher mode data with a large uncertainty. Therefore, this data was considered unreliable and eliminated from the composite dispersion curve. The remaining composite experimental dispersion curve was divided into 50 frequency bins distributed evenly on a log scale between 1 to 100 Hz. For each bin, the mean phase velocity and standard deviation were calculated forming the mean dispersion curve for the vibroseis active-source Rayleigh wave data.

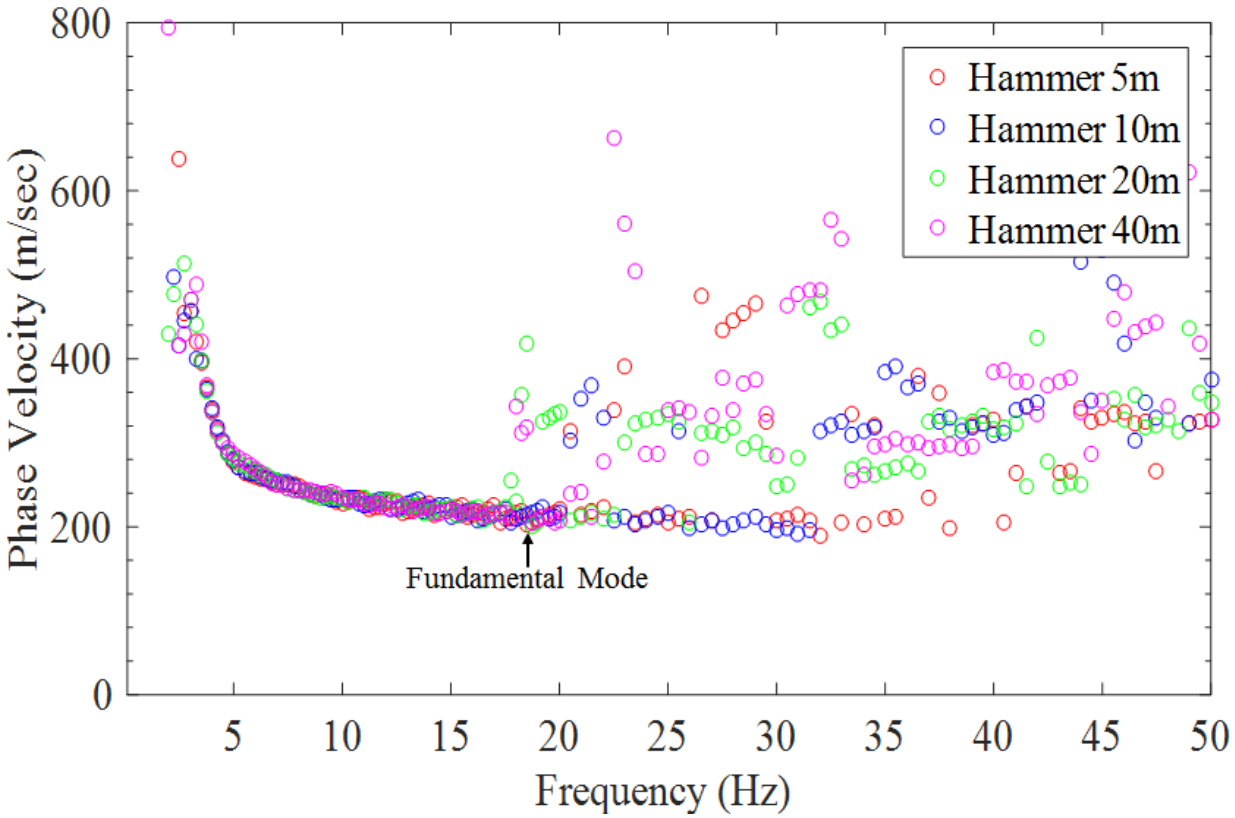

Figure 3. 7: Active-source vibroseis Rayleigh wave dispersion data for an example site. The dispersion data at the lowest line, labelled as the fundamental mode is the expected fundamental dispersion data. The dispersion data points above the fundamental data are higher mode dispersion data.

3.3 L-Array Passive-Source Dispersion Data Processing

The microtremor array measurements (MAM) collected with the ambient-wavefield L-shaped array, were processed using two methods: the conventional frequency-wavenumber (f-k) method (Kelly 1967 and Harjes and Henger 1973) and the high-resolution frequency-wavenumber (HRFK) method (Capon 1969). The L-shaped array was constructed using only vertical geophones which were effective in capturing Rayleigh waves. However, no love wave data were recorded using the L-array.

3.3.1 L-Array f-k Processing

The f-k method was used to process the L-Array data in the Geopsy software suite (www.geopsy.org). In Geopsy, the time records were divided into 60 second time windows. Within each time window, 125 frequency bands were processed based on a log distribution between 0.1 and 20 Hz. For each analysis window and within each frequency bin, a search was performed in the wavenumber domain to attempt to find the phase velocity of the most evident and/or highest energy wave. In other words, the x and y wavenumber pair that resulted in the highest power output in the 2D wavenumber spectrum were selected at each frequency band, representing the Rayleigh wave velocity. Three spectral peaks (or three x and y pairs) within the wavenumber spectrum were chosen to allow the possibility of resolving higher modes for the inversion. For each time window, the phase velocity was calculated at each frequency. The dispersion data for all time windows were then joined together to form a composite dispersion curve. The mean phase velocity and standard deviation were calculated for 125 frequency bins spaced on a log scale from the composite dispersion curve to form a mean Rayleigh wave dispersion curve for the inversion.

3.3.2 L-Array HRFK Processing

The 2D HRFK method was also used to process the L-Array data along with the f-k method. The HRKF method is similar to the conventional f-k method and the set up in Geopsy (www.geopsy.org) for processing is essentially identical. The time records were divided into 60 second time windows. Within each time window, 125 frequency bands were formed on a log distribution between 0.1 and 20 Hz. The x and y wavenumber pair that resulted in the highest power output in the 2D wavenumber spectrum were selected at each frequency band, representing the Rayleigh wave velocity. Three spectral peaks (or three x and y pairs) within the wavenumber spectrum were chosen to allow the possibility of resolving higher modes for the inversion. For each time window, phase velocity was calculated at each frequency. The dispersion data for all time windows were then joined together to form a composite dispersion curve. The mean phase velocity and standard deviation were calculated in 125 frequency bins spaced on a log scale from the composite dispersion curve to form a mean Rayleigh wave dispersion curve for the inversion.

3.4 Circular Array Passive-Source Dispersion Data Processing

The microtremor array measurements (MAM) collected with the ambient-wavefield circular arrays, were processed using three methods: the conventional frequency-wavenumber (f-k) method (Kelly 1967 and Harjes and Henger 1973), the high-resolution frequency-wavenumber (HRFK) method (Capon 1969), and the modified spatial autocorrelation (MSPAC) method (Bettig el al. 2001). Since the broadband seismometers used in the circular arrays were three component seismometers, vertical and horizontal wave propagation were recorded. Therefore, both Rayleigh and Love wave data could be resolved from the circular array data sets using applicable methods.

3.4.1 Circular Array f-k Processing

Rayleigh and Love wave data were computed from the noise records from each of the circular arrays (50, 200, 500, 1000 (where applicable) meter diameter) vertical and horizontal components respectively using the standard f-k approach. The Rayleigh wave data were processed separately from the Love wave data as the two wave types have distinct relationships to shear wave velocity. In Geopsy (www.geopsy.org) the time records were divided into 180 second windows. The time windows were sampled between 0.1 to 20 Hz into 125 log spaced frequency samples. The Rayleigh or Love phase velocity x and y wavenumber pairs that resulted in the highest power output in the 2D wavenumber spectrum were selected at each frequency automatically by the Geopsy f-k toolbox. The dispersion data for all windows were combined to form the dispersion curve for an individual array.

The individual dispersion curves from each array were plotted together to form a singular composite dispersion curve. The dispersion curves from each array were then compared to identify locations where the dispersion curves significantly deviated from the composite trend of all arrays. Those dispersion points that deviated from the primary trend were considered effective mode data and were eliminated from the composite curve since the inversion algorithm cannot utilize effective mode data. Dispersion points outside of the array resolution limit (determined using the array response function in Geopsy; Wathelet *et al.*, 2008, i.e., those points with wavenumbers less than half the resolvable wavenumber $k_{min}/2$), were removed for the 200 and 50 meter arrays. For the 500 and 1000 meter arrays some data were allowed outside of the array resolution limit, for comparison purposes.

3.4.2 Circular Array HRFK Processing

The HRFK approach was used to compute Rayleigh and Love wave dispersion data from the noise recoded by each of the circular arrays (50, 200, 500, 1000 (where applicable) meter diameter) vertical and horizontal components, respectively. The Rayleigh wave data were processed separately from the Love wave data as the two wave types have distinct relationships to shear wave velocity. Prior to the HRFK processing, 180 second windows were selected over the time record for each array, to include the possibility for uncertainty analysis. For each time window, peak

wavenumber x and y pairs were selected at 125 frequency samples spaced on a log distribution between 0.1 and 20 Hz. Dispersion points outside of the array resolution limit (determined using the array response function in Geopsy; Wathelet *et al.*, 2008 i.e., those points with wavenumbers less than half the resolvable wavenumber $k_{min}/2$), were removed. Each array was processed independently and then combined to form a composite dispersion curve (Figure 3.8) from the 1000 (for applicable sites), 500, 200 and 50 meter arrays. Once compiled, the composite curve, was separated into 125 bins on a log scale between 0.1 and 20 Hz. For each bin, the mean phase (Rayleigh or Love) velocity and standard deviation were calculated.

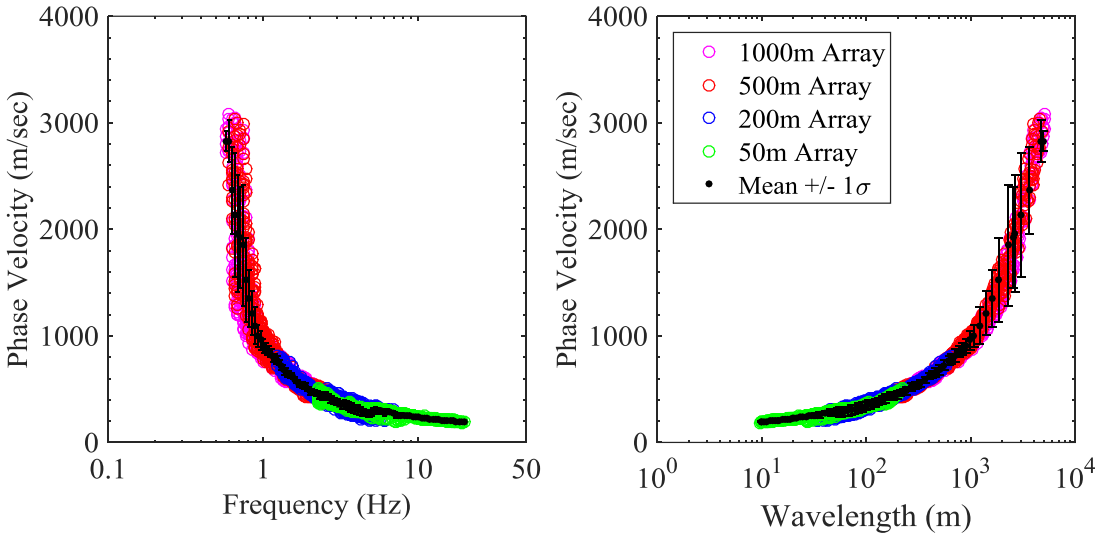

Figure 3. 8: An example of HRFK Rayleigh wave dispersion data from each of the applicable array diameters (500 (red), 200 (blue), and 50 (green) meter) for an example site. The mean and plus or minus standard deviation for each bin is shown as the black error bars.

3.4.3 Modified Spatial Auto-Correlation Processing

The modified spatial auto-correlation (MSPAC) method was used to develop Rayleigh dispersion data from microtremor array measurements recorded in the circular arrays. There are currently no established methods for processing Love wave data using the MSPAC method. MSPAC is a modification of the original SPAC method, which divides receiver pairs into sets of circular sub-arrays or rings. For each ring, an average auto-correlation value is calculated to allow for the processing of imperfect circles (Bettig el al. 2001). For the older SPAC approach, receiver pairs were required to have a constant radius (i.e. be perfect circles) from which the phase velocity over a range of frequencies was computed from spatially (azimuthally) averaged auto-correlation ratio.

For each array, the receiver pairs were split into five rings. The spatial auto-correlation data from these rings were then used in Geopsy (www.geopsy.org) to create a 3D histogram. The auto-correlations were developed by dividing the time records into 180 second time windows before

processing. Auto-correlation values were then calculated for each of the 125 frequency bins spaced on a log scale from 0.1 to 10 Hz for each time widow. Manual selection of the middle (average) and upper- and lower-bound phase velocities were made from the histograms over the applicable frequency ranges for each array diameter. The resulting dispersion curves with associated uncertainty were resamples between 0.1 and 10 Hz on a log scale into 125 sample bins. The MSPAC dispersion curves for each array diameter (Figure 3.9) individually contributed to the final dispersion curve and were not averaged into one composite MSPAC curve.

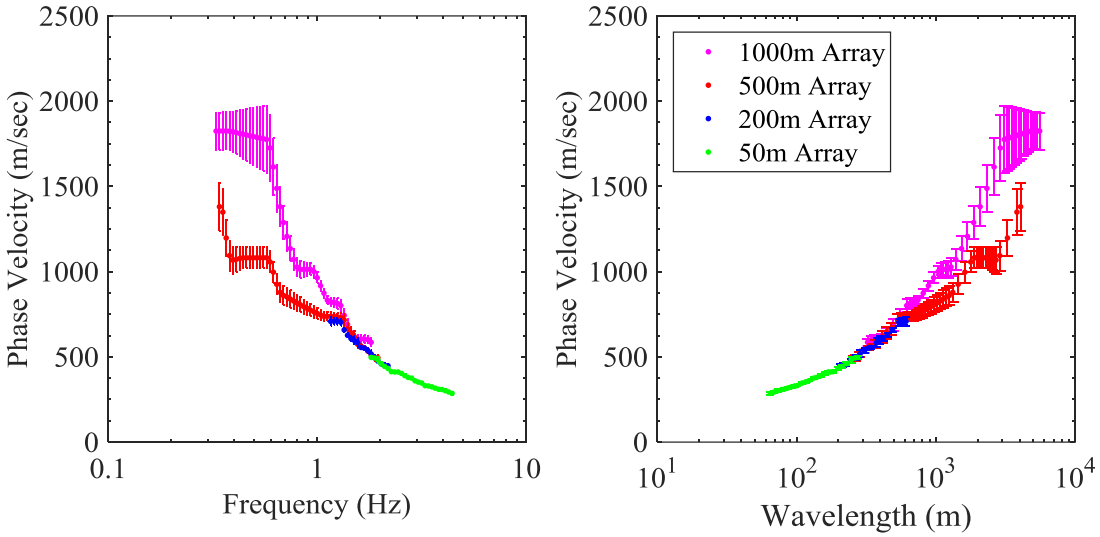

Figure 3. 9: An example of MSPAC Rayleigh wave dispersion data from each of the applicable array diameters (1000 (magenta), 500 (red), 200 (blue), and 50 (green) meter). The mean and plus or minus standard deviation of each bins is shown as the appropriately colored error bars for each array diameter.

3.5 Horizontal-to-Vertical Spectral Ratio Data Processing

The horizontal and vertical components of ambient wavefield noise collected using the circular arrays were used to calculate a horizontal-to-vertical spectral ratio for each noise record. The ratio is calculated by first computing the spectral response of each time record (V, N-S, E-W) and dividing the squared average of the two horizontal components (North-South and East-West) by the vertical component. General guidelines established by the SESAME project were followed for the processing (SESAME 2004). Similar to the passive-source MAM processing, the time records for each of the ten sensors in the array were broken into 180-second windows. The results from each time window were used to create an average spectral response curve for each array. The peaks within the array represent velocity contrasts where a stiffer layer underlies a softer layer. Typically, the peak at the lowest frequency represents the fundamental period of the site. An example H/V response curve is shown in Figure 3.10 with the measured site period.

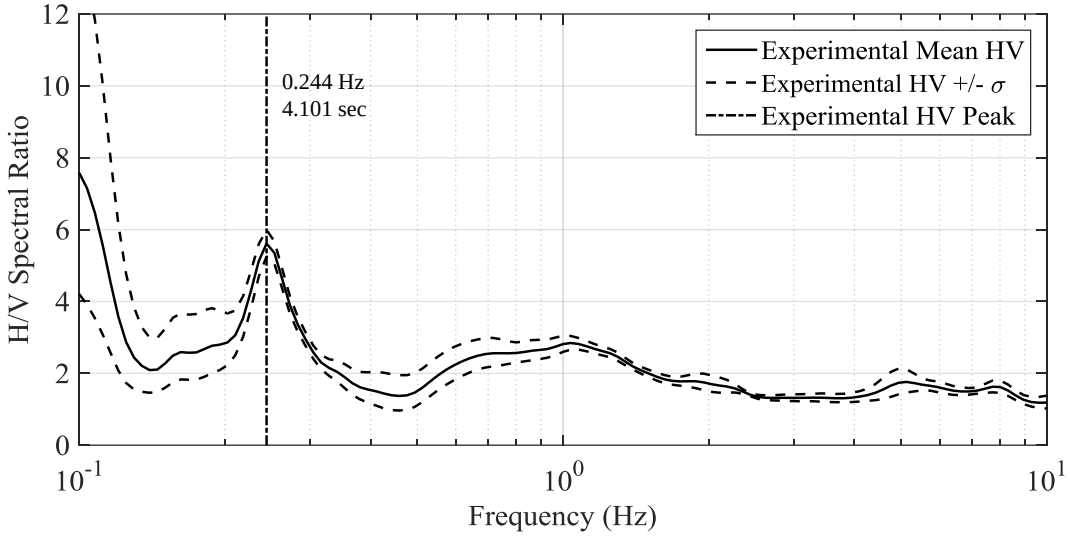

Figure 3. 10: An example horizontal-to-vertical spectral response curve.

3.6 Dispersion Comparison

The dispersion data from the active-source and MAM (f-k, HRFK and MSPAC) methods were combined into a single composite dispersion curve as shown in Figure 3.11. The active source data is over a frequency range generally higher than that of the HRFK and MSPAC data. Likewise, the HRFK data is over a frequency range typically higher than the MSPAC data, but mostly lower than the active data. Whereas, the MSPAC data is effectively the lowest frequency data and typically represents the data of the stiffest and deepest soil layers.

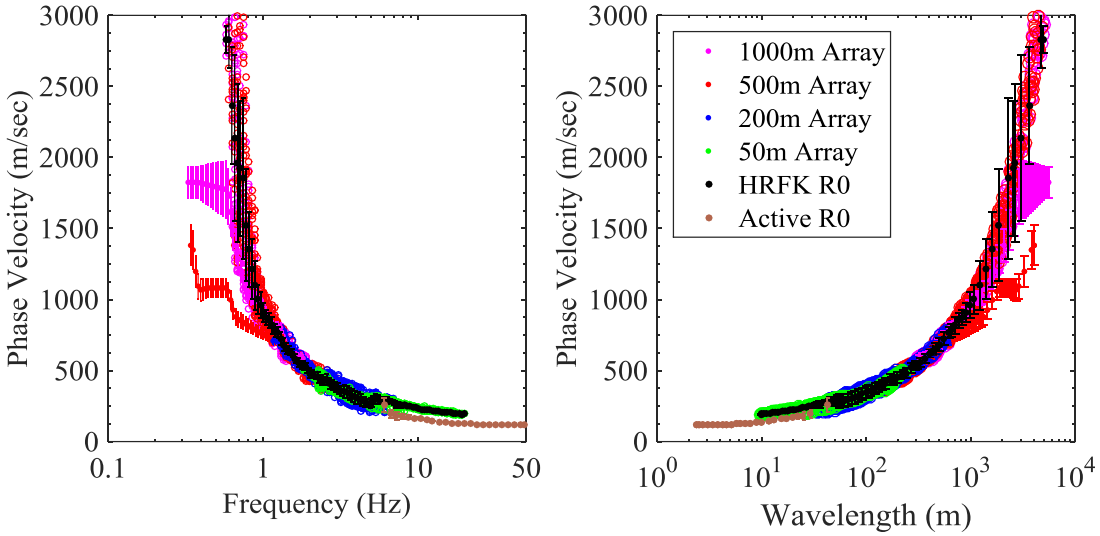

Figure 3. 11: An example of the composite dispersion curve for each of the methods used in this investigation: active-source Rayleigh wave data (Active R0), high-resolution frequency-wavenumber Rayleigh wave data (HRFK R0) and Rayleigh wave data from the modified spatial auto-correlation method (MSPAC) for each array.

At some sites, multiple modes were identified in the dispersion analysis. These higher mode sections of the dispersion curve have a higher velocity than the lower or fundamental mode velocity at the same frequency. Therefore, the higher mode data typically plots above the lower or fundamental mode data. Where the velocity of one section of the curve dips below or rises above the velocity of the general trend of the dispersion curve, this is considered a region of effective mode. Similarly, if the lower mode dispersion curve rises up to the higher mode or the reverse happens this is an area of effective mode. Since the inversion program within Geopsy, Dinver (www.geopsy.org), cannot utilize effective modes these regions must be eliminated. An example of a final composite experimental dispersion curve is provided in Figure 3.12. For this final curve, the dispersion data modes have been clearly identified and labeled as fundamental Rayleigh wave data (R0), first higher mode Rayleigh wave data (R1), and first higher mode Love wave data (L1). No dispersion data of one mode crosses over or converges on the dispersion data of a different mode, which shows that there is likely no effective mode data remaining in the experimental dispersion curve that would interfere with the results of the inversion process.

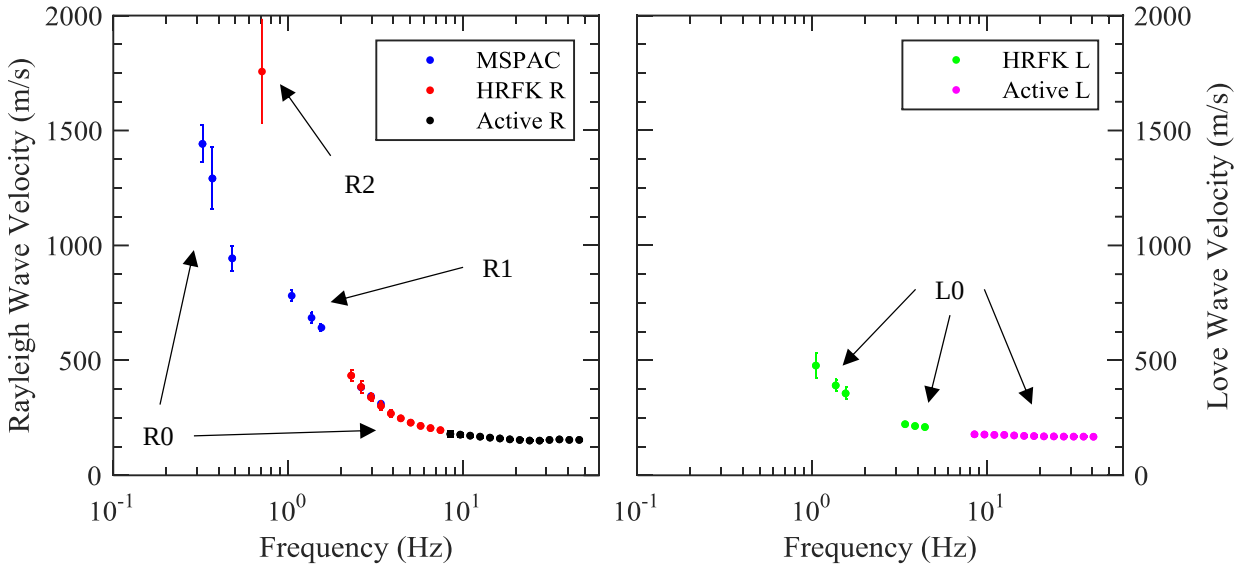

Figure 3. 12: An example of a final composite dispersion curve with any effective mode data eliminated and mode assignments as denoted by the arrows: fundamental Rayleigh wave data (R0), first higher mode Rayleigh wave data (R1), and first higher mode Love wave data (L1).

3.7 Inversion

Geopsy was used to perform a joint inversion of the final composite experimental dispersion curve along with the site period in Dinver (www.geopsy.org) to obtain the shear wave velocity profile for each site. The inversion uses the fundamental site period to help constrain the depth of bedrock and the global stiffness of the velocity model. However, for this study, the bedrock depth for each site were fixed in the inversions to the depths defined by the CUSVM (Ramírez-Guzmán *et al.*, 2012). The CUSVM is a velocity model developed by Ramírez-Guzmán *et al.*, 2012 through a project funded by National Science Foundation. This velocity model includes several urban areas in Arkansas, Tennessee, Kentucky, Missouri and Indiana. Dinver utilizes a neighborhood algorithm, which randomly generates V_s profiles within user defined constraints on velocity (V_s and V_p), depth, Poisson's ratio, density, and the number of layers in the soil profile. To obtain accurate shear wave velocity profiles from the inversion, these constraints must be well defined. The geologic data collection discussed in Chapter 3 was used to develop the parameterization for each site. A well-defined parameterization will be beneficial for Dinver in reducing the generation of erroneous velocity models. For each V_s profile generated, Dinver creates a corresponding theoretical dispersion curve from the generated V_s profile and compares this to the experimental dispersion curve. Dinver computes an overall 'closeness' between the experimental data and the generated theoretical dispersion model, which is known as the misfit. The algorithm Dinver runs on, attempts to minimize this misfit at each point along the experimental dispersion curve.

The process of minimizing the misfit in the velocity model takes many iterations; in this investigation approximately one to two million models were generated for each site. As Dinver generates V_s profiles and their corresponding dispersion curve, the associated misfit is calculated and automatically recorded with the V_s profile and theoretical dispersion curve. A representative sample of the top 1000 best fit velocity profiles and dispersion curves are then exported from Geopsy. A sample of 1000 profiles is considered sufficient to minimize variability in the median V_s profile for the site (Teague *et al.*, 2016). The median V_s for each layer is then computed from the lowest misfit 1000 profiles and is the representative V_s profile for the site, contrary to the idea that the lowest misfit profile is the best fit profile (Teague *et al.*, 2015). An example of the top 1000 V_s profiles, the top 50 V_s profiles, the lowest misfit profile, and the median profile are presented in Figure 3.13. Also included are the velocity constraints on the inversion, the counted five percent and 95 percent velocity intervals, and sigma natural log of the V_s profiles to show the variation in the velocity profiles.

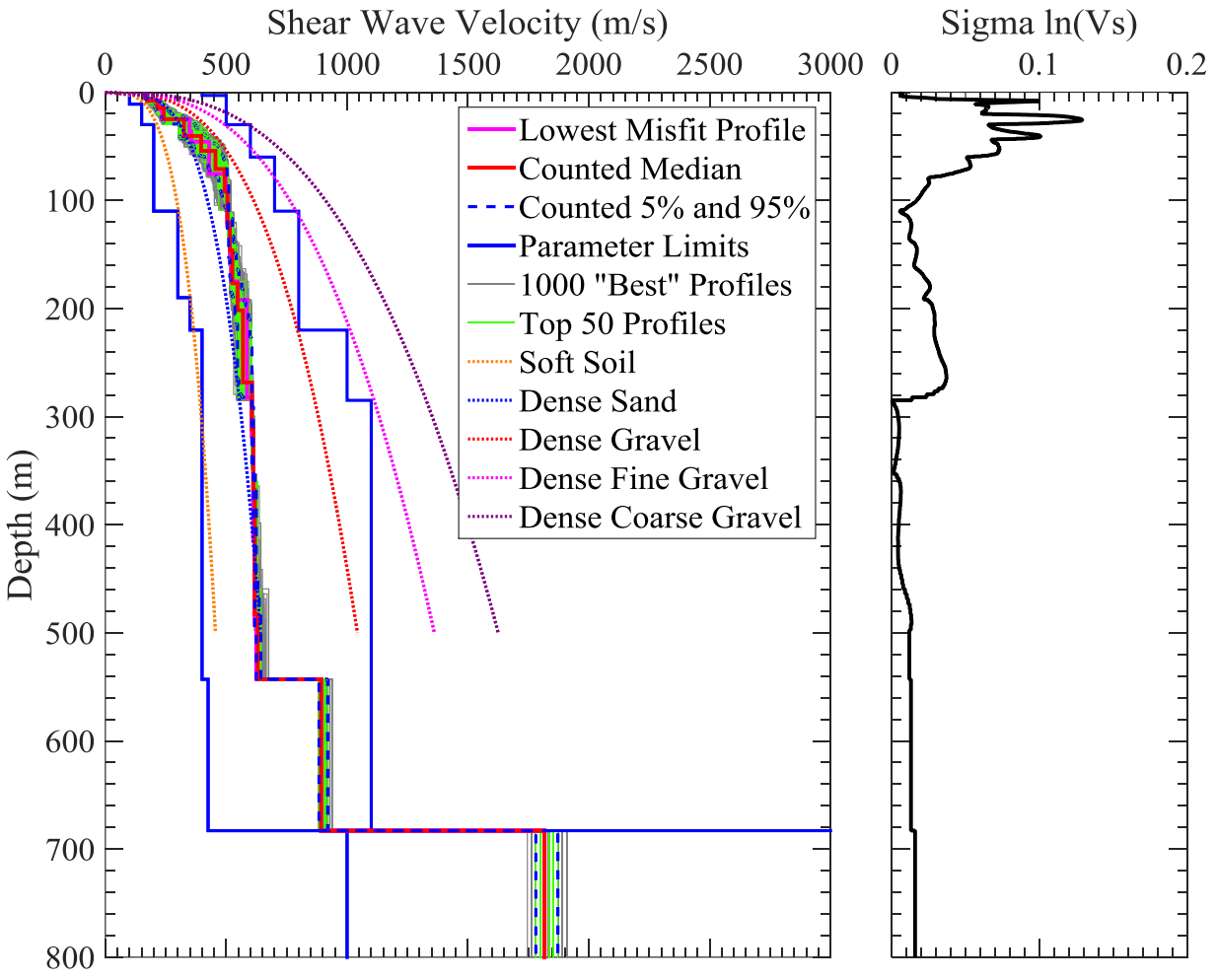

Figure 3. 13: An example of the top 1000 V_s profiles, the top 50 V_s profiles, the lowest misfit profile, and the median profile are presented. Also included are the velocity constraints on the

inversion, the counted five percent and 95 percent velocity intervals, and sigma natural log of the V_s profiles to show the variation in the velocity profiles.

CHAPTER 4
Dynamic Site Characterization Results and 3D Velocity Model

4.1 Introduction

In this chapter, the results of the dynamic site characterization measurements made at each site including the dispersion curves, V_s profiles, and horizontal-to-vertical spectral ratios are discussed. The V_s profiles for the 15 sites are compared across the Embayment to understand trends in the subsurface velocity structure. Finally, the creation of the 3D velocity model of the Mississippi Embayment is presented along with a summary of uncertainty estimation and definition of geologic layer boundaries.

4.2 Results from All Sites

The results of the dynamic site characterization measurements include: (1) experimental dispersion data measured in the field along with theoretical dispersion curves computed from the generated shear wave velocity profiles, (2) horizontal-to-vertical spectral ratio (HVSR) curves computed from the generated shear wave velocity profiles, and (3) shear wave velocity profiles from the inversion.

4.2.1 Dispersion Results

Summarized in Figure 4.1 are the Rayleigh wave experimental and theoretical dispersion data from the inversions for all 15 sites that were part of the study. The sites are organized (a-f) in the figure according to depth of bedrock. Theoretical Rayleigh wave dispersion curves include the 1000 lowest misfit theoretical dispersion curves and the median dispersion curve (calculated from the median of the 1000 lowest misfit V_s profiles). Experimental dispersion data can include fundamental, first higher, and second higher mode data. Effective mode data were eliminated through an iterative inversion process to isolate modes that represent only one mode and are not a combination of modes. A site map showing the location of each site is provided in Chapter 3. Typically, the experimental dispersion data were fundamental mode from 1-3 Hz up to approximately 60 Hz. Lower frequency data (below 1-3 Hz) were typically fundamental or first higher mode data, however, for the Athelstan site (j) the experimental data below 1.5 Hz was second higher mode. Furthermore, most sites had portions of the experimental dispersion data fit by the second higher mode theoretical dispersion curve. The interpretation of the data below 1-3 Hz was particular difficult as assigning the correct mode of propagation was quite complex requiring many iterations during the inversion process.

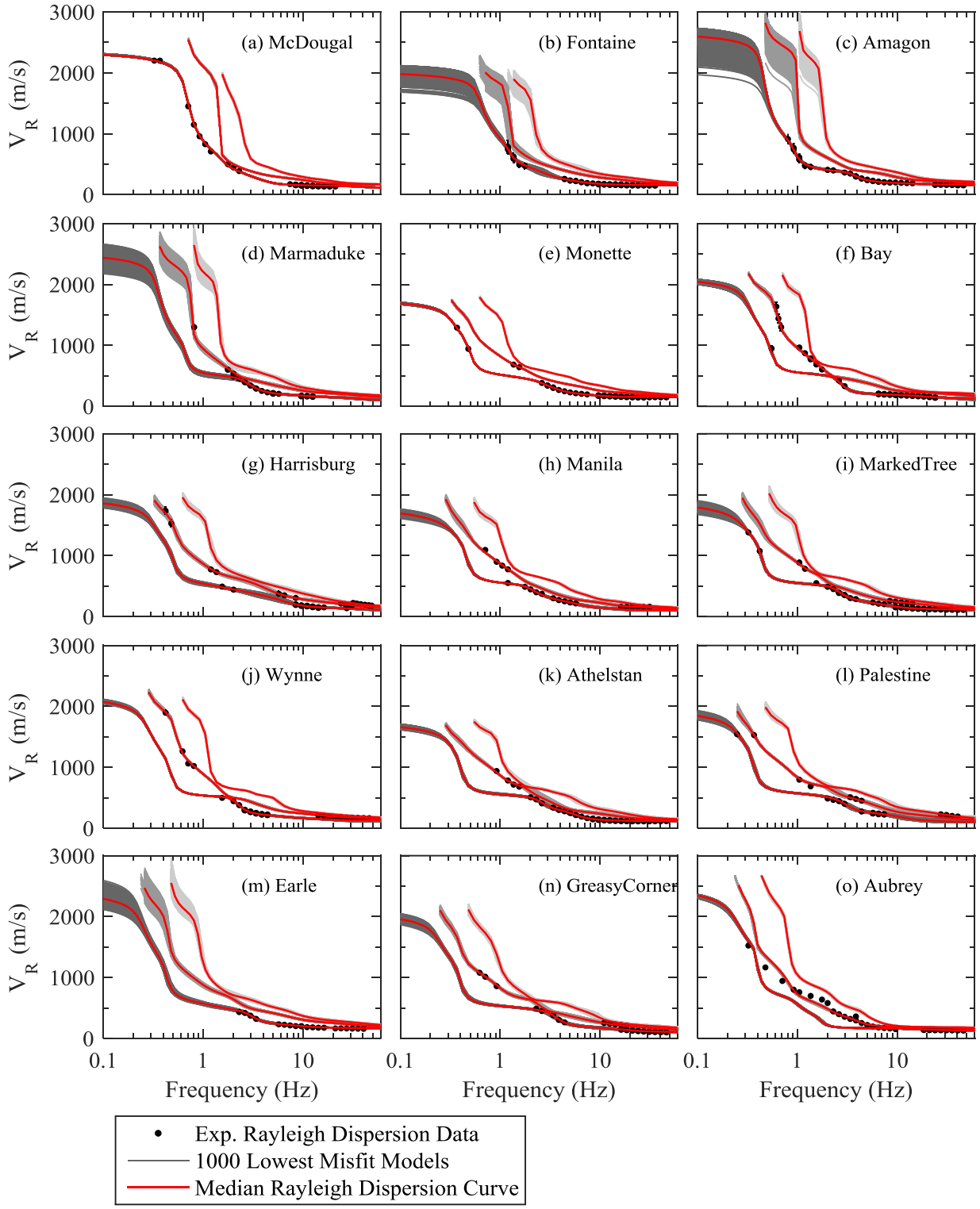

Figure 4. 1: Rayleigh wave dispersion modelling for each site in this study. Experimental dispersion data are compared with the theoretical dispersion models for the median velocity profile and the 1000 lowest misfit V_s profiles. Theoretical models are presented for each mode included in the inversion process.

Summarized in Figure 4.2 are the Love wave experimental and theoretical dispersion data from the inversions for all 15 sites. Theoretical Love wave dispersion curves include the 1000 lowest misfit theoretical dispersion curves and the median dispersion curve (calculated from the median of the 1000 lowest misfit V_s profiles). Experimental dispersion data include fundamental and first higher mode data. Effective mode data were eliminated through an iterative inversion process to isolate modes. For the shallowest sites (a – f), the experimental Love wave data were primarily fit by the fundamental mode theoretical dispersion model or eliminated due to it being an effective mode. For the remaining sites (g – o), at frequencies greater than approximately 1 Hz, the experimental dispersion data were fundamental mode, whereas, the data below 1 Hz typically transitioned to the first higher mode.

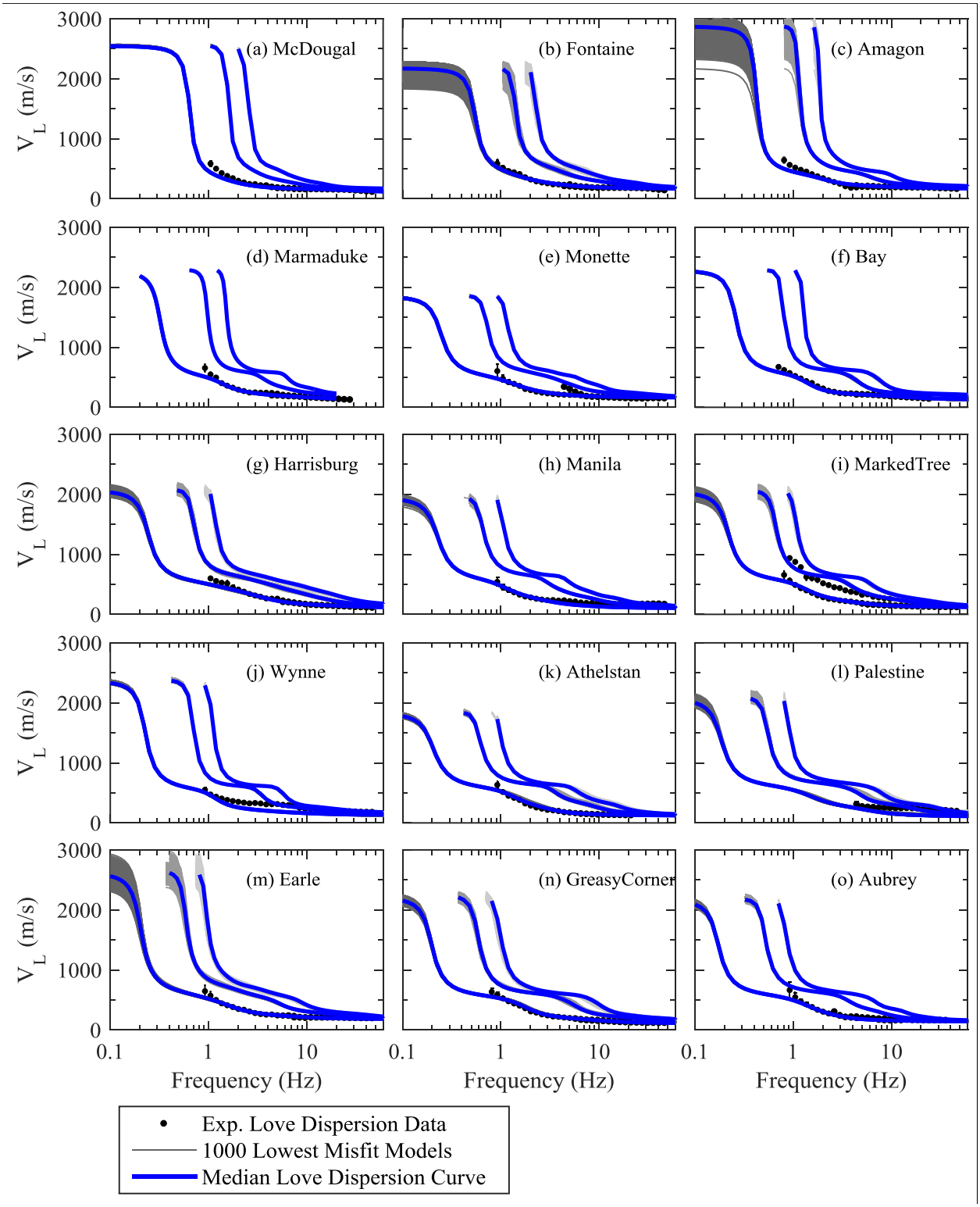

Figure 4. 2: Love wave dispersion modelling for each site in this study. Experimental dispersion data are compared with the theoretical dispersion models for the median velocity profile and the 1000 lowest misfit profiles. Theoretical models are presented for each mode included in the inversion process.

4.2.2 HVSR Curves

Summarized in Figure 4.3 and Table 4.1 are the HVSR experimental and theoretical results from all 15 sites. For each site, the peak spectral ratio and the mean experimental HVSR curve with the associated plus- and minus- one standard deviation bounds of the curve are provided. The theoretical spectral peak and HVSR curve for each site were computed from the median V_s profile. Experimental HVSR curves, corresponding to the ellipticity curve for each site, ranged from 0.188 Hz to 0.614 Hz. The ellipticity peak estimated using the median V_s profile for each site ranged from 0.192 to 0.614 Hz and were each within one standard deviation of and less than 4% different than the mean experimental peaks. In addition to the low frequency peaks, a majority of sites (exceptions: Fontaine and McDougal) have minor peaks or secondary peaks in the experimental data, which meet the criteria for a clear peak per SESAME (2004). These minor peaks may be a factor of odd harmonics or an artifact of a shallow stiff material relative to the overlying soils such as the Memphis sand formation. However, these peaks were not used in the analysis of the sites. Bedrock depth from the CUSVM are also included in Table 4.1 and compared to the experimental HVSR peak in Figure 4.4. Lower HVSR peaks typically correspond to sites with deeper bedrock depth. Furthermore, the bedrock depth and peak HVSR measurements from the Rosenblad *et al.*, 2009 are included for comparison and are in agreement with the northeast Arkansas sites. However, the bedrock depth and HVSR of Rosenblad *et al.*, 2009 range from 586-847 meters and 0.24-0.38 Hz, cover a smaller range than the northeast Arkansas sites. A power-law fit to the northeast Arkansas bedrock depth-fundamental frequency points has been developed as $h=116.268f_0^{-1.355}$, where h is the bedrock depth taken from CUSVM and f_0 is the HVSR peak frequency, i.e., fundamental frequency.

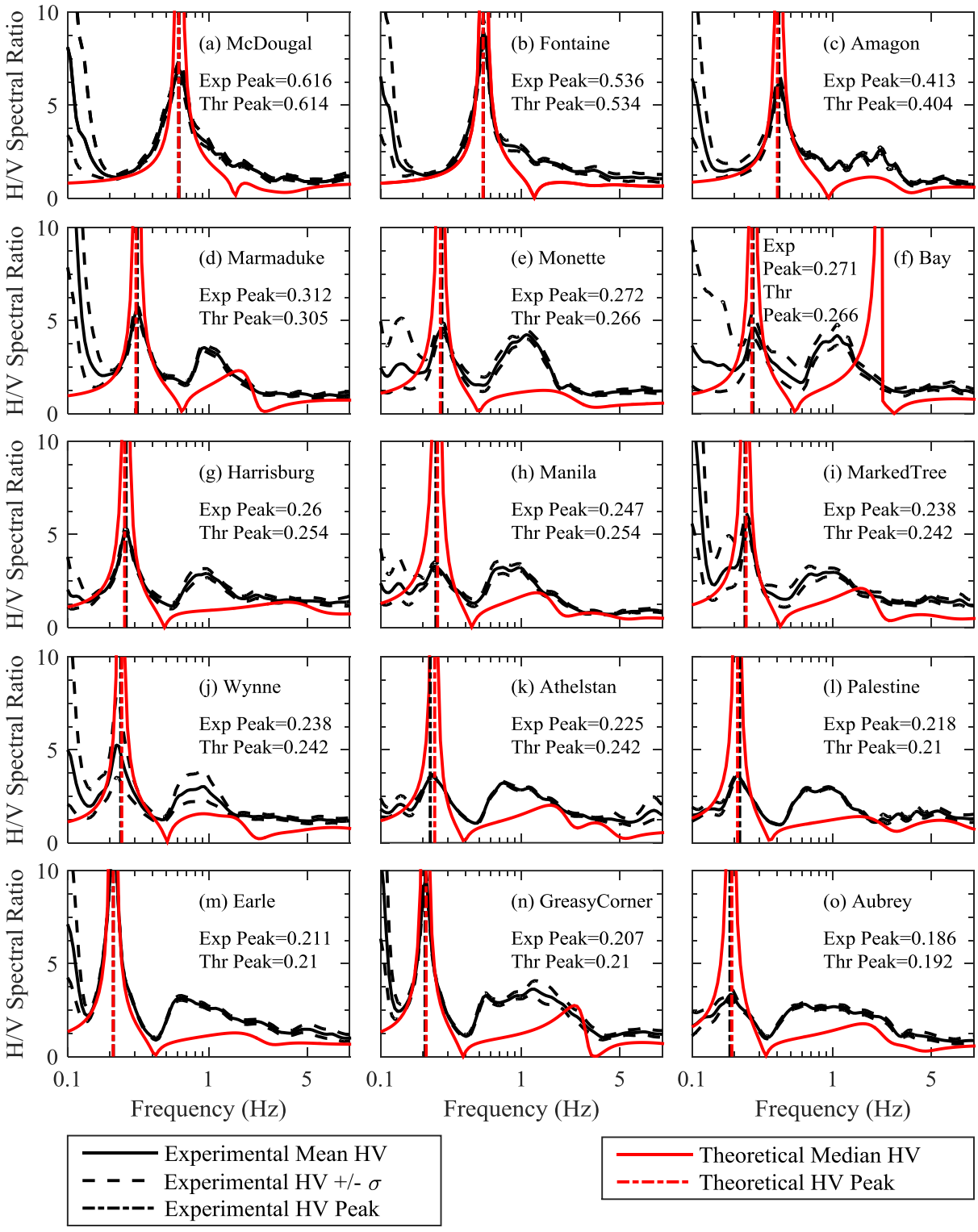

Figure 4. 3: Theoretical HVSR curves generated from the median V_s profile compared to the experimental HVSR curves for each site with associated peaks.

Table 4. 1: Experimental HVSR peak and associated standard deviation (Std), the theoretical peak associated with the ellipticity curve generated from the median of the 1000 lowest misfit Vs profiles, the percent difference between the experimental and theoretical values, and the bedrock depth from the Central United States Velocity Model (Ramirez-Guzman *et al.*, 2012) for each site.

Site Name	Experimental Mean, f_0 (Hz)	Experimental Std (Hz)	Theoretical Median (Hz)	Percent Difference	CUSVM Bedrock Depth, h (m)
McDougal	0.616	0.024	0.614	0.26%	252
Fontaine	0.536	0.008	0.534	0.29%	291
Amagon	0.413	0.012	0.404	2.11%	326
Marmaduke	0.312	0.009	0.305	2.24%	492
Bay	0.271	0.012	0.266	2.05%	587
Monette	0.272	0.020	0.266	2.09%	677
Harrisburg	0.260	0.010	0.254	2.22%	701
Manila	0.247	0.018	0.254	2.96%	813
Marked Tree	0.238	0.011	0.242	1.51%	853
Wynne	0.225	0.008	0.231	2.83%	853
Athelstan	0.238	0.028	0.242	1.69%	858
Palestine	0.218	0.024	0.210	3.86%	958
Earle	0.211	0.004	0.210	0.52%	1018
Greasy Corner	0.207	0.005	0.210	1.26%	1069
Aubrey	0.186	0.025	0.192	3.04%	1114

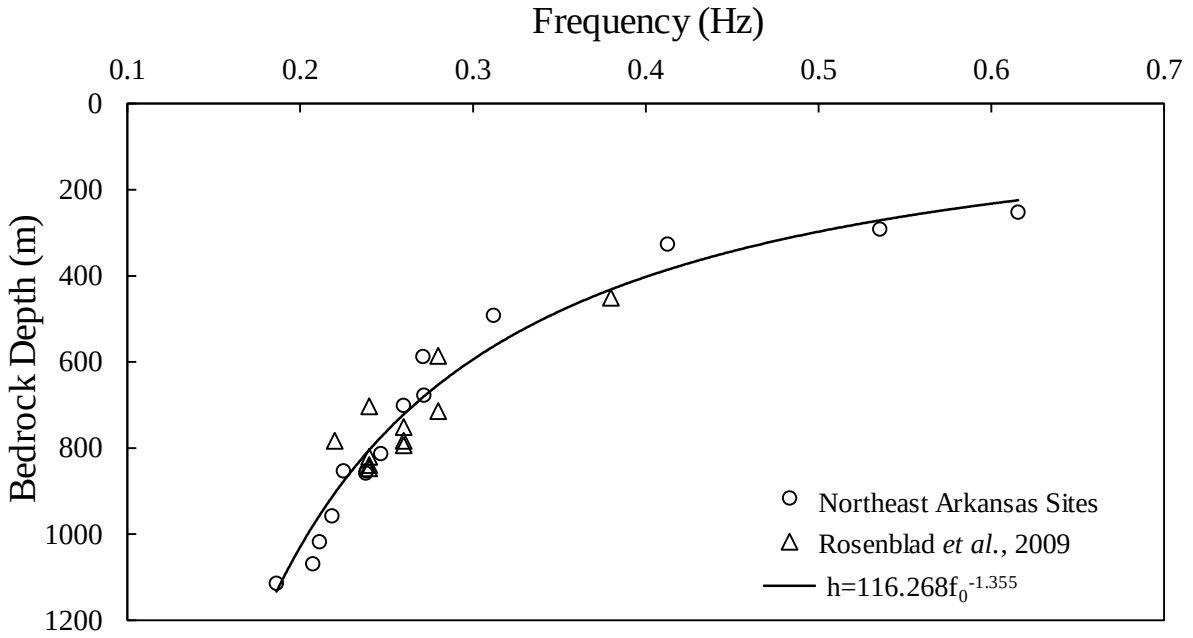

Figure 4. 4: Bedrock depth from the CUSVM compared with the experimental HVSR peak measured at each site.

4.2.3 V_s Profiles

In Figure 4.5, the 1000 lowest misfit V_s profiles are shown with the median V_s profile (V_s and depth for each layer), and the counted 5th and 95th percent confidence intervals at one meter depth increments for the 1000 lowest misfit V_s profiles. The standard deviation on natural logarithm of Vs values are calculated as a mean to observe the change in Vs magnitude. This term would be called σln(Vs) throughout the rest of the report. The variation in σln(Vs) with depth are included adjacent to the set of V_s profiles for each site. Geologic layering from the parameterization created for each site and based on the CUSVM are included for each site. The median V_s profiles for each site are summarized in Table 4.2 and the V_{S30} values are summarized in Table 4.3 with upper and lower bound V_{S30} estimates for each site in this study. V_{s30} values were computed from the median of the 1000 lowest misfit V_s. Median V_{s30} estimates ranged from 197 m/s - 250 m/s for the 15 sites. The median V_{S30} estimates had a standard deviation (5% and 95% estimates) of between 5-10% with only few sites being between 10-20%. Various building design codes (e.g. NEHRP) separate sites into classes for earthquake engineering design based on the V_{S30}, which is the time average Vs over the top 30 meters.

The bedrock depth at sites in this study ranged from 250 meters to over 1100 meters with the shallow sites located toward the eastern portion of the Embayment and the deeper sites located toward the Mississippi River on the western side of the state similar to bedrock maps by Dart (1995) and Ramírez-Guzmán *et al.,* (2012). Bedrock at each site is typically characterized by a

sharp increase in V_s and σln(Vs) (See Figure 4.5). Median bedrock velocity ranged 1800 m/s to 2800 m/s, with an average velocity of 2200 m/s across all sites. These estimates for Paleozoic bedrock V_s are consistent with estimates from the literature although there is certainly variability in the estimates (Romero and Rix 2005, Rosenblad and Goetz 2009, Ramirez-Guzman *et al.*, 2012).

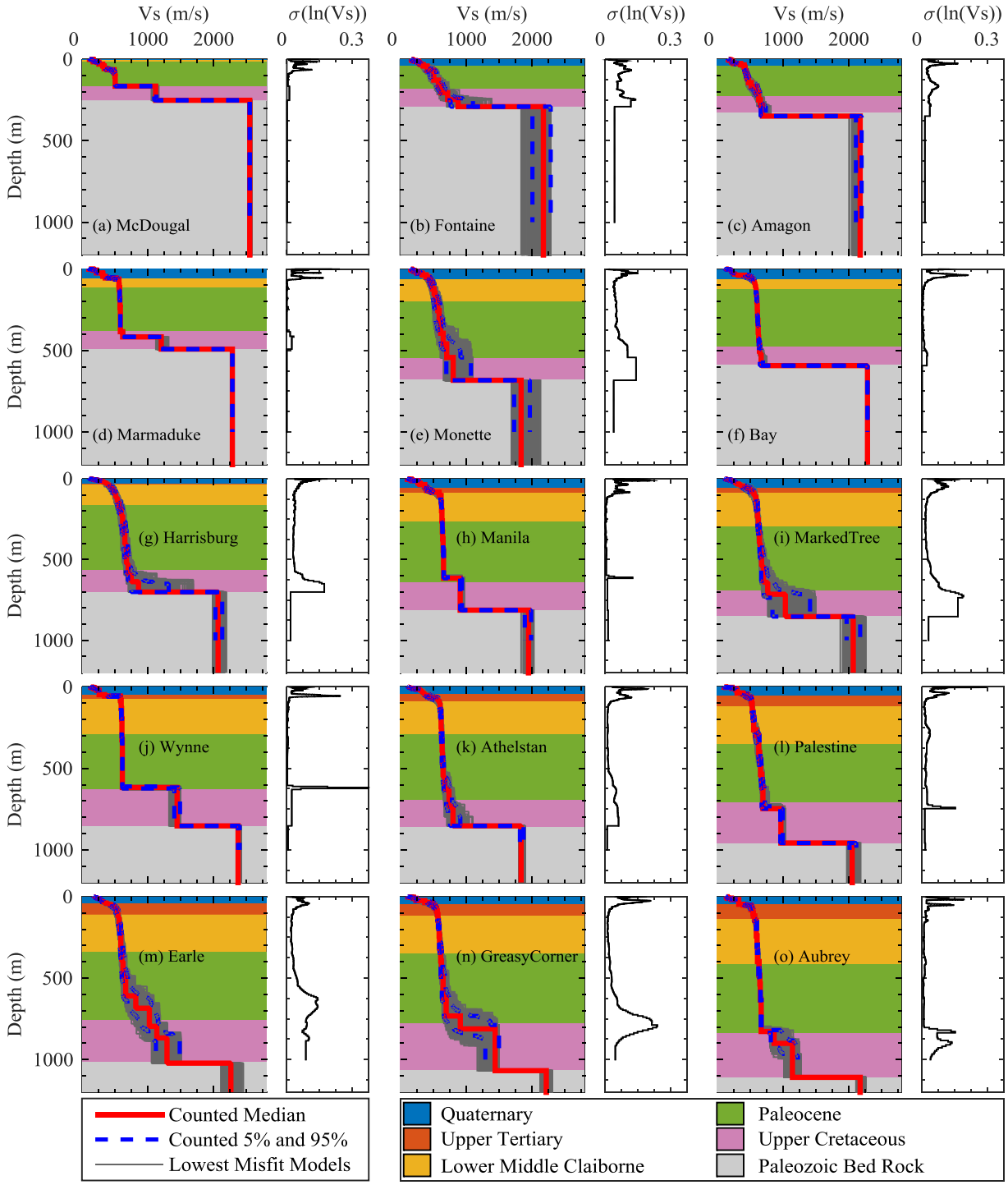

Figure 4. 5: V_s profiles from the inversion of surface wave data at the fifteen Northeastern Arkansas sites. V_s profiles from 1000 lowest misfit models are in gray, and median (V_s and depth for each layer) and 5th/95th percentile V_s confidence intervals of the top 1000 Vs profiles are in red and blue, respectively. The σln(Vs) of the top 1000 Vs profiles for a given depth are summarized in the plot to the right of the inverted shear wave velocity profiles.

Table 4. 2: Median Vs profiles from each site in this study with depth to the top of the layer and Vs of each layer.

McDougal		Fontaine		Amagon		Marmaduke		Monette		Bay		Harrisburg		Manila	
Depth (m)	V_s (m/s)	Depth (m)	V_s (m/s)	Depth (m)	V_s (m/s)	Depth (m)	V_s (m/s)	Depth (m)	V_s (m/s)	Depth (m)	V_s (m/s)	Depth (m)	V_s (m/s)	Depth (m)	V_s (m/s)
0.0	114	0.0	168	0.0	171	0.0	104	0.0	161	0.0	131	0.0	114	0.0	106
1.0	164	1.9	175	2.1	180	1.1	164	1.7	166	1.7	175	1.2	158	1.6	115
4.0	167	5.3	187	4.5	203	4.2	175	4.8	176	3.8	209	4.9	183	3.4	161
7.8	172	9.1	226	8.0	219	7.5	219	8	206	8.0	222	7.3	244	7.1	174
16	234	13	273	18	247	24	307	14	249	19	232	12	298	12	270
19	258	18	289	26	358	27	317	25	331	31	295	18	346	27	299
30	315	27	310	34	411	45	354	37	392	38	454	27	382	36	372
41	338	33	349	49	425	55	519	51	438	49	527	35	410	53	399
58	384	42	408	72	442	62	562	68	465	65	556	44	439	73	479
64	488	68	508	95	458	99	564	90	489	78	573	56	466	83	590
84	500	128	579	120	476	115	570	123	513	96	584	71	490	104	620
104	505	163	620	144	518	128	572	148	529	117	593	89	512	144	626
165	1119	205	719	167	595	179	577	177	550	148	599	116	538	197	632
252	2548	247	878	204	631	235	583	206	570	173	605	144	565	261	639
		291	2173	249	656	385	618	255	590	212	611	182	596	329	643
				282	690	417	1204	315	614	255	614	225	617	372	650
				349	2173	492	2284	394	651	300	620	276	636	441	656
								459	705	349	625	331	651	616	909
								543	803	403	631	406	677	813	1948
								683	1835	451	643	526	701		
										518	669	591	749		
										593	2284	637	859		
												701	2068		

Table 4.2 continued: Median Vs profiles from each site in this study with depth to the top of the layer and Vs of each layer.

Marked Tree		Wynne		Athelstan		Palestine		Earle		Greasy Corner		Aubrey	
Depth (m)	V_s (m/s)	Depth (m)	V_s (m/s)	Depth (m)	V_s (m/s)	Depth (m)	V_s (m/s)	Depth (m)	V_s (m/s)	Depth (m)	V_s (m/s)	Depth (m)	V_s (m/s)
0.0	120	0.0	135	0.0	121	0.0	107	0.0	183	0.0	114	0.0	140
1.6	136	2.5	147	1.0	131	1.7	130	1.7	193	2.0	160	1.3	152
4.5	166	3.6	177	4.7	153	3.4	226	4.6	207	4.2	197	7.1	164
7.5	217	7.5	189	8.6	210	9.3	286	8.2	239	11	237	10	217
12	252	12	227	14	310	18	304	12	275	24	371	18	329
21	287	21	262	30	346	37	387	21	298	37	487	47	399
33	354	48	344	39	376	45	459	30	339	55	527	53	517
47	441	56	584	54	442	64	517	40	402	71	549	80	543
61	508	83	596	66	556	85	524	50	466	87	562	101	550
79	561	133	602	80	590	104	534	60	505	110	572	118	572
104	590	198	608	99	605	151	545	73	530	144	578	147	596
142	608	325	614	135	617	188	555	98	546	182	590	241	608
193	614	617	1445	193	620	263	596	127	565	241	596	296	614
241	626	853	2371	258	626	300	632	174	577	315	614	399	639
295	637			329	635	402	648	228	590	394	624	483	650
343	643			402	641	451	661	313	605	491	650	536	656
401	656			480	650	536	681	397	623	621	697	635	669
455	676			552	676	618	697	490	664	732	911	828	866
541	704			631	739	747	969	609	818	812	1440	901	1145
641	769			736	801	958	2052	685	1024	1068	2217	1109	2173
715	1037			853	1835			796	1137				
853	2068							867	1291				
								1022	2261				

Table 4. 3: V_{S30} estimates at each site, computed from the median V_s profiles and the 5% and 95% counted profiles as the lower and upper bounds, respectively.

Site	V_{S30} (m/s)		
	5% Lower	Median	95% Upper
McDougal	184	197	210
Fontaine	217	235	256
Amagon	201	227	254
Marmaduke	187	209	237
Bay	193	211	232
Monette	191	220	249
Harrisburg	218	249	288
Manila	184	203	227
Marked Tree	182	213	244
Wynne	186	206	219
Athelstan	187	215	252
Palestine	209	239	275
Earle	233	249	278
Greasy Corner	180	218	244
Aubrey	198	215	237

4.2.4 Comparison of V_s Profiles

In Figure 4.6, the median V_s profiles from all 15 sites, with the Upper Cretaceous layers highlighted with red solid line, are presented along with the reference V_s profiles for various soil types from Lin *et al.,* (2014). The reference Vs profiles are for soft soil, dense sand, dense gravel, dense fine gravel and dense coarse gravel. The median V_s profiles exclude the bedrock velocities to keep the focus of Figure 4.6 on the soil velocity. Despite the velocity variation due to differences in the locations of geologic boundaries at each site, there is a generally good trend between the V_s profiles at all sites. The range of soil velocity between the sites is consistent with the range of the dense sand and dense gravel reference V_s profiles of Lin *et al.,* 2014. The Upper Cretaceous layers are highlighted as this geologic layer has the largest variation in V_s between the sites varying between 600-1400 m/s. This variation is expected due to the depth of the Upper Cretaceous layer at each site and the lower resolution with depth of the surface wave methods used in the study.

Despite the general consistency in the V_s profiles, there are some consistent differences in the V_s between approximately 50-200 meters as the V_s profiles are compared from the Western edge of the Embayment to the Mississippi River. To illustrate this point, the sites are broken up into three regions as shown in Figure 4.7 (i.e., the outer, middle, and inner region). The V_s profiles for three sample sites, Amagon, Harrisburg, and Marked Tree from outer, middle and inner region, respectively are shown in Figure 4.8. The V_s profiles are divided into three depth ranges as 0-61 meters, 61-167 meters, and below 167 meters. While the V_s profiles are consistent in 0-61 meters, 61- 167 meter is characterized by a 9-24% variation in V_s between the sites.

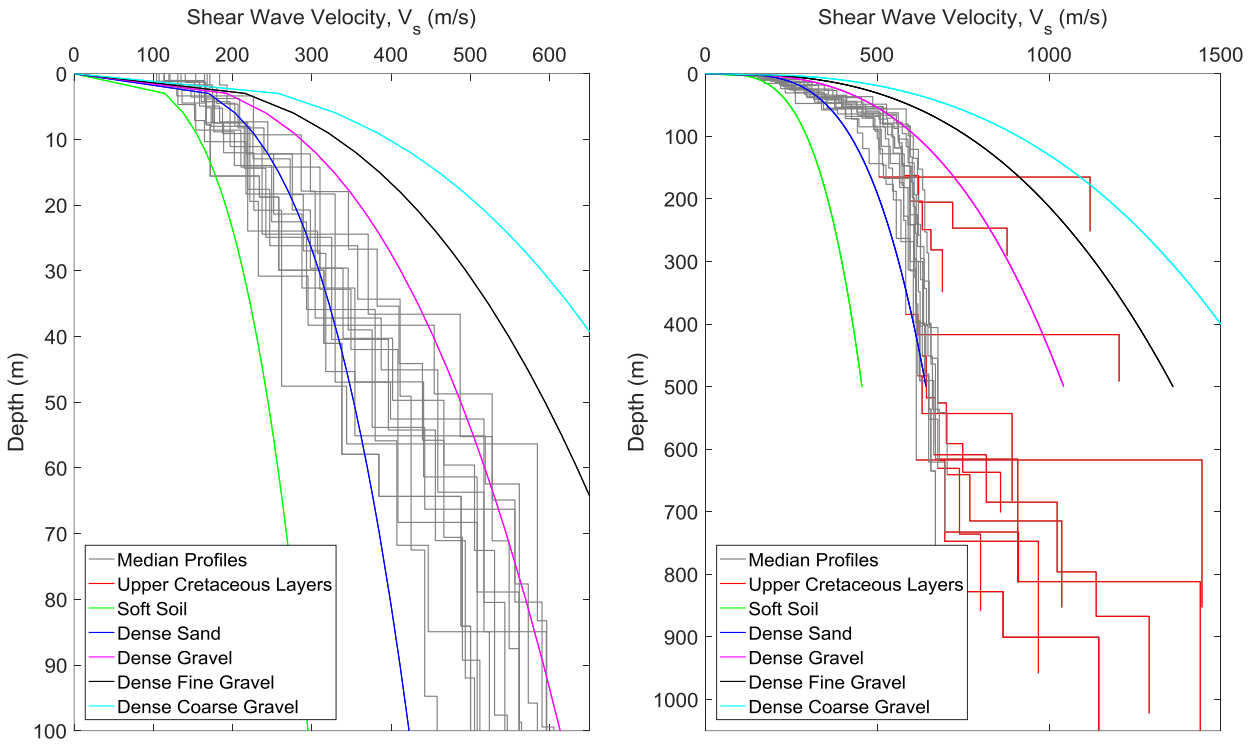

Figure 4. 6: Median V_s profiles from each of the 15 sites in this study with the Upper Cretaceous layers highlighted (a) in the first 100 meters and (b) down to 1100 meter. The reference velocity profiles for five different soil types from Lin *et al.*, (2014) are also provided (soft soil, dense sand, dense gravel, dense fine gravel, and dense coarse gravel) for comparison.

Also in Figure 4.8, the geologic layers provided by the CUSVM for each of the three sites are shown. The geologic layers in 61-167 meter range for the Amagon, Harrisburg/Marked Tree sites consist of Paleocene, and Lower Middle Claiborne, respectively. However, the V_s profiles of the sites in 61-167 meter range, are at odds with the geologic layers provided by the CUSVM, i.e., the older Paleocene layer at the Amagon site should have the highest V_s. However, the Amagon site has the lowest V_s in 61-167 meter range (9-24% lower). In addition, there are some inconsistencies between the V_s of the Lower Middle Claiborne layer at the Harrisburg and Marked Tree sites (i.e., a 9% difference between these V_s profiles in 61-167 meter range). This brings into question the overall accuracy of the geologic maps established as part of the CUSVM. After examining the other V_s profiles in these regions, similar trends appear throughout the study area (the largest difference is at the Amagon site). This indicates the CUSVM may have some inaccuracies in the western region (outer region in Figure 4.7) of the Mississippi Embayment.

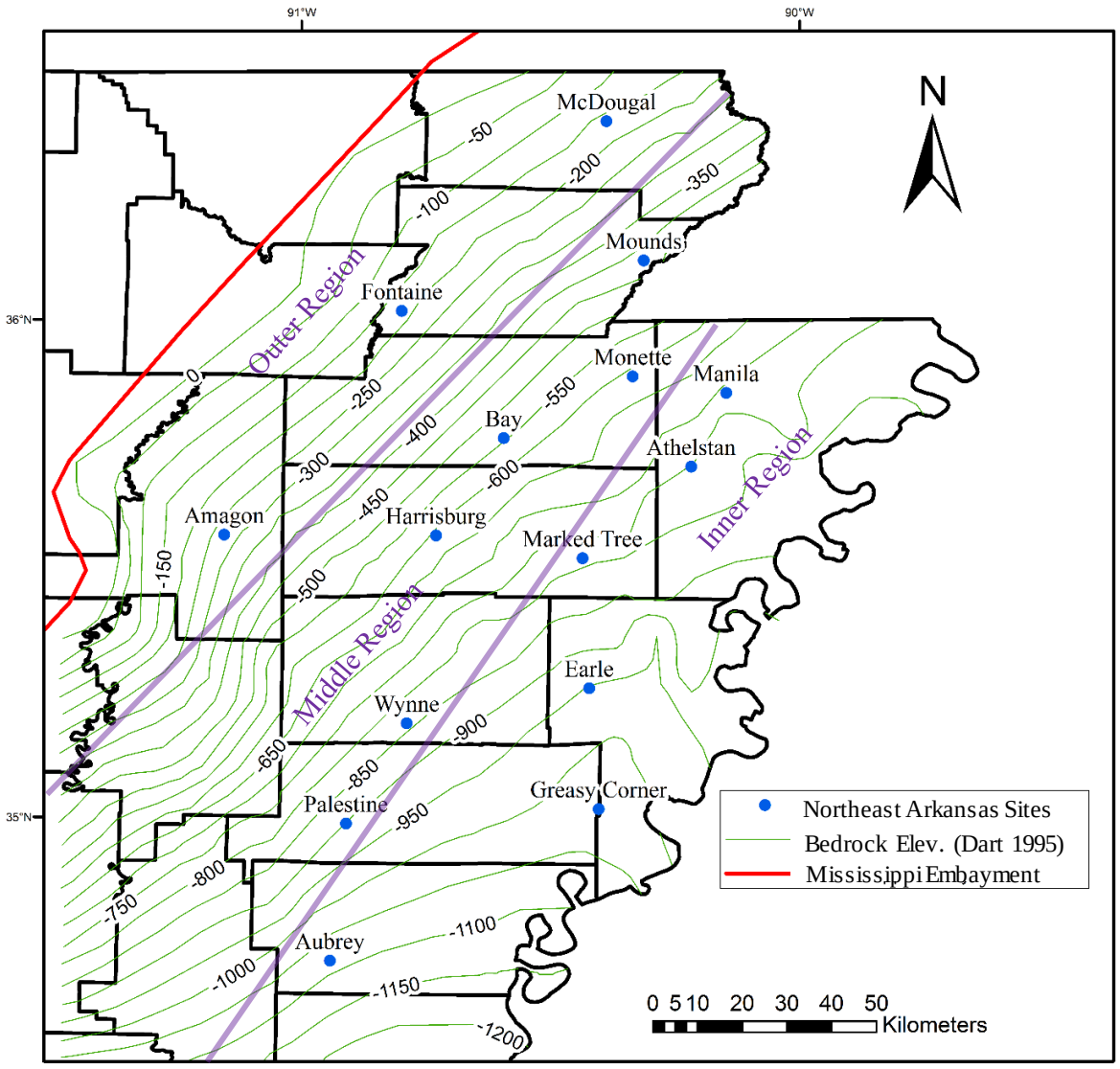

Figure 4. 7: Contours of bedrock elevation from Dart (1995) with testing locations for all 15 sites in Northeast Arkansas with the boundary line of the Mississippi Embayment. The area is separated into three regions: outer, middle, and inner regions denoting the area of mischaracterization in the CUSVM boundaries of the Paleocene and Lower Middle Claiborne layers.

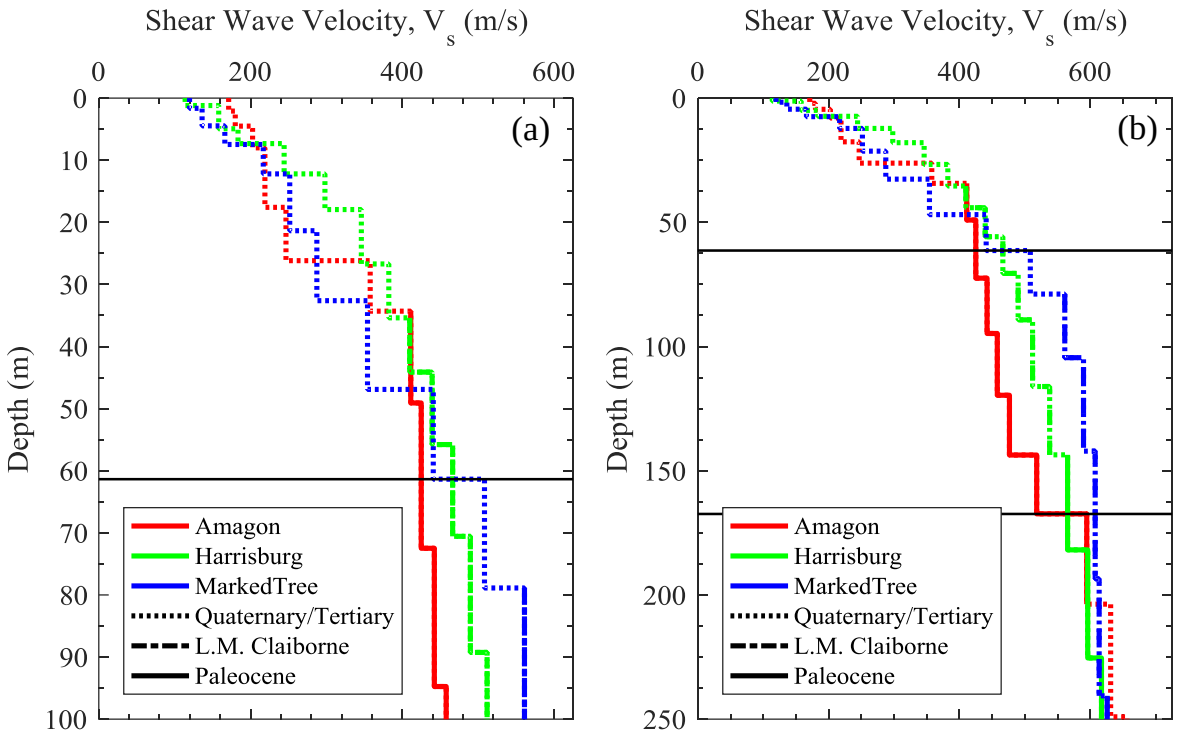

Figure 4. 8: Vs profile comparison for Amagon, Harrisburg and Marked Tree sites, each representing three different regions of northeast Arkansas spreading from west to east. a) shows the Vs profiles down to 100 meter, while b) shows the Vs profiles down to 250 meter. Here, each color represents a site and within each color type the line type represents different layer type in that site.

4.3 Development of the UA_MEVM

To develop a 3D velocity model of the Arkansas portion of the Mississippi Embayment, reference V_s profiles for each geologic layer need to be established based on the geologic layering and V_s profiles at each site. Those reference V_s profiles can then be applied to the larger CUSVM region established by Ramirez-Guzman *et al.*, (2012) in order to develop the full 3D velocity model.

4.3.1 Defining Reference V_s Profiles

To develop the reference V_s profiles for each geologic layer, the median Vs profile of each 15 sites is used. The following steps were conducted on each of the 15 sites median profile. First, data point at each one-meter increment depth was taken from the median Vs profile. Second, these data points were broken up into the five different geologic layers from the CUSVM. Third, combining the data points of all the 15 sites, power law fitting for each geologic layer was conducted utilizing the Equation 4.1. Figure 4.9 (a) through 4.9 (e) shows the power law fitting of Quaternary layer,

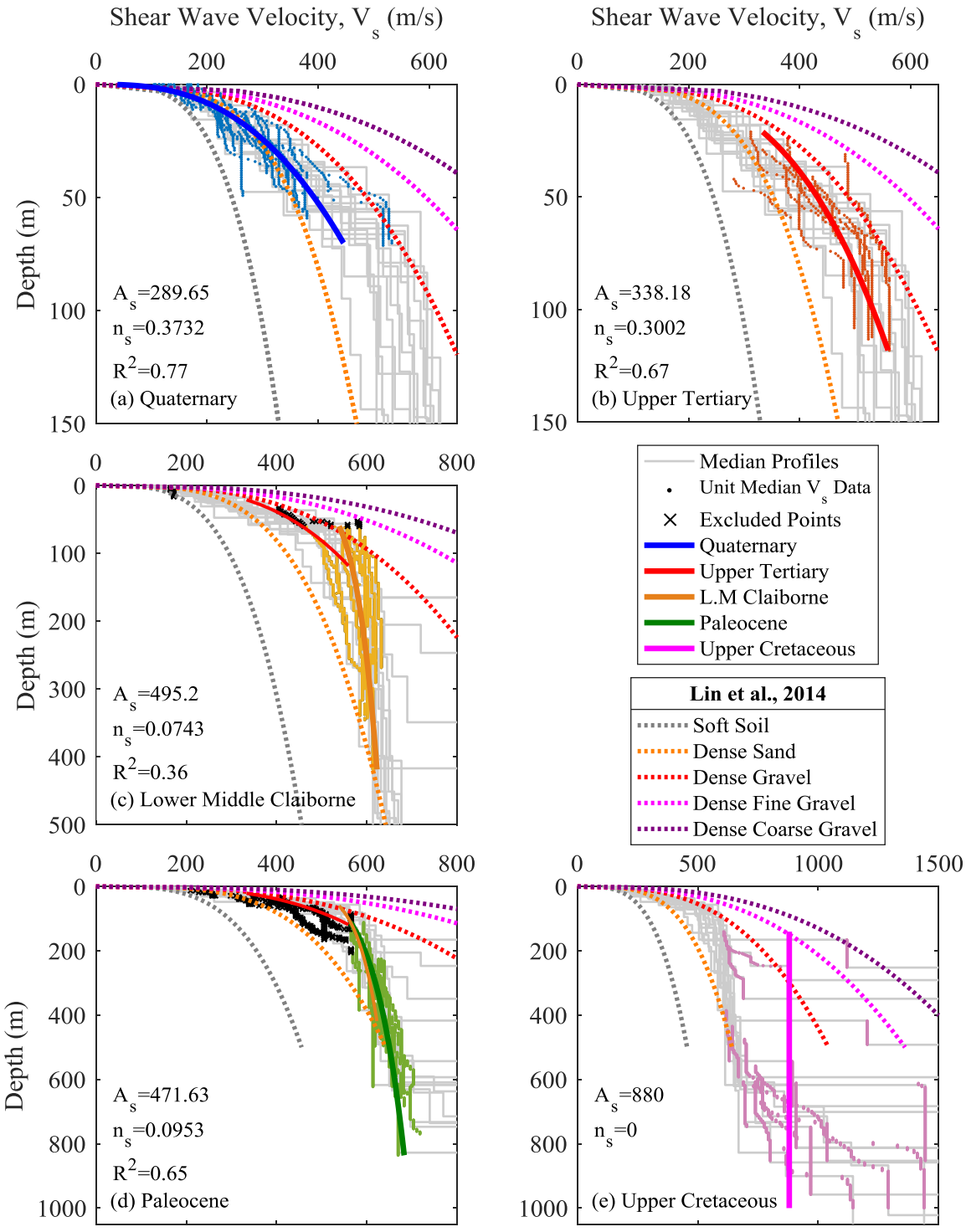

Figure 4. 9: Layer specific power-law fit through each incremental velocity data point in corresponding layers for all the 15 sites.

Upper Tertiary layer, Lower Middle Claiborne layer, Paleocene layer, and Upper Cretaceous layer, respectively. Each of the power law fitting for corresponding layer has its own color class, matching with the data points utilized for that layer's fitting (e.g. the thick blue line in Figure 4.9 (a) represents the Quaternary layer's power law fitting, and the blue dot points represents the data points of Quaternary layers of 15 sites used for this fitting). Thus, the general black dots shown in the legends (as unit median Vs data), representing median Vs profile at one meter increment depth would have different colors depending on their layer type (e.g. blue for Quaternary, red for Upper Tertiary). The Lin *et al.*, 2014 reference V_s profiles are included in each panel for comparison. For the Lower Middle Claiborne and Paleocene layers, some data (black x's) were excluded from further analysis (could be observed in Figure 4.9 (c) and (d)) because of the potential errors in the assigned geologic layers from the CUSVM discussed in Section 4.2.

For the V_s data in each geologic layer, a power-law function of the form of Equation 4.1 were fit to the V_s data to develop reference V_s profiles for each geologic layer.

$$V_s = A_s * (\sigma'_o/P_a)^{n_s} \qquad \text{Equation 4.1}$$

Where A_s is shear wave velocity corresponding to one atmosphere mean effective stress, σ'_o is the mean effective stress at the depth of interest, P_a is atmospheric pressure (1 atm), and n_s is the empirical normalized mean effective stress exponent. The power law function (Equation 4.1) fitting parameters (A_S and n_S) for each geologic layers are provided in Table 4.4. Equation 4.1 fit the Quaternary, Upper Tertiary, and Paleocene with R^2 greater than 0.64 (see Figure 4.9), however, the R^2 of the Lower Middle Claiborne indicates a poor fit ($R_2 = 0.35$). This may be a factor of the spread of the V_s data in the Lower Middle Claiborne which lacks a clear trend of a power law function, despite having, on average, a lower σln(Vs) than the other three layers (1.77% compared to a minimum of 0.223%). Note that a power law function was not fit to the Upper Cretaceous in Panel (e). Significant variability (approximately 500 m/s) exists in the velocity estimates for this layer. Therefore, the value proposed by the CUSSO of 880 m/s (Woolery *et al.*, 2016) was utilized for any Upper Cretaceous layer. Because none of the geologic layers had V_s data that extended to the full depth of the V_s profiles, the fits for a particular geologic layer are only shown for depths where V_s data was present for that geologic layer.

Comparing the resulting reference V_s profiles for each layer, the Quaternary layer in panel (a) and the Upper Tertiary layer in panel (b) result in the lowest V_s estimates for a particular depth (approximately 17% and 9% softer than the Lower Middle Claiborne, respectively). This is consistent with the idea that young geologic layers should have relatively lower average velocities than the aged layers (Hayati *et al.*, 2009). The Lower-Middle Claiborne reference V_s profile in panel (c) is very similar to the Paleocene layer with typically only a 2% difference between the estimated V_s values. As mentioned earlier, the Upper Cretaceous, were fit with a singular V_s value of 880 m/s based on the CUSSO estimates due to the high variability of the V_s estimates for the geologic layer. The bedrock velocity was set equal to the mean of all 15000 possible bedrock values from the inversions: 2200 m/s.

Due to the large variability in the V_s data in the upper 30 meters of the soil for each geologic layer, which can be up to 73%, it is not recommended that the reference V_s profiles developed in this study be used to estimate V_s in the upper 30 meters of a location. Site specific measurements should be used to determine the V_s of the upper 30 meters of soil.

Table 4. 4: Parameters for the velocity model equation and uncertainty estimates.

Geologic layer	A_s (m/s)	n_s	$\sigma_{ln(Vs)}$	ρ (kg/m^3)
Quaternary	290	0.3736	0.0582	1700
Upper Tertiary	341	0.2900	0.0546	1700
Lower-Middle Claiborne	494	0.0753	0.0177	1800
Paleocene	472	0.0956	0.0223	1900
Cretaceous	880	0	0.0679	2100

4.3.2 Consideration of Uncertainty

In addition to the power-law functions fit to each layer, an associated measure of uncertainty was computed. For each layer, the incremental velocity values computed for the 1000 lowest misfit V_s profiles of each site were combined. Variation was computed by taking the σln(Vs) for each one meter increment of a layer. At each increment, there may be up to 1000 V_s values from each site, i.e. a total of up to 15000 V_s values from the all 15 sites. Due to high local soil variability in the top 30 meters, data shallower than this threshold were excluded from the computation of uncertainty. The mean of all standard deviation values below 30 meters were then computed for each layer. The standard deviation of the bedrock velocity was computed from the set of 15000 possible bedrock V_s values from all fifteen sites in this analysis. Standard deviation values are included in Table 4.4.

4.3.3 Assigning Geologic Interfaces and Reference V_s Profiles in 3D Model

The boundaries of the geologic layers are defined based on the CUSVM (Ramírez-Guzmán *et al.,* 2012). The CUSVM includes several geologic layers including the Quaternary, Upper Tertiary, Lower Middle Claiborne, Paleocene, Cretaceous, and Paleozoic layers. The geologic composition of each of these layers is defined in Section 1.4 of this report. In CUSVM, the geologic layer points are in a grid of approximately 5.5 kilometers spacing and with five meter depth increments down to 2500 meters deep. For the UA_MEVM, the four nearest points from the CUSVM to the site of interest are used to find the layer boundaries using a nearest neighbor algorithm to produce a weighted average depth to each geologic layer interface. For each layer, sub-layering is defined using a layer ratio of approximately 1.5. Given the depth, soil type, and density of each layer, V_s may be estimated using Equation 4.1 along with the appropriate reference V_s profile parameters.

Because of the potential errors in the CUSVM discussed earlier, limitations were placed on what depths each reference V_s profile parameter could be used to estimate V_s regardless of the

geologic layer provided by the CUSVM. The Lower-Middle Claiborne reference V_s profile, was only applied for depths greater than 60 meters due to a lack of data above 60 meters during the fitting process and a poor fit between the V_s data and the reference V_s profile. For layers defined as shallower than 60 meters and Lower-Middle Claiborne in the CUVSM, the Upper Tertiary reference V_s profile was used because it fit well with the Lower-Middle Claiborne data, which was shallower than 60 meters in Figure 4.9c. A similar substitution was made for the Paleocene geologic layer for depths shallower than 100 meters, where the Lower-Middle Claiborne reference V_s profile was utilized. The Upper Cretaceous layer of panel (e) may consist of various soils and rock formations; consequently, significant variability (approximately 500 m/s) exists in the velocity estimates of this study for this layer. Therefore, the values proposed by the CUSSO, approximately equal to 880 m/s, were utilized for any Upper Cretaceous layer.

4.4 UA Mississippi Embayment Velocity Model

4.4.1 GUI for the UA Mississippi Embayment Velocity Model (UA_MEVM)

Presented in Figure 4.10, is an example of the graphical user interface for the University of Arkansas, Mississippi Embayment Velocity Model (UA_MEVM) produced as a standalone executable (i.e. UA_MEVM.exe) using Matlab. This simple to use application was developed to incorporate the functions for the model, which identify geologic layer boundaries, defines sub-layers within each layer, and solve for V_s of each layer using Equation 4.1 and the parameters from Table 4.4 for the applicable geologic layer. With the application, the user simply enters the desired site location coordinates in latitude and longitude and clicks "Solve." A V_s profile is displayed on the left portion of the interface and the table on the right is populated with layer depth, thickness, V_s (± standard deviation), and density values. Due to local soil variability in the near surface, the model excludes the first 30 meters; therefore, in-situ V_s characterization must be carried out in the first 30 meters of the desired site.

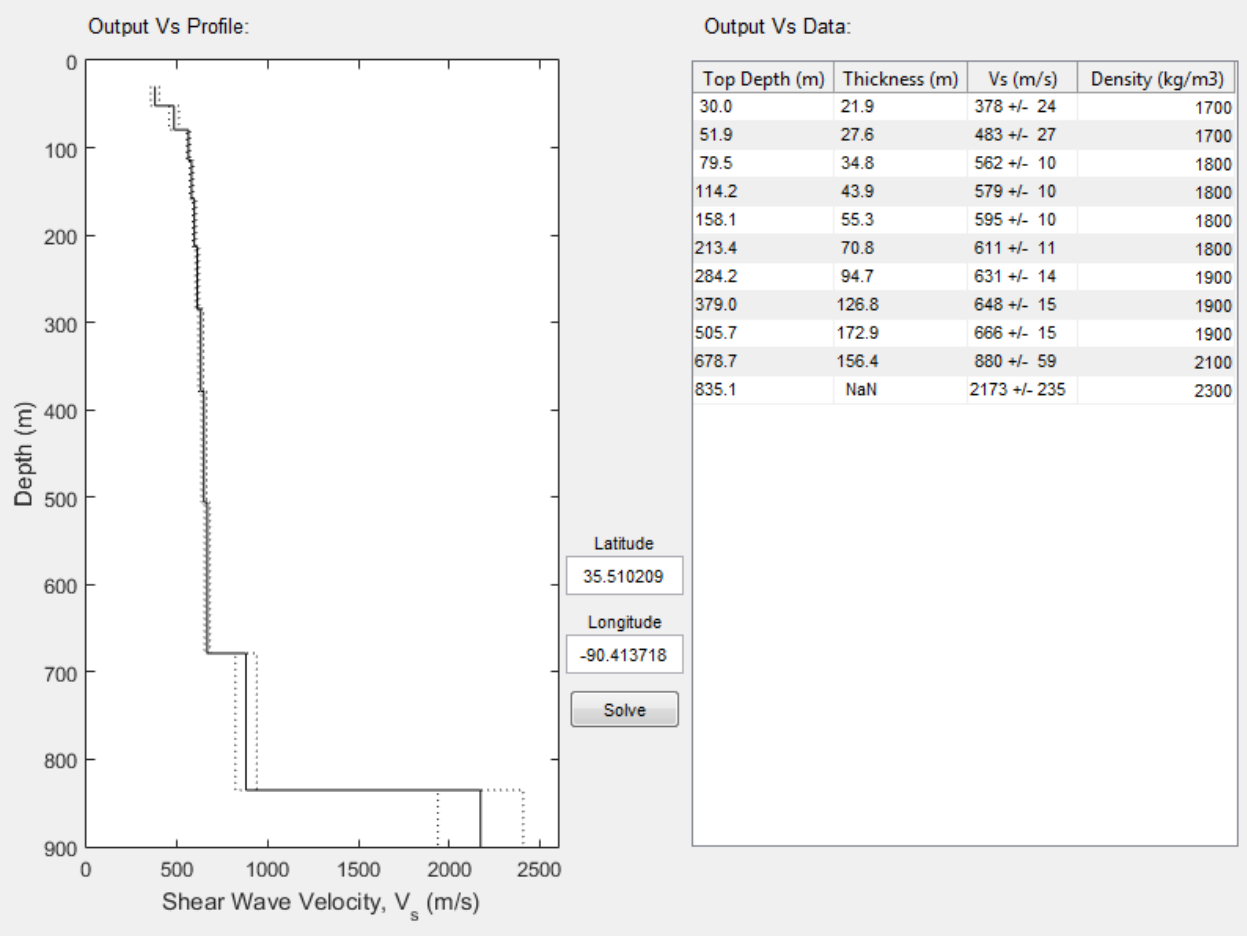

Figure 4. 10: An example of output data from the UA_MEVM for the ARDOT building in Marked Tree Arkansas.

4.4.2 Combining Shallow and Deep Shear Wave Velocity

The UA_MEVM, discussed in the previous section, can be used to generate a V_s profile for a specific site from a depth of 30 meters down to bedrock. For a SSGMRA, this deep V_s profile has to be combined with the shallow V_s profile at each location. This shallow V_s profile should be measured at the site of interest and should extend to 30 meters to 60 meters below the surface. This shallow profile is necessary due to the increased uncertainty/variability in the near surface materials. While the combination of the shallow and deep V_s profiles is beyond the scope of the current project, we feel that it is necessary to provide some guidance on how to combine these profiles. However, be aware that the method for combining the profiles detailed in this section is for general guidance only and has not been fully tested. Testing and validation of this approach should be accomplished in future projects.

To measure the shallow V_s profile of a site, both invasive and non-invasive methods can be used. Invasive methods such as Crosshole, Downhole, or SCPT require one or multiple boreholes or a CPT rig to conduct. These methods measure the layering and V_s of a site directly by placing sensors or sensors and source below the surface in a borehole or CPT cone. The V_s is directly measured by knowing the distance between source and receiver and the travel time between source and receiver. These methods are proven to provide accurate results in a variety of conditions and often require less sophisticated analyses. However, they are not without complexity or uncertainty. The downside of these tests are the additional cost of drilling borehole/boreholes. A simple breakdown of the equipment required for each invasive method is detailed in Table 4.5. While invasive methods are commonly used for dynamic site characterization, this project did not utilize these methods. Guidelines for using downhole surveys for determining shear wave velocity can be found from ASTM D7400-14, Crice (2011), Redpath (2007) etc. and a guideline for using Crosshole for determining shear wave velocity can be found from ASTM D4428/D4428M.

Table 4. 5: Equipment needed for site characterization using invasive methods.

Method	Depth of Investigation	Equipment Required
Downhole Survey	V_s (~<60 meters)	One borehole geophone system (Geostuff BHG3), Seismograph or dynamic signal analyzer, source (sledgehammer or any other), wooden plank, one cased borehole to desired depth.
Crosshole Survey	V_s (~<60 meters)	Two borehole geophone instruments (Geostuff BHG3), Seismograph or dynamic signal analyzer, source (in hole source), Three cased borehole to desired depth, slope inclinometer instrument.
SCPT	V_s (~<60 meters)	CPT equipment with seismic geophone and source plank.

Non-invasive methods, such as surface wave methods, have also been proven accurate in a variety of conditions and have the advantage of only requiring sensors and source to be placed on the ground surface. This often reduces the cost of developing V_s profiles for a site. Non-invasive methods for determining V_s are spilt into two main categories: body wave methods and surface wave methods. Body wave methods include seismic refraction and seismic reflection methods, while surface wave methods include the SASW, MASW, MAM. It is not recommended to conduct ReMi measurements to determine the Vs profile. While this method has gained popularity due to its "blackbox" type processing, significant errors in the Vs profiles due to wavefield assumptions have been shown by a number of authors (Beekman (2008), Cox and Beekman 2011). The use of each of the methods for site characterization was discussed earlier in the report. The equipment required to conduct surface wave testing for development of shallow V_s profiles is shown in Table 4.6. In addition to equipment needed to estimate the shallow V_s profile, three component broadband sensors and digitizer will be required to collect data for HVSR analysis to estimate the site period. The use of the fundamental site period to combine the shallow and deep V_s profiles is discussed below.

Table 4. 6: Items needed for site characterization (shallow) using non-invasive surface wave methods.

Depth of Investigation	Item	Count	Use
V_s depth (<60m)	4.5 Hz Horizontal Geophones*	24	Active source MASW testing (Love wave)
	4.5 Hz Vertical Geophones	24	Active source MASW testing (Rayleigh wave)
	Refraction Cables	1-2	Active source MASW testing
	Geode Seismographs	1	Active source MASW testing/L-array testing
	Sledgehammer with Trigger Cable	1	Active source MASW testing
	Strike Plate	1	Active source MASW testing (Rayleigh wave)
	Strike Beam*	1	Active source MASW testing (Love wave)
	Tape Measures	2-3	Sensor layout
	Laptop Computer	1	Recording data

*Optional equipment

In order to generate a site specific V_s profile in the Mississippi Embayment using a shallow V_s profile collected at the site and deep V_s profile from the UA_MEVM, the following are required:

I. Shallow site specific Vs profile (30-60 meters depth)
II. Fundamental frequency (f_0) for the site using the HVSR method
III. Deep V_s profile using UA_MEVM

Items I & II need to be determined experimentally at the specific site of interest using methods described earlier in the report. Item III can be determined using the UA_MEVM as specified in the previous section. While the shallow and deep V_s profiles can be directly combined by simply translating from one V_s profile to the other at the maximum depth of the shallow V_s profile, an improved V_s profile can be obtained by using the f_0 at the site determined from HVSR to insure that the global stiffness of the generated V_s profile represents the site to the best degree possible. To do this, the linear transfer function should be computed for the initial combined V_s profile

generated at the site. This can be done using the linear option in any site response program such as DEEPSOIL. The f_0 determined from the transfer function can then be compared to the f_0 estimated for the site from the HVSR measurements. If the transfer function f_0 is less than the HVSR f_0, this indicates the V_s profile is too soft (V_s is too low) and the V_s profile should be adjusted upward to insure the transfer function f_0 value is within an acceptable error when compared to the HVSR f_0. If the transfer function f_0 is greater than the HVSR f_0, this indicates the V_s profile is too stiff (V_s is too high) and the V_s profile should be adjusted to downward to insure the transfer function f_0 value are within an acceptable error.

From the methodology above, a single V_s profile can be determined for the site of interest. However, AASHTO Section 3.4.3.2 requires that uncertainty in the V_s be accounted for in the SSGMRA, therefore multiple V_s profiles should be considered for the site. These profiles can be generated by increasing or decreasing the V_s of each layer in the profile by some percent error (i.e., +/- 20%) or a randomization model such as Toro (1995) can be used to randomize the V_s profile to account for uncertainty. The Toro (1995) model uses a statistical approach to account for uncertainty in a more scientific way than simply using bounding upper and lower V_s profiles. The use of bounding V_s profiles has been shown to poorly represent the uncertainty of the V_s profile (Cox and Teague 2016). Therefore, the randomization option is recommended. Software packages such as DEEPSOIL or STRATA may be used to perform the randomization.

CHAPTER 5
SITE-RESPONSE ANALYSIS CASE STUDY

5.1 Monette, Arkansas Bridge Site Background

Monette, Arkansas is located on the eastern edge of Craighead County in northeast Arkansas as shown in Figure 5.1. Just east of Monette, Highway 18 crosses the Cockle Burr Slough, a 200-foot wide canal that connects into the St. Francis River. Recently, as part of Job CA1001, that expanded Highway 18 to four lanes and rerouted it to bypass north of Monette, a new 329-foot long by 78-foot wide bridge was constructed to cross the Cockle Burr Slough. The main components of the bridge include nine 327-foot long continuous steel girders and six pile bents. The new structure occupies the same location as the old bridge and was built in stages so that traffic could still flow over the old structure until two lanes of the new bridge could be opened. The lowest bridge chord is 7.5 feet above the design flood elevation, which is 6.8 feet higher than the previous structure that crossed the canal. Figure 5.2 shows several details of the bridge during construction. The overall cost of the project was $13.7 million, of which $2.82 million was for bridge construction.

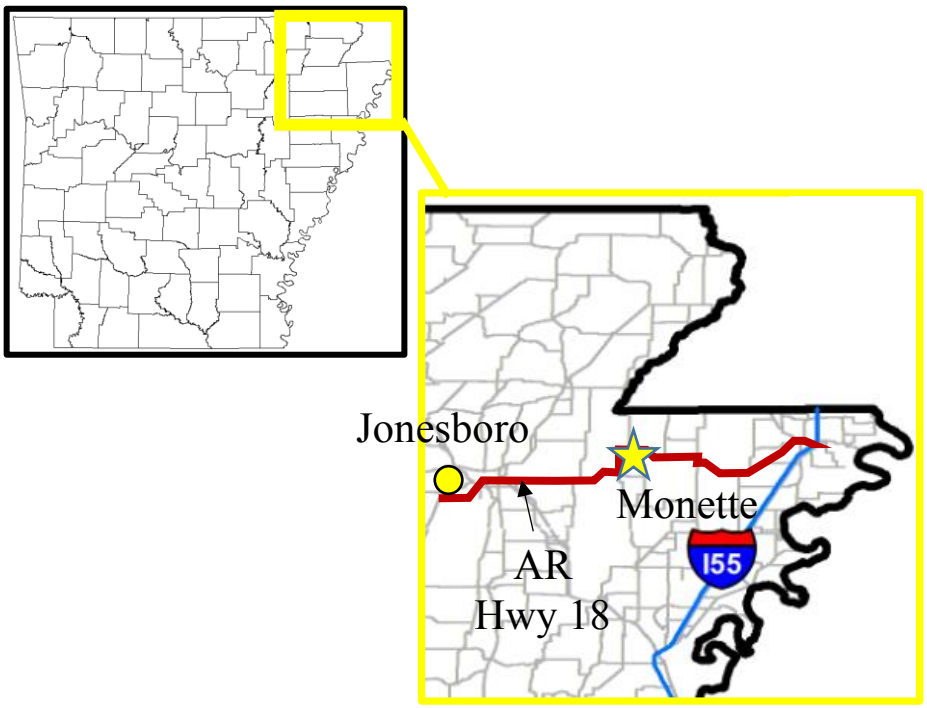

Figure 5. 1: Location of Monette in relation to Arkansas state map, Jonesboro, Arkansas, and Arkansas Hwy. 18.

Figure 5. 2: Monette Bypass Bridge construction. Top Left – Second phase of deck construction. Top Right – South side of bridge (looking East bound) crossing Cockle Burr Slough. Bottom Left – View of steel girders and pile bent 3. Bottom Right – View of restrainer block on bent 1.

The subsurface conditions at the site are characterized by mainly sandy soils with the exception of a clay layer between 10 feet and 20 feet below existing grade according to ARDOT borings located at each end of the bridge. Some trace gravel exists in layers below 50 feet. Soil information at the bridge end bents are detailed in Figure 5.3. The soil at the site classifies as an AASHTO site class D based on blow count. More soil information, such as borings and ARDOT geotechnical recommendations can be found in Appendix B. General procedure design values include a design PGA value of 0.917 g, an S_{DS} value of 1.641 g, and an S_{D1} value of 0.694 g, which corresponds to an AASHTO seismic performance zone of 4. This high seismic hazard is the result of the site's close proximity to the Reelfoot Rift, the main fault system of the NMSZ.

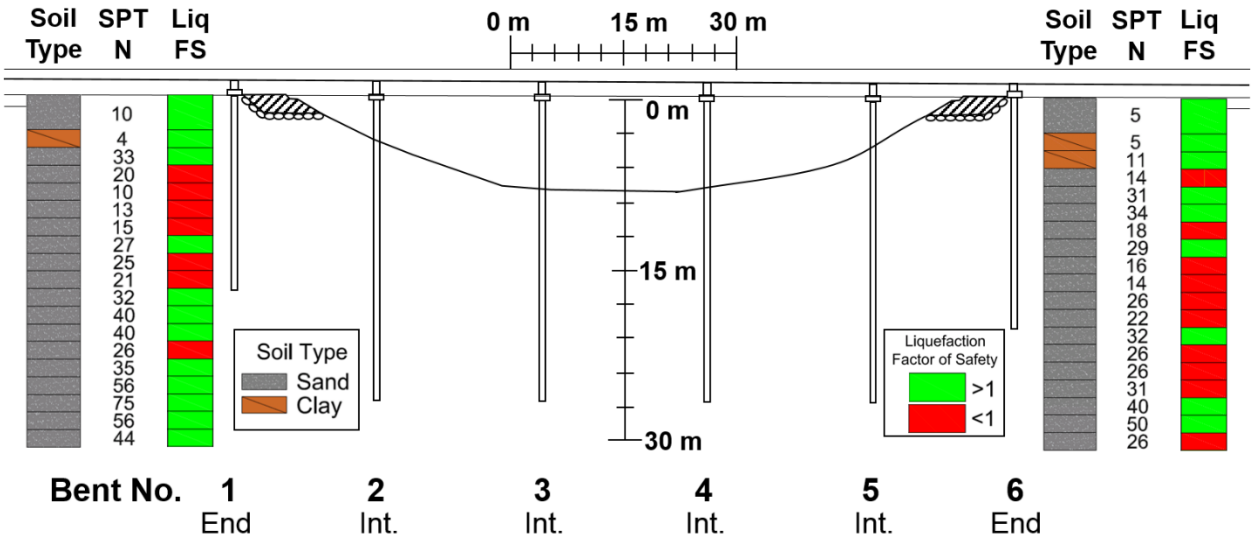

Figure 5. 3: Elevation view of Monette Bypass Bridge with bent numbering, soil conditions, and liquefaction potential determined from ARDOT boring information. N values represent raw blow counts from SPT measurements. Note: 1.5:1 vertical to horizontal scale.

5.2 Site-Response Methodology

To conduct an SSGMRA, there are three main steps: (1) characterize the small-strain V_s of the soil profile down to bedrock, (2) collect and adjust appropriate input earthquake acceleration time histories, and (3) simulate the propagation of input ground motions from bedrock to the ground surface using appropriate numerical analyses. Each of these steps has its own challenges that can contribute to the overall uncertainty in surface ground motion estimates.

5.2.1 Dynamic Site Characterization

To determine the small strain V_s profile at the Monette, Arkansas site, a combination of active source multi-channel analysis of surface waves (MASW), passive source microtremor array measurements (MAM), and horizontal to vertical spectral ratio (HVSR) measurements were carried out. These methods were outlined in Chapter 3. The theoretical fits for the Rayleigh, Love, and HVSR experimental data are shown in Figure 5.4 for the 1000 lowest misfit V_s profiles. The 1000 lowest misfit V_s profiles are also shown in Figure 5.4. To conduct the SSGMRA, 10 V_s profiles (shown in green in Figure 5.4), were randomly selected from the top 1000 lowest misfit profiles.

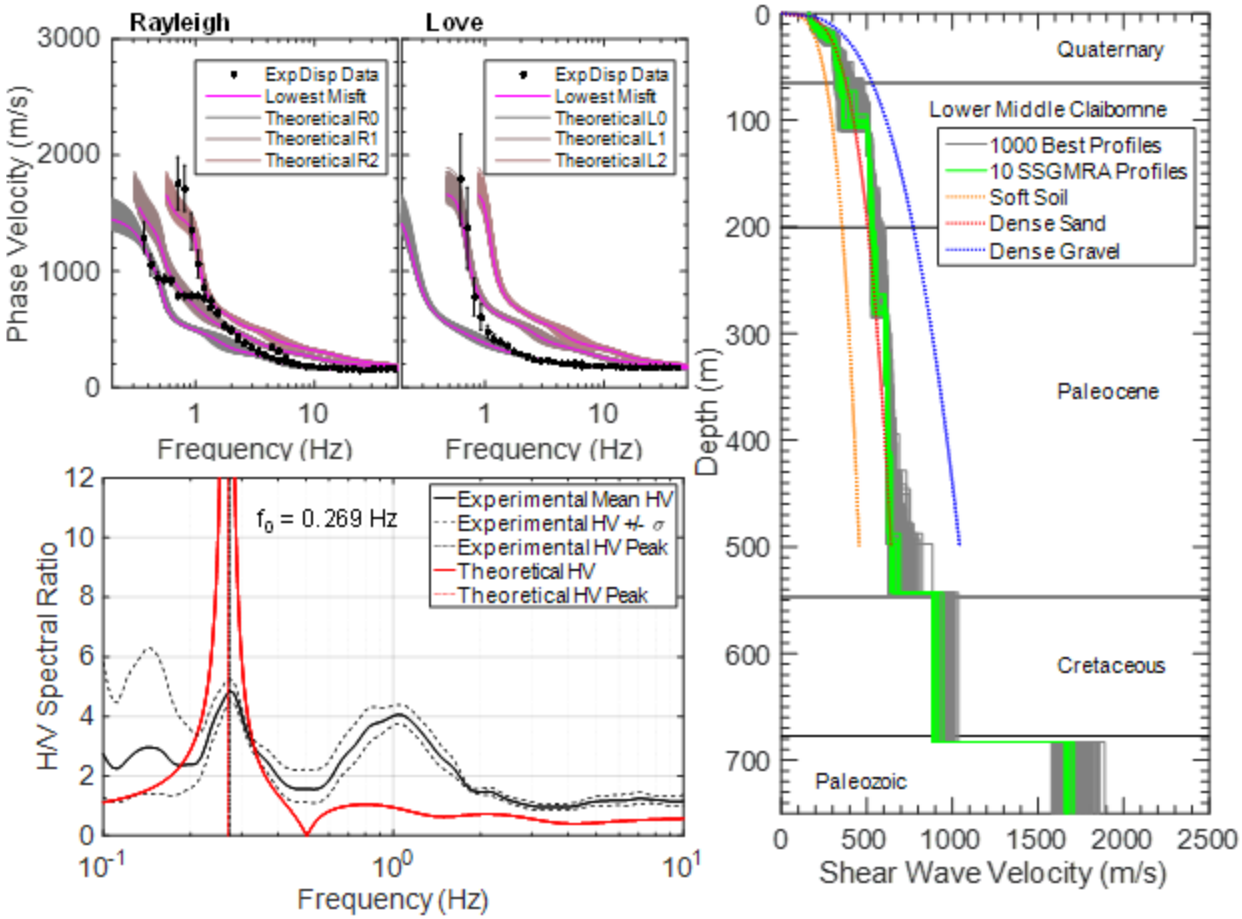

Figure 5. 4: Top Left – Rayleigh and Love wave experimental dispersion data fit with theoretical curves. Bottom Left – Experimental horizontal to vertical spectral ratio fit with theoretical curves. Right – 1000 lowest misfit shear wave velocity profiles from inversion and 10 randomly selected shear wave velocity profiles used in SSGMRA. Also shown are reference V_s curves from Lin *et al.*, (2014) used to constrain the inversion process and the geologic boundaries taken from the CUSVM.

5.2.2 Input Ground Motions

A deaggregation was performed using the USGS Unified Hazard Tool for the Conterminous U.S. 2008 v3.2 Edition (USGS 2017). Deaggregation results indicated that a singular scenario governs the seismic hazard at all periods: a modal magnitude 7.7 earthquake at a distance between 22 and 23 kilometers. The UHS for Site Class A was chosen as the design target spectrum over the period range from 0.01 to 2 seconds, which is an appropriate target spectrum if conservative estimates of response are acceptable (NEHRP 2011). The UHS is shown in Figure 5.5. It should be noted that the UHS is an ergodic target spectrum as recommended by the AASHTO code. A user guide for the USGS Unified Hazard Tool that is used for both deaggregation and obtaining the target spectrum is provided with the deliverables (TRC 1603_UHS Guide).

The AASHTO Guide Specifications for LRFD Seismic Bridge Design states that response-spectrum-compatible time histories shall be developed from representative recorded earthquake

motions. Rathje *et al.*, (2010) argued that these time histories have the greatest influence on site-response results. Large magnitude ground motions at short distances have never been recorded in the Central United States. Therefore, as part of a Nuclear Regulatory Commission project, earthquake acceleration time histories from various regions were adjusted to encompass the frequency content expected from an earthquake occurring in the Central and Eastern United States (McGuire *et al.*, 2001). All rock outcrop motions from the McGuire *et al.*, 2001 study are provided in the deliverables, but a CD containing the ground motion files can be obtained for free by request from DISTRIBUTION.Resource@nrc.gov (https://www.nrc.gov/reading-rm/doc-collections/nuregs/contract/cr6728/). The selected input acceleration time histories from McGuire *et al.*, (2001) were restricted to those with magnitudes and distances consistent with the deaggreagtion (Kramer 2012). Quantitative rules of thumb for selecting ground motions, which align with those defined in Cox *et al.*, 2012, include the following:

- Distance from r/2 to r*2.
- Magnitude from (M_W – 1) to (M_w + 1).
- PGA from the target spectrum PGA/2 to the target spectrum PGA*2 (PGA/3 to PGA*3 is acceptable if necessary).
- As many different earthquake locations as possible.
- Duration typically > 10 seconds.

It is best to first select all of the ground motions that have similar magnitudes and distances from the design scenario, and then narrow down those preliminary motions based on the rules listed above to 10-20 motions. Ultimately, ten input ground motions, listed in Table 5.1, were selected.

Table 5. 1: Summary of selected input ground motions (McGuire *et al.*, 2001).

File Name	**Earthquake**	**PGA (g)**	**Magnitude M_w**	**Distance R (km)**	**Duration (s)**
SHL090	Cape Mendocino	0.585	7.1	33.8	14.6
SHL000	Cape Mendocino	0.648	7.1	33.8	14.4
GBZ000	Kocaeli, Turkey	0.454	7.4	17	7.3
DAY-TR	Tabas, Iran	0.947	7.4	17	9.7
DAY-LN	Tabas, Iran	0.993	7.4	17	8.8
GYN000	Kocaeli, Turkey	0.313	7.4	35.5	8.3
TCU128-N	Chi-Chi, Taiwan	0.305	7.6	9.7	29.9
TCU046-W	Chi-Chi, Taiwan	0.336	7.6	14.3	18.8
TCU047-W	Chi-Chi, Taiwan	0.7	7.6	33	12.9
TCU047-N	Chi-Chi, Taiwan	1.168	7.6	33	10.8

RspMatch (2009) was used to match the ten selected ground motions to the UHS target spectrum (Hancock *et al.*, 2006). According to AASHTO (2011), input rock acceleration time

histories should be adjusted, either by scaling or spectral matching, to match the seismic hazard consistent with the bridge site. Advantages of spectral matching include reduction of record-to-record variability, which reduces output variability and also enhancement the select frequencies with no unconservative bias in response (NEHRP 2011). RspMatch2009 was used to spectrally match input rock outcrop motions to the UHS target spectrum using two passes from 1 Hz to 100 Hz and from 0.5 Hz to 100 Hz, respectively. Ground motions were spectrally matched or scaled to the UHS target spectrum from at least $0.5T_n$ to $2T_n$. A tutorial on RspMatch is provided with project deliverables (TRC 1603_RspMatch Processing Guide).

5.2.3 Simulating Wave Propagation

To perform the site response analysis, the software program DEEPSOIL 6.1 was utilized (Hashash *et al.,* 2016). It has been shown to produce appropriate site response results for sites with deep sedimentary deposits, such as those in the Mississippi Embayment, because of its short period accuracy (Zheng *et al.,* 2010, Hashash and Park 2001).

Within DEEPSOIL, a new model for small-strain nonlinearity and strength, termed the GQ/H model, has recently been implemented (Groholski *et al.,* 2016). The GQ/H model uses a shear strength asymptote to constrain the maximum shear strength that can be obtained for each layer with the goal of matching both the small-strain and large-strain portions of the soil backbone curve. It does so by following a fitting procedure that slightly increases the shear modulus reduction curve from the reference curve at higher strains. This eliminates the need for manually implied shear strength corrections, which were previously required in older models to account for strain-hardening behavior. The GQ/H model was used to fit corrected curves to the Darendeli (2001) modulus reduction and damping curves for each soil layer using the MRDF-UIUC reduction factor fitting procedure (Philips and Hashash 2009, Hashash *et al.*, 2016). These dynamic soil properties were not randomized because no reasonable variability parameters could be determined (Malekmohammadi and Pezeshk 2015).

Soil type, plasticity, and blow count information was obtained from ARDOT boring logs and used in calculations for dynamic soil properties. For layers below the final boring depth, sand reference curves were assigned. Target shear strength values were estimated using either a SPT blow count to shear strength correlation based on ARDOT boring logs or a Mohr-Coulomb behavior shear strength assuming a friction angle of 30° and no cohesion. Layering for the soil profile was divided up to provide a maximum analysis frequency of at least 25 Hz.

Due to the limitations and advantages of each type of analysis, EQL and NL analysis results were weighted equally to obtain an overall design response spectrum. EQL analyses can produce a very flat response at high frequencies due to high damping values at sites where high shear strains are expected (Griffiths *et al.,* 2016a), and underestimates ground motions at high frequencies for thick soil deposits (Romero and Rix 2001). NL analyses can better predict soil behavior under large strains from strong ground motions at soft soil sites because it accounts for changes in soil properties at each time step (Kim *et al.,* 2016). However, EQL analysis is still the most common method in practice (Rathje *et al.,* 2010) and has proved to be valuable for studies within the NMSZ (Liu and Stephenson 2004).

The final site-response spectrum should be a weighted average, preferably a 50%-50% average, of EQL and NL amplification ratios multiplied by the AASHTO site class A spectrum for the site. Amplification ratio can be obtained by dividing the median output surface response, whether it be EQL or NL, from DEEPSOIL by the median of the input ground motions.

Maximum shear strains from each analysis should be checked. Analyses producing shear strains greater than 5% should be rerun using different target shear strengths at the maximum strain interfaces or discarded.

The delineated design spectrum for all periods shall be determined as follows:

- (1) The maximum of 2/3 AASHTO design spectrum determined from the general procedure and the resulting site-response spectrum.
- (2) The minimum of (1) and the AASHTO design spectrum determined from the general procedure.

5.3 1-D Site-Response Analysis Results

A delineated design response spectrum was developed and shown in Figure 5.5d for the Monette site using the site-response acceleration response spectrum, the upper limiting AASHTO site class D design response spectrum, and the lower limiting two-thirds AASHTO site class D design response spectrum. The scaled input motions are shown in Figure 5.5a, the EQL results are shown in Figure 5.5b, the NL results are shown in Figure 5.5c, and the combined EQL and NL results are shown in Figure 5.5d. The delineated design response spectrum is the greater of either the site-specific response spectrum or two-thirds of the general response spectrum and is always less than or equal to the AASHTO site class D response spectrum obtained from the general procedure.

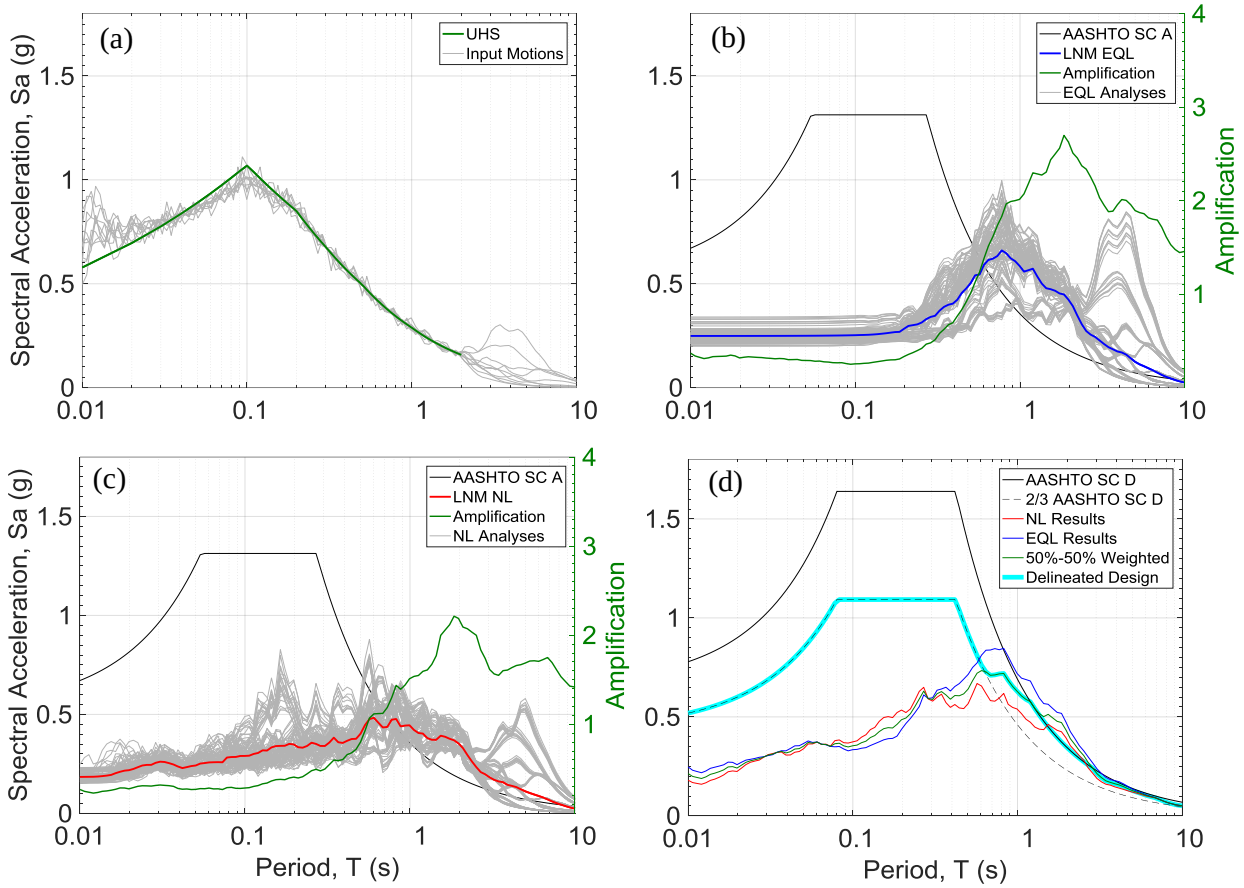

Figure 5. 5: Site specific ground motion response analysis results for the Monette, AR bridge site a.) scaled input motions and uniform hazard spectrum (UHS), b.) equivalent linear (EQL) analyses surface response with lognormal median (LNM) of EQL results, LNM EQL spectral ratio (surface output/input), and AASHTO Site Class A spectrum c.) nonlinear analyses surface response with LNM of NL results, LNM NL spectral ratio (surface output/input), and AASHTO Site Class A spectrum and d.) LNM of EQL results, LNM of NL results, 50% EQL-50% NL weighted results, AASHTO Site Class D Spectrum, 2/3 AASHTO Site Class D Spectrum, and delineated design spectrum. NL and EQL results are the LNM spectral ratio times the AASHTO site class A response spectrum.

Results from this analysis indicate a general linearly increasing response from the PGA (i.e., 0.01 seconds) to approximately 0.2 seconds. The EQL analysis response spectrum begins to exceed the two-thirds AASHTO site class D design spectrum at around 0.6 seconds – 0.7 seconds, which is similar to the results presented in Cox *et al.*, (2012) for a Blytheville, Arkansas site. The NL response spectrum begins to exceed the two-thirds AASHTO design spectrum around 0.8 seconds. As expected, the NL analyses resulted in lower accelerations than the EQL analyses for most periods. The smooth peak of the site-response spectrum indicates that no wave energy entrapment is expected for the soft soil site.

Also illustrated in Figure 5.5b and c, amplification of input rock motions begins around 0.5 seconds and continues until a peak amplification of 2.7 times and 2.2 times is reached at 1.85

seconds for EQL and NL analyses, respectively. This amplification is consistent with that observed in Cox *et al.*, (2012). Rogers *et al.*, (2007) also observed this type of period migration for three Missouri River highway bridge sites. This causes higher potential for constructive interference with long period bridges. Figure 5.5 (b) and (c) also shows the deamplification of spectral acceleration from 0.01 second to 0.5 second range. Design of structures in northeast Arkansas with a natural period in this range will benefit from the lower design spectral acceleration estimated by a SSGMRA compared to those estimated using the general procedure. This attenuation is also consistent with previous Mississippi Embayment SSGMRA research (Cox *et al.*, 2012, Liu and Stephenson 2004, Zheng *et al.*, 2010, Malekmohammadi and Pezeshk 2015).

Maximum strain levels reached 1.57% for EQL analyses and 1.54% for NL analyses as shown in Figure 5.6. The TCU128-N record (M_w = 7.6 in Chi-Chi, Taiwan, Table 5.1) produced the highest maximum shear strains out of all of the selected input records. This record has the longest duration and shortest distance from fault rupture of all the records. It was also among records with the highest magnitudes. Zheng *et al.*, (2010) observed similar shear strain magnitudes using their average V_s profile for Osceola, AR. These shear strain values are less than those observed by Cox *et al.*, (2012), but the input ground motion was greater for their Blytheville site versus the Monette site.

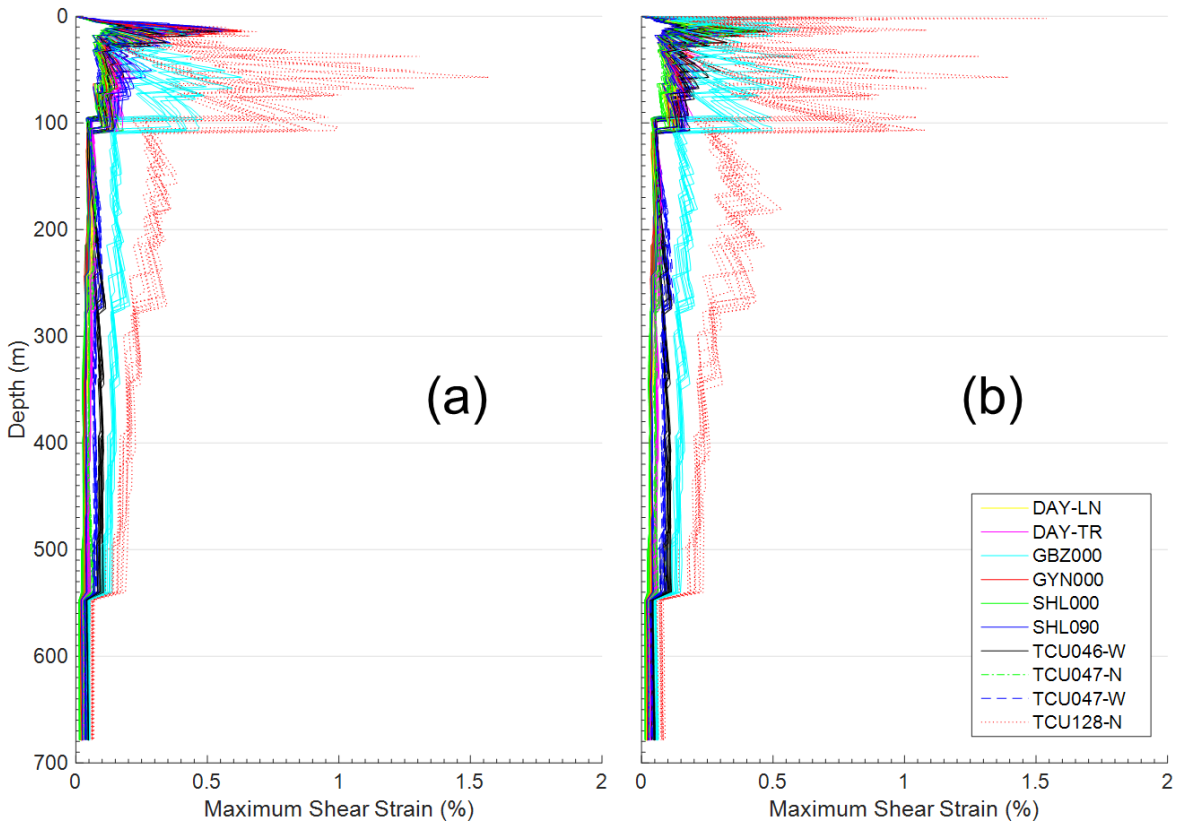

Figure 5. 6: Maximum shear strains profiles for a.) equivalent linear analyses and b.) nonlinear analyses.

5.4 Implementing SSGMRA Results in ARDOT Design

This section details how the results from the SSGMRA will be incorporated into the current ARDOT design methodology. Since this study followed ARDOT procedures for seismic design of bridges during the redesign of the Monette bridge, many of the items needed to incorporate the SSGMRA results have already been worked out as part of the redesign process.

5.4.1 AASHTO Site Classification

The time averaged shear wave velocity in the top 30 meters can be calculated per AASHTO 3.10.3.1 in order to determine seismic site class. This V_{S30} value along with some site specific information can be used with AASHTO Table 3.10.3.1-1 to determine the updated site classification.

5.4.2 AASHTO Seismic Performance Zone

There is also the potential for improving the seismic performance zone. The S_{D1} value, i.e., the spectral acceleration value at a period of 1 second, can be taken from the delineated design response spectrum (see Figure 5.7). This updated spectral acceleration at 1 second can be used with Table 3.10.6-1 in AASHTO to determine the updated seismic performance zone.

5.4.3 Bridge Design

The delineated design acceleration response spectrum determined from SSGMRA will be used in place of the general AASHTO design response spectrum in WinSEISAB for performing dynamic analyses, as illustrated in Figure 5.8. DRIVEN can still be used to determine pile capacities with no changes of the soil profile required.

5.4.4 Liquefaction Analysis

The PGA value should be taken as the acceleration at the lowest period shown on the delineated design spectrum (see Figure 5.7), which is typically 0.01 seconds. This value should be used in the spreadsheets utilized by ARDOT to estimate liquefaction potential.

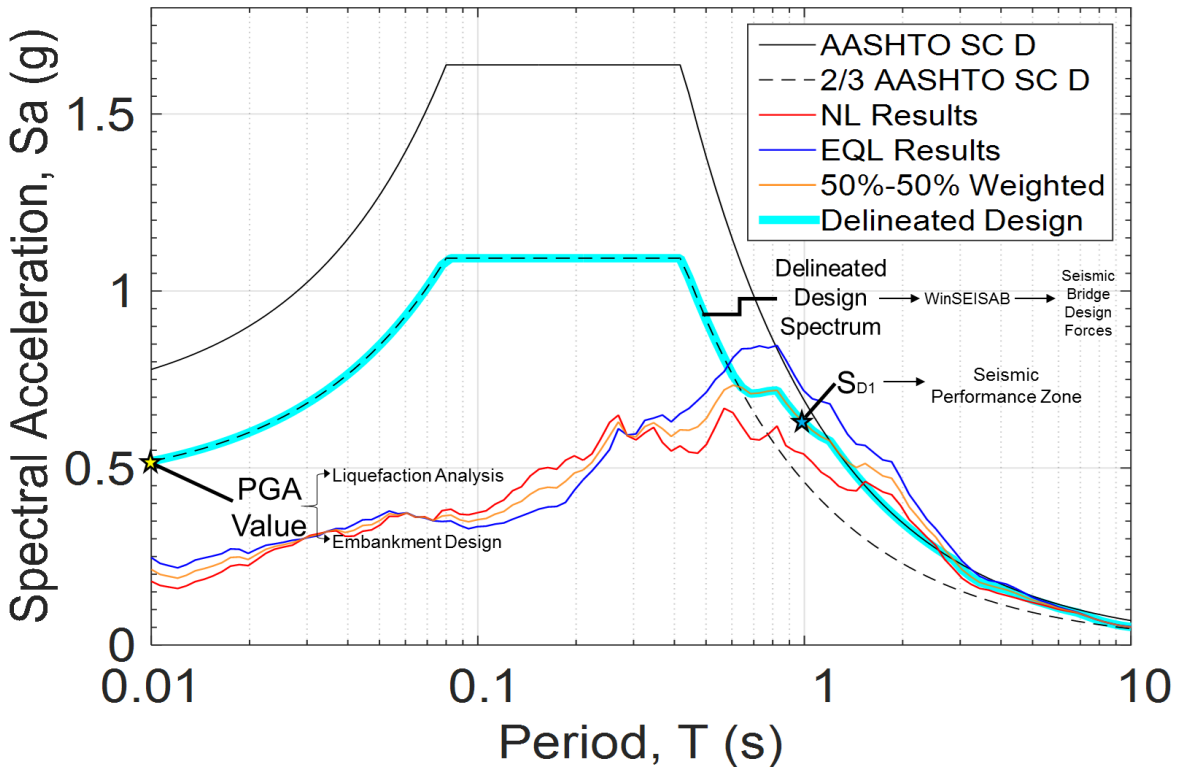

Figure 5. 7: Example updated design acceleration response spectrum determined from SSGMRA with important values highlighted.

5.4.5 Embankment Design

This PGA value is also used in embankment design. As per the ARDOT Materials Division, half of the PGA value taken from the delineated design spectrum will be used in slope stability analysis.

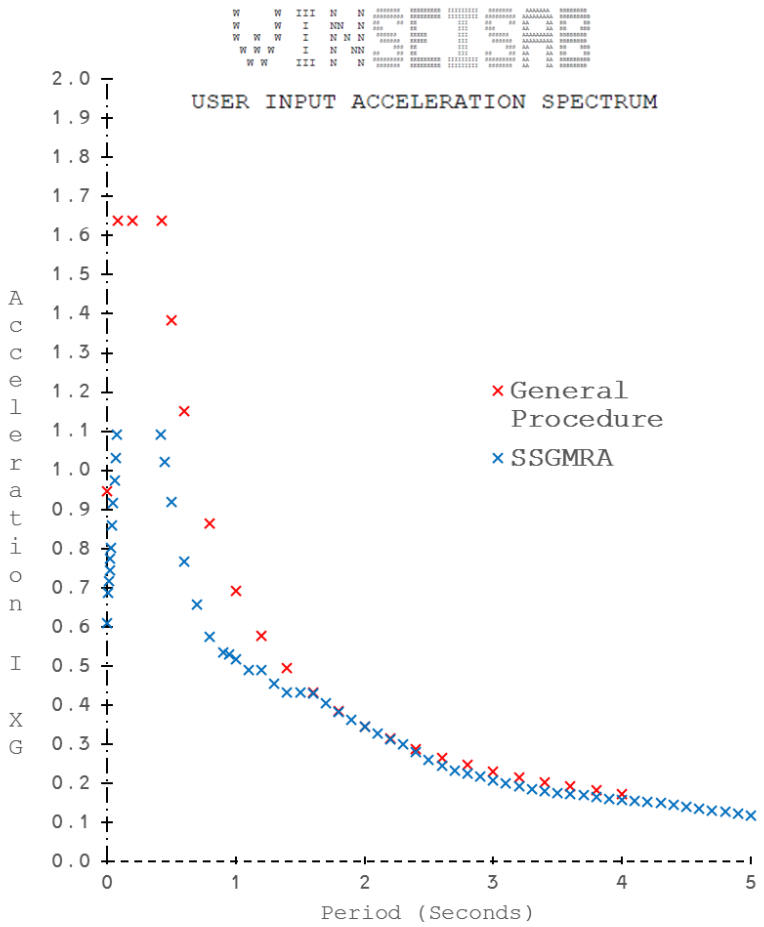

Figure 5. 8: WinSEISAB input acceleration spectrum with general procedure design spectrum (red) versus SSGMRA design spectrum (blue).

CHAPTER 6
SEISMIC BRIDGE DESIGN

6.1 Original Bridge Design Specifications

The superstructure of the Monette bypass bridge, presented in Figure 5.3, consists of a 8.75 inch thick deck slab and nine 327 foot long continuous W36x135, Grade 50W steel girders spaced at 9 foot. The girders are supported by two end stub abutments (termed end-bents herein) and four intermediate pile-bents, and are equipped with bumper bars, which are assumed to transfer the lateral load to the substructure by striking against a steel bumper plate attached to the end bents during seismic excitation.

An important aspect of the composite deck is the concrete restrainer block system, presented in Figure 5.2. The restrainer blocks, the bridge's main ERS, are designed to resist transverse seismic loads. At end abutments, concrete was cast over the first 18 inches of the girders and diaphragms leaving approximately 5 inches of web and bottom flange exposed. Subsequently, four 2 foot-1 inch tall by 4 foot-6 inch wide restrainer blocks were cast on top of the end bents. With this interlocking system of the composite deck and the abutments, transverse movement is restricted during a seismic event.

Nine 18 inch diameter closed end concrete filled steel pipe piles of 0.5 inch wall thickness are integrated into the bottom of each end bent. Similarly, nine 24 inch x 0.5 inch closed end concrete filled steel pipe piles are integrated into the bottom of each of the four intermediate bents.

From WinSEISAB®, a dynamic analysis program that analyzes bridge structures to determine the seismic demand placed on various bridge components (WINSEISAB 2009), the bridge has a longitudinal period of 1.272 seconds and a transverse period of 0.365 seconds before joint lockup. After joint lockup, the longitudinal period changes to 0.360 seconds. The program also outputs mass participation per mode and total accumulated mass participation along with the vibration characteristics of the structure. ARDOT seismic design calculations and dynamic analyses are included in Appendix C.

6.2 Bridge Redesign Based on SSGMRA

Four major components of the bridge project were considered in the seismic redesign: restrainer blocks, columns, piles, and approach embankment. While there may be additional components that would benefit from being redesigned using the post SSGMRA response spectrum, these likely would result in limited cost savings compared to the components mentioned above. The redesign of each of the components used the same ARDOT design methodology as the original project to yield the most accurate cost savings values for the redesign. To maintain the intricacies of the original structure, which is important for the cost-savings analysis, two redesign options were considered that used similar components as the original design. These two options were (1) use 24 inches diameter intermediate bent piles and 18 inches end bent piles (same design as original structure), or (2) downsize the intermediate bent piles to 18 inches diameter piles, which uses only 18 inches piles for the entire structure. These two options are discussed below in detail, and calculations for each are included in Appendix D and Appendix E respectively.

6.2.1 24 in Intermediate Bent Piles

A new dynamic analysis was performed in WinSEISAB® (WINSEISAB 2009) using the delineated design acceleration response spectrum from the SSGMRA. The reduction in notable loads and load effects is outlined in Table 6.1. From this analysis, there is a linear type of relationship between the reduction in design accelerations and some seismic forces/effects. In particular, column axial load, column transverse moment, and lateral force on restrainer blocks were all reduced by approximately 33% (i.e., the same reduction in the short period range of the updated design response spectrum).

Table 6. 1: Load/load effect reduction due to SSGMRA for 24 inch intermediate bent pile design.

Design	**Load/Effect**	**Pre SSGMRA**	**Post SSGMRA**	**Unit**	**% Reduction**	**Location**	**AASHTO Methods/ Criteria**
Restrainer Block Design	$F_{T\ Max}$	2999	1999	*kip*	33.3%	Load Case 4	5.7.5 5.8.3.3 5.8.4
Column Design	P_{max}	330	220	*kip*	33.5%	Bent 3, Column 4, LC 4	6.9.5.1 4.5.3.2.2b 6.12.2.2.3 6.9.2.2 4.7.4.5
	$M_{T\ Max}$	464	309	*kip-ft*	33.3%	Bent 3, Column 4, LC 4	
	$M_{L\ Max}$	124	110	*kip-ft*	11.3%	Bent 2 Column 1, LC3	
Pile Length Design	$P_{required}$	530	432	*kip*	18.5%	Interior Bent Piles (2-5)	
	$P_{required}$	136	130	*kip*	4.2%	End Bent Piles (1,6)	

The reduction in lateral forces on the bridge allowed a reduction in restrainer block size. The height and transverse width of the blocks were reduced while the lateral width of the blocks were not adjusted. From a construction perspective, it is easier to cast the blocks flush with the face of the abutment. The height of the blocks was reduced from 25 inches to 21 inches, and the transverse width was reduced from 54 inches to 35 inches. Shear and moment reinforcement was redesigned considering the reduction in lateral forces, which resulted in a reduction of about 500 lb of rebar.

For the columns, 1/16 inches section loss was assumed due to corrosion or scour. Since the columns were structurally sound as 24 inches diameter piles with the original seismic load, they were satisfactory for the reduced seismic load. The axial pile capacity was then checked while considering the effect of potentially liquefiable layers. With the reduction in PGA, liquefaction hazard was reanalyzed. ARDOT utilizes a deterministic approach for liquefaction analysis. Liquefaction potential was evaluated using SPT blow counts for the Youd *et al.,* (2001), Cetin *et al.,* (2004), and Idriss and Boulanger (2008) methods. However, little difference in potentially liquefiable layers was observed between the methods due to the poor soils at the site. One layer between 20 ft and 25 ft at bent 6 changed from potentially liquefiable (FS<1) to non-liquefiable (FS>1) when considering the reduced SSGMRA PGA. Liquefaction analyses calculations using both the AASHTO general procedure PGA and the SSGMRA PGA can be found in Appendix F.

DRIVEN® (DRIVEN 2001) was used to input the soil profile from boring log information and to determine the pile capacities at given depths. DRIVEN pile capacity calculations can be found in Appendix G. The skin friction resistance of the pile was reduced in layers at which the factors of safety for liquefaction were less than 1.0. Even though there was only small change in the potentially liquefiable layers, the reduction in axial load caused some piles to reach required capacity at shallower depths than in the original design. The intermediate bent pile lengths were reduced by 4 feet each, resulting in a total reduction of 144 feet of 24 inches diameter piling. The greatest length change was estimated at bent 6. The original bent 6 piles reached the required axial capacity at 50 feet. However, since piles are not allowed to bear in liquefiable layers, the design length of these piles had to be extended through the liquefiable layer to 65 feet. The reduced axial load from SSGMRA allowed the piles to reach the required capacities at 42 feet and bear in a dense sand layer. This resulted in a total reduction of 207 feet of 18 inches diameter pipe piling. The complex soil layering at bent 1 prevented any reduction in pile length. It should be noted that the pile length reductions are based on design calculations and true as-built pile lengths may vary. However, the as-built length is likely to be reduced by a similar amount compared to the design lengths due to the decreased axial demand.

6.2.2 18 in Intermediate Bent Piles

The dynamic analysis for the structure with 18 inches diameter intermediate bent piles showed an even larger reduction in column loads than the 24 inches diameter intermediate bent pile structure. However, restrainer block forces and pile forces were not reduced as significantly. The pre and post SSGMRA loads for the 18 inches diameter intermediate bent pile structure are presented in Table 6.2.

Table 6. 2: Load/load effect reduction due to SSGMRA for 18 in intermediate bent pile design.

Design	Load/Effect	Pre SSGMRA	Post SSGMRA	Unit	% Reduction	Location	AASHTO Methods/ Criteria
Restrainer Block Design	$F_{T\ Max}$	2999	2598	*kip*	13.4%	Load Case 4	5.7.5 5.8.3.3 5.8.4
Column Design	P_{max}	330	163	*kip*	50.7%	-	6.9.5.1 4.5.3.2.2b 6.12.2.2.3 6.9.2.2 4.7.4.5
	$M_{T\ Max}$	464	160	*kip-ft*	65.5%	-	
	$M_{L\ Max}$	124	40	*kip-ft*	67.4%	-	
Pile Length Design	$P_{required}$	530	359	*kip*	32.3%	Interior Bent Piles (2-5)	
	$P_{required}$	136	130	*kip*	4.0%	End Bent Piles (1,6)	

Even though the reduction in lateral forces was not as great as for the 24 inch diameter column structure, a reduction in restrainer block size was still achieved. The height of the blocks was reduced from 25 inches to 23 inches, and the transverse width was reduced from 54 inches to 35 inches. There was also a reduction in the reinforcement needed, which amounted to about a 250 lb reduction in rebar.

The axial loads and moments were found for several different columns on respective bents and load cases in order to capture the design load envelope. The magnified moments and flexural resistance of the pile was calculated. Then, the combined axial compression and flexural resistance was checked for the several different columns and load cases. Displacement requirements (P-Δ) were then checked. Other significant limit states, such as Strength I, were also satisfied.

With the large reduction in load/load effects for the columns comes a reduction in section capacity. However, the 18 inch diameter piles were determined to be satisfactory as columns. The designs for the end bents (bents 1 and 6) are the same as those for the 24 inch diameter column redesigned structure. This is due to both end bent piles being 18 inches in diameter for both cases, and the change in seismic load between the two structures is relatively small because of their fully supported lengths. Intermediate pile lengths were reduced by 4 feet each compared to the original pile lengths. Lengths were again reduced for bent 6 piles by about 23 feet compared to the original ARDOT design. Again, pile lengths at bent 1 could not be reduced.

6.2.3 Other Aspects of Bridge Design

It is important to note other bridge aspects that could benefit from reduced seismic demand. In particular, the seismic design of the bridge approach embankments that are designed based on a seismic slope stability analysis. Reducing this design PGA, would provide a potential cost savings. Figure 6.1 shows the reduced embankment reinforcement by using the reduced PGA from SSGMRA. For the original design, slope stability analyses were conducted for the embankments which indicated 8 layers of 9,000 lb/ft geogrid reinforcement on 1 foot vertical spacing and extending 100 feet beyond the abutment were required to satisfy stability requirements. Using the

updated SSGMRA PGA, stability of the embankment was achieved using 4 layers of 2000 lb/ft geogrid reinforcement on 1 foot vertical spacing and extending 100 feet beyond the abutment. This significantly reduced both the quality (lower tensile strength) and quantity (approximately half the area required) of geogrid required for the job.

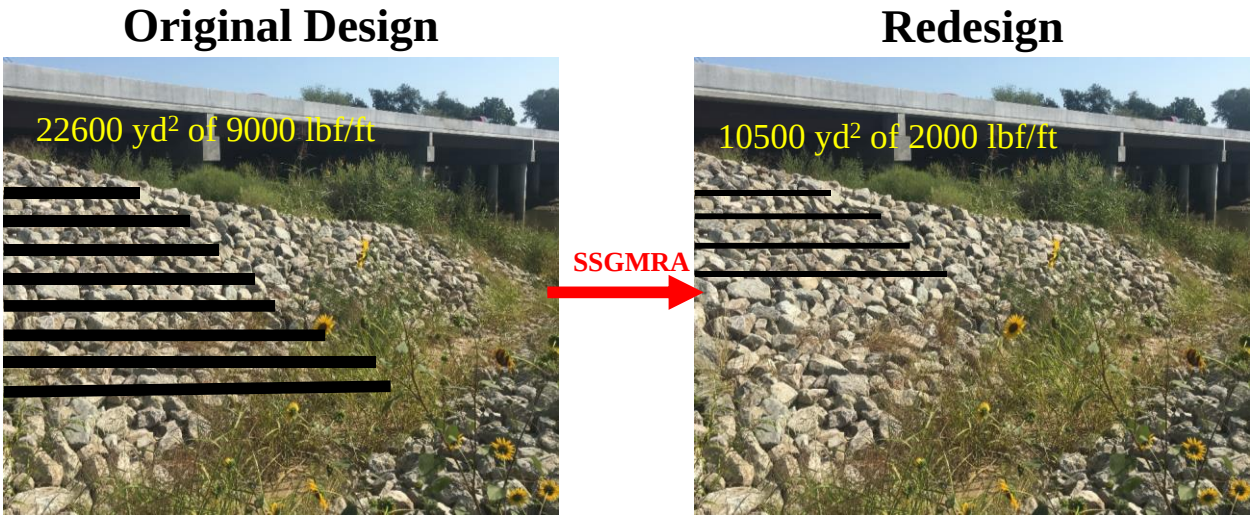

Figure 6. 1: Original embankment reinforcement design versus embankment design after using reduced PGA from SSGMRA.

CHAPTER 7
COST-SAVINGS ANALYSIS

Cost savings analyses was conducted using both redesign options discussed above. Tables 7.1 and 7.2 outline the cost savings for each analysis compared to the original bid items for the 24 inch structure and 18 inch structure, respectively. Cost savings calculations can also be found in Appendix H. The redesign savings, which is directly based on the original bid documents for the structure with 24 inch diameter intermediate piles are outlined in Table 7.1. A total savings of $164,089 was determined for this bridge redesign, which represents a 5.82% reduction in the cost of the project with respect to the original bid. The savings for the structure with 18 inch diameter intermediate piles are listed in Table 7.2. A total savings of $206,992 was determined for this structure, which represents a 7.34% reduction in the cost of the project. These cost reductions are consistent with other findings from Ketchum *et al.*, (2004). The majority of the savings for each structure is from the reduction in pile lengths and sizes as well as the reduction in strength and area of embankment reinforcement. A slight savings from the reduction in restrainer block design was also estimated.

Table 7. 1: Cost savings associated with 24 inch intermediate bent piles bridge redesign. Cost in USD.

Original Design					24" Intermediate Bent Piles			
Quantity	**Unit**	**Item**	**Winning Bid Unit Cost**	**Total**	**Redesign Quantity**	**Unit Cost**	**Total**	**Savings**
1.00	LS	REMOVAL OF EXISTING BRIDGE	$85,000.00	$ 85,000.00				
100.00	CUYD	UNCLASS EXCAVATION FOR STRS-BR	$35.00	$ 3,500.00				
269.40	CUYD	CLASS S CONCRETE-BRIDGE	$705.00	$ 189,927.00	266.131	705	$187,622.36	$ 2,304.64
782.90	CUYD	CLASS S (AE) CONCRETE-BRIDGE	$685.00	$ 536,286.50				
59.80	GAL	CLASS1 PROTECT. SURF. TREATMENT	$150.00	$ 8,970.00				
31960.00	LB	REINF STEEL BRIDGE (GR 60)	$1.20	$ 38,352.00	31460	1.2	$ 37,752.00	$ 600.00
168640.00	LB	EPOXY COATED REINF STEEL (GRADE 60)	$1.10	$ 185,504.00	168140	1.1	$184,954.00	$ 550.00
1080.00	LF	STEEL SHELL PILING (18" DIAM)	$125.00	$ 135,000.00	873	125	$109,125.00	$ 25,875.00
3060.00	LF	STEEL SHELL PILING (24" DIAM)	$140.00	$ 428,400.00	2916.00	140	$408,240.00	$ 20,160.00
687.00	LF	PILE ENCASEMENT	$105.00	$ 72,135.00				
502910.00	LB	STR. STEEL IN BEAM SP. (M 270. GR 50W)	$1.58	$ 794,597.80				
7340.00	CUIN	ELASTOMERIC BEARINGS	$2.00	$ 14,680.00				
156.00	LF	SILICONE JOINT SEALANT	$40.00	$ 6,240.00				
1.00	EACH	BRIDGE NAME PLATE	$1,200.00	$ 1,200.00				
825.00	SQYD	FILTER BLANKET	$3.00	$ 2,475.00				
446.00	CUYD	DUMPED RIPRAP	$48.00	$ 21,408.00				
58.80	CUYD	APPR. GUTTER	$430.00	$ 25,284.00				
240.96	CUYD	APPR. SLABS	$400.00	$ 96,384.00				
40800.00	LB	REINF. STEEL-RDWY	$1.00	$ 40,800.00				
22600	SQYD	EMBANKMENT REINFORCEMENT	$6.00	$ 135,600.00	10500	2	21000	$ 114,600.00
			TOTAL	$2,821,743.30		**TOTAL SAVINGS**		**$164,089.65**
						% OF ORIGINAL COST		**5.82%**

Table 7. 2: Cost savings associated with 18 inch intermediate bent pile bridge redesign. Cost in USD.

Original Design					18" Intermediate Bent Piles			
Quantity	**Unit**	**Item**	**Winning Bid Unit Cost**	**Total**	**Redesign Quantity**	**Unit Cost**	**Total**	**Savings**
1.00	LS	REMOVAL OF EXISTING BRIDGE	$85,000.00	$ 85,000.00				
100.00	CUYD	UNCLASS EXCAVATION FOR STRS-BR	$35.00	$ 3,500.00				
269.40	CUYD	CLASS S CONCRETE-BRIDGE	$705.00	$ 189,927.00	266.503	705	$187,884.62	$ 2,042.38
782.90	CUYD	CLASS S (AE) CONCRETE-BRIDGE	$685.00	$ 536,286.50				
59.80	GAL	CLASS1 PROTECT. SURF. TREATMENT	$150.00	$ 8,970.00				
31960.00	LB	REINF STEEL BRIDGE (GR 60)	$1.20	$ 38,352.00	31710.00	1.2	$ 38,052.00	$ 300.00
168640.00	LB	EPOXY COATED REINF STEEL (GRADE 60)	$1.10	$ 185,504.00	168390.00	1.10	$185,229.00	$ 275.00
1080.00	LF	STEEL SHELL PILING (18" DIAM)	$125.00	$ 135,000.00	3789	125	$473,625.00	$ (338,625.00)
3060.00	LF	STEEL SHELL PILING (24" DIAM)	$140.00	$ 428,400.00	0	140	$ -	$ 428,400.00
687.00	LF	PILE ENCASEMENT	$105.00	$ 72,135.00				
502910.00	LB	STR. STEEL IN BEAM SP. (M 270. GR 50W)	$1.58	$ 794,597.80				
7340.00	CUIN	ELASTOMERIC BEARINGS	$2.00	$ 14,680.00				
156.00	LF	SILICONE JOINT SEALANT	$40.00	$ 6,240.00				
1.00	EACH	BRIDGE NAME PLATE	$1,200.00	$ 1,200.00				
825.00	SQYD	FILTER BLANKET	$3.00	$ 2,475.00				
446.00	CUYD	DUMPED RIPRAP	$48.00	$ 21,408.00				
58.80	CUYD	APPR. GUTTER	$430.00	$ 25,284.00				
240.96	CUYD	APPR. SLABS	$400.00	$ 96,384.00				
40800.00	LB	REINF. STEEL-RDWY	$1.00	$ 40,800.00				
22600	SQYD	EMBANKMENT REINFORCEMENT	$6.00	$ 135,600.00	10500	2	21000	$ 114,600.00
			TOTAL	$2,821,743.30		**TOTAL SAVINGS**		**$206,992.39**
						% OF ORIGINAL COST		**7.34%**

Savings based on each SSGMRA benefit area are shown in Table 7.3. For this site, no savings could be obtained from reevaluating the AASHTO Site Classification based on shear wave velocity because the new classification did not change with respect to the original classification based on blow count. Also, no savings could be attained by reevaluating the AASHTO Seismic Performance Zone. The site is so close to the NMSZ fault system that even a 33% reduction in the S_{D1} value could not reduce the Seismic Performance Zone to the less stringent zones 1 or 2. In addition, since liquefaction was still determined to be likely at the site, performance zone 4 is still required regardless of the updated S_{D1} value.

Table 7. 3: Cost savings associated with each bridge design categorized by SSGMRA benefits.

	Cost Savings for Monette Bridge	
SSGMRA Benefits	24" Column Structure	18" Column Structure
AASHTO Site Classification	-	-
AASHTO Seismic Performance Zone	-	-
Liquefaction Analysis	$0	$0
Bridge Design	$49,489.65	$92,392.39
Embankment Design	$114,600.00	$114,600.00
TOTAL	**$164,089.65**	**$206,992.39**

In order to separate the cost savings benefit of SSGMRA due to reduced seismic demands and due to reduced liquefaction potential, pile design was carried out first using the post-SSGMRA reduced load for axial demand and the pre-SSGMRA PGA of 0.917g for liquefaction analysis. The cost reduction associated with this analysis was attributed to the reduced axial demand. This reduction was compared to a design using the post-SSGMRA reduced load for axial demand and the post-SSGMRA reduced PGA of 0.611g for determining the cost savings associated with the liquefaction analysis.

For both the 24 inch diameter column structure and the 18 inch diameter column structure, no cost savings was attributed to the liquefaction analysis. Only one layer, which is at bent 6 from 20-25 feet, converted from liquefiable to non-liquefiable when considering the reduced PGA from SSGMRA. This layer only provided 7.5 kips more of skin friction capacity when considering the layer as non-liquefiable.

For the 24 inch diameter column structure, the reduction in cost by reducing the pile length was primarily a result of the reduced axial load from SSGMRA. This is illustrated in Figure 7.1 where the design pile lengths are compared for the Original Design (OD), design with Reduced Axial Demand (RAD), and design with Reduced Liquefaction Potential (RLP). For bent 1 piles, the original design piling was tipped at 55 feet. While the pile could reach required axial capacity at 50 feet, the pile was extended to a non-liquefiable layer at 55 feet to insure the pile end bearing was in a non-liquefiable layer. With the reduced axial demand from SSGMRA in the RAD analysis, the piles could have been tipped at 45 feet. However, this would put their tips directly at

the interface of a liquefiable layer. Therefore, the piles were extended past the liquefiable layer to 55 feet. Therefore, the complex layering at Bent 1 prevented any cost savings.

For intermediate piles (Bents 2-5), the original design required the piles extend to 90 feet to reach the required axial capacity. The reduced axial demand from SSGMRA allowed the piles to be tipped at 86 feet resulting in some cost savings.

The biggest length change was estimated at Bent 6. The original Bent 6 piles reached the required axial capacity at 50 feet. However, since piles are not allowed to bear in liquefiable layers, they had to be extended through the liquefiable layer to 65 feet. The reduced axial load from SSGMRA allowed the piles to reach the required capacities at 42 feet.

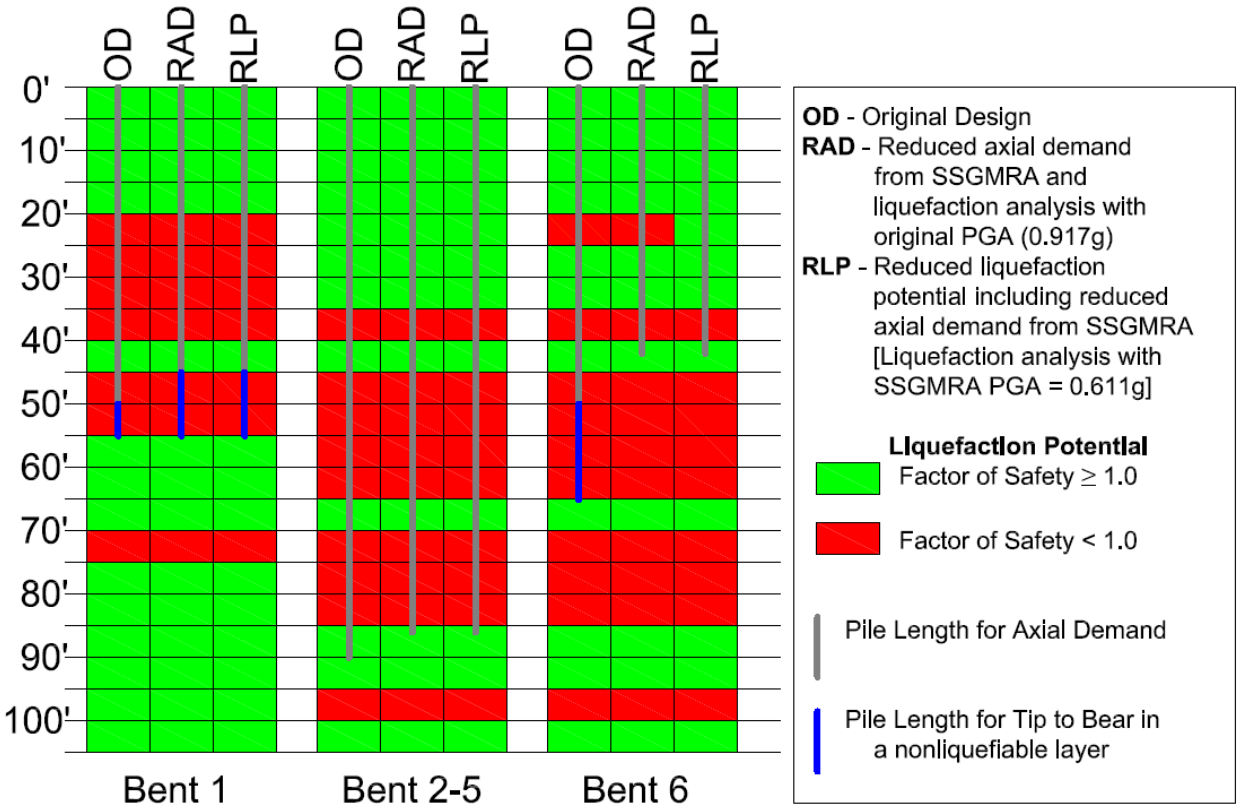

Figure 7. 1: Comparison of pile lengths for 24" intermediate pile structure.

For the 18 inch diameter column structure, the reduction in cost by reducing the pile length was also primarily a result of the reduced axial loads. No cost savings was achieved due to the liquefaction analysis.

The design cases for the end bents (bents 1 and 6) are the same as those for the 24 inch diameter column structure. This is due to all end bent piles being 18 inches in diameter for both cases, and the change in seismic load between the two structures is relatively small because of their fully

supported lengths. If the original structure were designed using 18 inch piles, the lengths of the intermediate piles would need to be 100 feet to achieve the required skin friction. The additional length for the 18 inch piles is required because of the lower surface area of the 18 inch piling compared to the 24 inch piling, resulting in a lower skin friction per foot of pile. However, when considering the reduced axial demand due to SSGMRA, the pile lengths could be reduced to 86 feet. This scenario is illustrated in Figure 8.2.

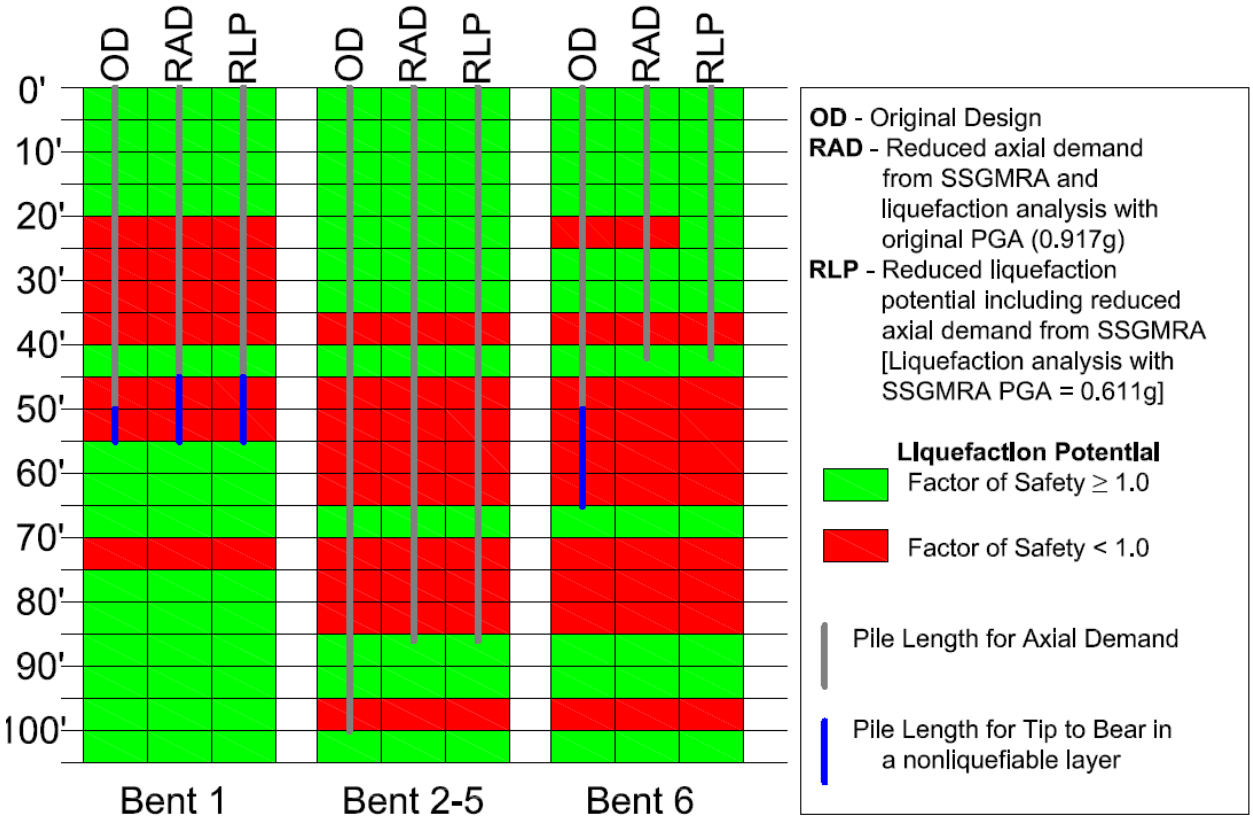

Figure 7. 2: Comparison of pile lengths for 18" intermediate pile structure.

Embankment design savings were calculated by comparing the pre-SSGMRA Geogrid requirements with the post-SSGMRA requirements. Slope stability analyses were performed by the ARDOT Geotechnical Section for both cases. With the pre-SSGMRA PGA of 0.917g, 8 layers of Geogrid of T_{allow}=9000 lbf/ft on a 2 feet vertical spacing were needed. For the post-SSGMRA PGA of 0.611g, only 4 layers of Geogrid of T_{allow}=2000lbf/ft on a 2 feet vertical spacing were needed. Based on information provided by Tensar, a geotechnical company specializing in Geogrid production and applications, a unit cost of $6/SY was used for the 9000 lbf/ft Geogrid and a unit cost of $2/SY was used for the 2000lbf/ft Geogrid. Ultimately, this resulted in a $114,600 savings for embankment design.

From the findings of this research, a gross cost savings of approximately $200,000 was estimated for the Monette, AR bridge as a results of performing SSGMRA. Assuming an average

savings of $200,000 per bridge, and considering an average of 20 bridges built per year in Arkansas seismic regions (based on ARDOT data from January 2005-December 2014 for bridges in Districts 1,2,5,6, and 10), performing SSGMRA could potentially result in a $4,000,000 per year savings for ARDOT. Originally, Ketchum *et al.,* (2004) noted that bridges that have a design PGA of 0.3g-0.4g will not benefit from SSGMRA, which limited the areas where SSGMRA could be used to lower bridge cost to areas of very high seismic demands. However, this may not be the case for many Arkansas bridges in the Mississippi Embayment. In Ketchum *et al.,* (2004) study, only the reduction in the size of individual elements was considered. While this may be appropriate for determining changes in bridge structural cost, this does not consider the potential cost savings which can be achieved due to other less straight forward elements. For example, a reduction in PGA, even if only from 0.3g, could potentially cause some soil layers to change from liquefiable to non-liquefiable. Also, the reduction could cause the site to change from a seismic performance zone of 4 or 3 to 2 or 1. This can have a large impact in the overall cost of the bridge project.

Compared to the Monette site, we expect a larger benefit from SSGMRA for sites where soil conditions, especially liquefaction potential, are more reasonable (i.e., factors of safety closer to one). For example, several soil layers at the Monette site had very low factors of safety against liquefaction. Sites with denser sands layers or lower pre-SSGMRA PGA values, which may potentially liquefy under the pre-SSGMRA PGA, may change to layers unlikely to liquefy under the post-SSGMRA lower PGA value. In other words, the likelihood of seeing benefit at sites where the factor of safety against liquefaction is low (i.e. FS < 0.2) is not as great as if the factor of safety were closer to 1.0 (i.e. FS > 0.6 – 0.7).

For long period bridges (i.e. bridge with long spans and a natural period range between 1.5 seconds and 10 seconds), the SSGMRA may result in higher accelerations at the bridge natural period. In these cases, it is acceptable to use the AASHTO code based general acceleration design spectrum instead of the higher SSGMRA spectrum. However, actual ground motions produced by the design earthquake will likely be more similar to those predicted by the SSGMRA. The AASHTO code even warns that at deep, soft soil sites, long period bridges may be under-designed at a significant risk if the general procedure is used to obtain the design response spectrum. Therefore, using the higher SSGMRA design response spectrum could be warranted. However, most ARDOT bridges in NEA are considered to be short period structures.

There are a number of complex factors that play a role in determining if SSGMRA will provide a cost-savings benefit. Assuming that a significant cost-savings will come from reduced design accelerations alone may be true in some instances, but for most cases, several other considerations must be taken in determining the value in performing SSGMRA. These complex variables include the magnitude of PGA, the S_{D1} value used in determining seismic performance zone, soil liquefaction resistance at depth, bridge length and structural type, foundation type, and depth to competent soil layers among others. Further studies are needed to determine the sensitivity of all of these factors and their roles in cost-savings associated with SSGMRA.

CHAPTER 8
SUMMARY OF CONCLUSIONS AND RECOMMENDATIONS

Dynamic site characterization testing was conducted at 15 sites located throughout Northeast Arkansas. These sites were chosen based on the location of current or potential ARDOT bridge job locations. However, if the area near or around the job site could not accommodate testing (i.e., too urban, poor soil conditions, no landowner permission) or there was another job site within close proximity, other locations were explored. An attempt was also made to distribute the sites across Northeast Arkansas as much possible to understand the distribution of dynamic soil properties across in the region and aid in the development of the 3D velocity model of the area. From the sites tested, only the Mounds and Harrisburg sites were not located in close proximity to an ARDOT job. These sites were tested to provide a more consistent distribution across the Northeast Arkansas area.

Dynamic site characterization at each site was conducted using a number of methods including P-wave refraction, active source multi-channel analysis of surface waves (MASW), and passive source microtremor array measurements (MAM). P-wave refraction was conducted at each of the testing locations to help locate the water table (i.e., line of saturation) below the surface. Active source MASW utilizing both Rayleigh and Love type surfaces waves was also conducted at each site using a sledgehammer source to understand the dynamic properties of the very near surface materials. The use of both Rayleigh and Love type surface waves increases the robustness of the testing and helps ensure the correct mode assignments are made during the analysis process (Wood *et al.,* 2014). At select sites, Rayleigh wave MASW was conducted using a Vibroseis source in order to develop deeper active source dispersion data for comparison with passive source dispersion data.

Passive source testing (MAM) was conducted at each of the testing sites to understand the dynamic properties of the soil and rock layers at deeper depths. At each site, 2D circular arrays of 10 broadband sensors with diameters of 50, 200, and 500 meters were used to measure microtremors (i.e., background noise). At select sites, 1000 meter diameter circular arrays were used for comparison with the smaller diameter arrays. Also at select sites, an L-array of geophones were used for passive surface testing in addition to the circular arrays. For each site, a common center point for the circular arrays was maintained where possible. The P-wave refraction, active MASW (Rayleigh and Love) using a sledgehammer source, and L-array passive testing was conducted near the center point of the circular array where possible. Testing around a common midpoint helps reduce the influence of lateral variability on surface wave measurements and ensure each method is measuring similar soil and rock properties. The active MASW testing using a Vibroseis source was often conducted away from the center of the array due to site constraints (i.e., the vibroseis truck could not access locations away from roads). Therefore, testing was often conducted on the nearest farm or public road to the center of the array.

Both Rayleigh wave and Love wave dispersion curves and HVSR peaks were developed at each project site. This data were used in a multi-modal joint inversion to determine the Vs profile from the surface to bedrock at each site. Using the Vs profiles at each site, reference Vs profiles were developed for each geologic layer in the Mississippi Embayment. The reference Vs profiles along with the 3D geologic model of the Embayment were used to develop the UA_MEVM. This model was packaged into a simple to use executable (UA_MEVM.exe), which is provided as a

distributable with this report. A discussion is provided for recommendations on performing shallow (<30 meters) V_s characterization and combining these with the deep profiles generated in the model for preliminary SSGMRA.

The V_s profiles developed to bedrock (depth of 680 meters) at a Monette, Arkansas ARDOT bridge site were used to conduct a SSGMRA for the bridge site using a combination of equivalent linear and completely nonlinear site-response analyses in DEEPSOIL in accordance with AASHTO 3.10.2.2. The results from both analyses demonstrate the attenuation of high frequency seismic waves and the amplification of long period waves within the deep sediments of the Mississippi Embayment. This attenuation at short periods lead to a reduction of 1/3 in the design acceleration response spectrum in the short period range (<1.0 seconds) for the bridge (AASHTO lower bound limit of 2/3 of the general procedure design response spectrum Monette, Arkansas site). Using the updated design response spectrum from SSGMRA, several aspects of the bridge were redesigned including the restrainer blocks, bents/columns, piles and pile lengths, and approach embankments. For each aspect, the size and/or quantity of the design element was able to be reduced. Using the original unit bid prices a cost-savings analysis was conducted. The majority of the cost savings associated with conducting a SSGMRA was related to reducing the length/size of piling for the bridge (~$90,000 savings) and a reduction in the quantity and quality of geogrid required to reinforce the approach embankment (~$114,000 savings). This resulted in a total gross potential cost-savings for the Monette bridge of $205,000 or approximately 7% of the original bid price of the project.

While this demonstrates the significant potential cost savings associated with conducting a SSGMRA for bridges located in the Mississippi Embayment, there are a number of complex factors that play a role in whether a SSGMRA will provide a cost-savings benefit to a project. Assuming that a significant cost-savings will be achieved for all Mississippi Embayment bridges is not appropriate. Complex variables including the magnitude of the PGA, the S_{D1} value used in determining seismic performance zone, soil liquefaction potential, bridge length and structural type, foundation type, depth to bedrock, and other items all play a role in determining the benefit of conducting a SSMGRA. Additional research is needed to determine the detailed influence of these parameters on the potential cost savings of conducting a SSGMRA.

REFERENCES

Aki, K. (1957). Space and time spectra of stationary stochastic waves, with special reference to microtremors. Bull Earthq Res Inst 35:415–456

American Association of State Highway and Transportation Officials (AASHTO), (2009). Guide Specifications for LRFD Seismic Bridge Design, 1st ed., AASHTO, Washington, D.C.

American Association of State Highway and Transportation Officials (AASHTO), (2012) AASHTO LRFD Bridge Design Specifications, 2st ed., AASHTO, Washington, D.C.

American Association of State Highway and Transportation Officials (AASHTO). (2014) "AASHTO LRFD Bridge Design Specifications," 7th ed., Washington, D.C.

American Association of State Highway and Transportation Officials (AASHTO). (2011) "Guide Specifications for LRFD Seismic Bridge Design," 2nd ed. Washington, D.C.

Arkansas Geological Survey. (2017) "Three Centuries of Earthquakes in Arkansas from 1699 through 2016," http://www.geology.ar.gov/maps_pdf/geohazards/Arkansas_Seismicity_Map.pdf

ASTM International. (2014). ASTM D7400-14 Standard Test Methods for Downhole Seismic Testing. Retrieved from https://doi.org/10.1520/D7400-14

ASTM International. (2014). ASTM D4428/D4428M-14 Standard Test Methods for Crosshole Seismic Testing. Retrieved from https://doi.org/10.1520/D4428_D4428M

Bakun, W.H. and Hopper, M.G. (2004). "Magnitude and locations of the 1811-1812 New Madrid, Missouri and the 1886 Charleston, South Carolina, Earthquakes", Bulletin of the Seismological Society of America, 94(1), 64-75.

Beekman, A. N. (2008). "A comparison of experimental ReMi measurements with various source, array, and site conditions" (Masters Thesis). University of Arkansas, Fayetteville, USA.

Bettig, B., Bard, P.Y., Scherbaum, F., Riepl, J., Cotton, F., Cornou, C., and Hatzfield, D. (2001) "Analysis of dense array noise measurements using the modified spatial auto correlation method (SPAC): application to the Grenoble area." Bollettino de Geofisica Teoria e Applicata, 42(3-4), 281-304.

Brahana, J.V., W.S. Parks, and M.W. Gaydos. (1987). Quality of Water from Freshwater Aquifers and Principal Well Fields in the Memphis Area, Tennessee. USGS Water-Resources Investigations Report 87-4052.

Capon, J. (1969) "High Resolution Frequency-Wavenumber Spectrum Analysis," Proceedings of IEEE, 57(8), 1408–1418.

Cetin, K.O., Seed, R.B., Kiureghain, A.D., Tokimatsu, K., Harder, L.F., Kayen, R.E., and Moss, R.E.S. (2004) "Standard Penetration Test-Based Probabilistic and Deterministic Assessment of Seismic Soil Liquefaction Potential," Journal of Geotechnical and Geoenvironmental Engineering 130(12), 1314-1340.

Coduto, D. P. (1999) Geotechnical Engineering: Principles and Practices, Prentice-Hall, Inc. Upper Saddle River, New Jersey 07458, 320.

Cox, B. R., & Beekman, A. N. (2011) "Intramethod variability in ReMi dispersion measurements and Vs estimates at shallow bedrock sites," Journal of Geotechnical and Geoenvironmental Engineering, 137(4), 354-362. DOI: 10.1061/(ASCE)GT.1943-5606.0000436.Cox, B.R., Ellis, T.B., and Griffiths, S.C. (2012) "Site-Specific Seismic Ground Motion Analyses for Transportation Infrastructure in the New Madrid Seismic Zone," Mack-Blackwell Rural Transportation Center. <http://ww2.mackblackwell.org/web/research/ALL_RESEARCH_PROJECTS/3000s/3032/MBTC-3032FinalReport.pdf>

Cox, B. Wood, C., Ellis, T., Teague, D. (2014). Synthesis of the UTexas1 Surface Wave Dataset Blind-Analysis Study: Inter-Analyst Dispersion and Shear Wave Velocity Uncertainty. 2014 Geo-Congress: Geo-Characterization and Modeling for Sustainability. Feb. 23-26, 2014, 850-859.

Cox, B.R., Teague, D.P. (2016). "Layering Ratios: A Systematic Approach to the Inversion of Surface Wave Data in the Absence of A-priori Information," Geophysical Journal International, 207, 422-438. (DOI: 10.1093/gji/ggw282).Cox, B., Wood, C. (2011) "Surface wave benchmarking exercise: methodologies, results, and uncertainties." GeoRisk 2011: Geotechnical Risk Assessment and Management. 845-852

Cramer, C.H., Gomberg, J.S., Schweig, E.S., Waldron, B.A., and Tucker, K. (2004) "The Memphis, Shelby County, Tennessee, Seismic Hazard Maps," U.S. Geological SurveyOpen File Report 2004-1294.

Crice, D., 2011. Near-surface, downhole shear-wave surveys: A primer. The Leading Edge, 30, 164-171.

Csontos, R. (2007). Three dimensional modeling of the Reelfoot Rift and New Madrid Seismic Zone. PhD Thesis, University of Memphis, Tennessee, 94 pp.

Darendeli, M. (2001) "Development of a New Family of Normalized Modulus Reduction and Material Damping Curves," Ph.D. Dissertation, Civil Engineering Dept., University of Texas, Austin, Texas.

Dart, R.L. (1995) "Maps of upper Mississippi Embayment Paleozoic and Precambrian Rocks, U.S. Geologic Survey, Miscellaneous. Field Study Map, MF-2284, 235-249.

Data Physics Corporation. (2016). SignalCalc Mobilyzer. Products and Solutions. <http://www.dataphysics.com/products-and-solutions/dynamic-signal-analyzers signalcalc/signalcalc-mobilyzer.html>.

Deschenes, M., Wood, C., Wotherspoon, L., Bradley, B., Thomson, E. (2018) "Development of deep shear wave velocity profiles in the Canterbury Plains, New Zealand," Earthquake Spectra (in review).

DRIVEN (1.2) (2001). Computer software. Logan, UT: Blue-Six Software, Inc. Federal Highway Administration.

Dunkin, J.W. (1965) "Computation of modal solutions in layered, elastic media at high frequencies," Bulletin of the Seismological Society of America, 55, 335–358.

Foti, S., Lai, C., Rix, G., and Strobbia, C. (2014). "Surface Wave Methods for Near-Surface Site Characterization. Boca Raton, FL: CRC Press.

Geometrics. (2017). Geode Ultra-Light Exploration Seismograph. Products > Seismographs. < http://www.geometrics.com/geometrics-products/seismographs/geode/>.

Goetz, R.P. (2009). Study of the Horizontal-to-Vertical Spectral Ratio (HVSR) Method for Characterization of Deep Soils in the Mississippi Embayment. Master's Thesis. University of Missouri-Columbia.

Gomberg, J., B. Waldron, E. Schweig, H. Hwang, A. Webbers, R. Van Arsdale, K. Tucker, R. Williams, R. Street, P. Mayne, W. Stephenson, J. Odum, C. Cramer, R. Updike, R. Hutson, and M. Bradley (2003). Lithology and shear velocity in Memphis, Tennessee. Bull. Seismol. Soc. Am. 93, 986–997.

Griffiths, S.C., Cox, B.R., Rathje, E.M. (2016) "Challenges associated with site response analyses for soft soils subjected to high-intensity input ground motions," Soil Dynamics and Earthquake Engineering 85, 1-10.

Griffiths, S.C., Cox, B.R., Rathje, E.M., Teague, D.P. (2016) "Mapping Dispersion Misfit and Uncertainty in V_s Profiles to Variability in Site Response Estimates," Journal of Geotechnical and Geoenvironmental Engineering 142(11), 04016062 1-12.

Groholski, D.R., Hashash, Y.M.A, Kim, B., Musgrove, M., Harmon, J., Stewart, J. (2016). "Simplified Model for Small-Strain Nonlinearity and Strength in 1D Seismic Site Response Analysis," Journal of Geotechnical and Geoenvironmental Engineering 142(9), 04016042 1-14.

Hancock, J., Watson-Lamprey, J., Abrahamson, N., Bommer, J.J., Markatis, A., McCoy, E., Mendis, R. (2006) "An Improved Method of Matching Response Spectra of Recorded Earthquake Ground Motion Using Wavelets," Journal of Earthquake Engineering 10(1), 67-89.

Hardeman, W. D. (1966). Geologic map of Tennessee west sheet. State of Tenn. Dept. of Conserv. Div. of Geol., scale 1:250,000

Harris, J.B., Street, R.L., Kiefer, J.D., Allen, D.L., Wang, Z.M. (1994) "Modeling Site Response in the Paducha, Kentucky Area," Earthquake Spectra 10(3), 519-538.

Hart, R.M., Clark, B.R., and Bolyard, S.E. (2008). Digital Surfaces and Thicknesses of Selected Hydrogeologic layers within the Mississippi Embayment Regional Aquifer Study (MERAS): U.S. Geological Survey Scientific Investigations Report 2008-5098, 33 p.

Hashash, Y.M.A., Musgrove, M.I., Harmon, J.A., Groholski, D.R., Phillips, C.A., and Park, D. (2016) "DEEPSOIL 6.1, User Manual".

Hashash, M.A., Park, D. (2001) "Non-linear one-dimensional seismic ground motion propagation in the Mississippi Embayment," Engineering Geology 62, 185-206.

Hashash, Y., Phillips, C. and Groholski, D. (2010) "Recent Advances in Non-Linear Site Response Analysis," Proc. of the Fifth International Conference on Recent Advances in Geotechnical Earthquake Engineering and Soil Dynamics, San Diego, California, OSP 4 22 pp.

Haskell, N. A. (1953) “The dispersion of surface waves on multilayered media, Bulletin of Seismological Society of America,” 43, 17–34.

Hayati, H., and Andrus, R.D. 2009. Updated liquefaction resistance correction factors for aged sands, *Journal of Geotechnical and Geoenvironmental Engineering*, 135(11): 1683-1692.

Hosman, R. L. (1996). Regional stratigraphy and subsurface geology of Cenozoic deposits, Gulf Coastal Plain, south-central United States. U.S. Geol. Surv. Profess. Pap. 1416-G, 35

Idriss, I. M., and Boulanger, R. W. (2008) "Soil Liquefaction during Earthquakes," Earthquake Engineering Research Institute, MNO- 12.

Ketchum, M., Chang, V., and Shantz, T., (2004). Influence of Design Ground Motion Level on Highway Bridge Costs, Report No. Lifelines 6D01, Pacific Earthquake Engineering Research (PEER) Center, University of California, Berkeley.

Kim, B., Hashash, Y.M.A., Stewart, J.P., Rathje, E.M., Harmon, J.A., Musgrove, M.I., Campbell, K.W., Silva, W.J. (2016) “Relative Differences between Nonlinear and Eqivalent-Linear 1-D Site Response Analyses,” Earthquake Spectra 32(3), 1845-1865.

Knopoff L. (1964) “A matrix method for elastic wave problems. Bulletin of Seismological Society of America,” 54, 431–438.

Kramer, S.L., Arduino, P., Sideras, S.S. (2012) “Earthquake Ground Motion Selection,” Washington State Transportation Center, <https://www.wsdot.wa.gov/research/reports/fullreports/791.1.pdf>

Ketchum, M., Chang, V., and Shantz, T. (2004) “Influence of Design Ground Motion Level on Highway Bridge Costs,” Pacific Earthquake Engineering Research (PEER) Center, Report No. Lifelines 6D01, University of California, Berkeley, California.

Lin, Y. C., Joh, S. H, and Stokoe, K. H. (2014) “Analyst J: Analysis of the UTexas 1 Surface Wave Dataset Using the SASW Methodology,” Geo-Congress 2014 Technical Papers: Geo-Characterization and Modeling for Sustainability. GSP 234. 2014.

Liu, W., Stephenson, W. (2004) “Seismic Reponse of Two Specific Sites in the New Madrid Seismic Zone,” Geotechnical Engineering for Transportation Projects (GeoTrans). Los Angeles, California, pp. 1682-1690.

Malekmohammadi, M., Pezeshk, S. (2015) “Ground Motion Site Amplification Factors for Sites Located within the Mississippi Embayment with Consideration of Deep Soil Deposits,” Earthquake Spectra 31(2), 699-722.

McGuire, R.K., Silva, W.J., Costantino, C.J. (2001) “Technical Basis for Revision of Regulatory Guidance on Design Ground Motions: Hazard- and Risk- consistent Ground Motion Spectra Guidelines,” NUREG/CR – 6728. <https://www.nrc.gov/docs/ML0131/ML013100012.pdf>

Mento, D.J., Ervin, C.P., McGinnis, L.D. (1986) “Periodic energy release in the New Madrid seismic zone,” Bulletin of the Seismological Society of America 76, 1001-1009.

Nanometrics. (2017). Centaur. Products > Digitizers. < http://www.nanometrics.ca/seismology/products/digitizers/centaur>.

Nanometrics. (2017). Trillium Compact Broadband Seismometer. Products > Broadband Seismometers. < http://www.nanometrics.ca/seismology/products/trillium-compact>.

NEHRP Consultants Joint Venture. (2011) “Selecting and Scaling Earthquake Ground Motions for Performing Response-History Analyses,” NIST GCR 11-917-15.

Nogoshi M. and T. Igarashi, (1971). On the amplitude characteristics of microtremor (part 2) (in japanese with english abstract). Jour. Seism. Soc. Japan, 24, 26-40.

Park, C.B., Miller, R.D. and Xia, J. (1999) “Multichannel analysis of surface waves.” Geophysics 64(3), 800-808.

Park, D. and Hashash, Y., (2005). Evaluation of Seismic Site Factors in the Mississippi Embayment. I. Estimation of Dynamic Properties. Soil Dynamics and Earthquake Engineering, Vol. 25, pp. 133 – 144.

Phillips, C., & Hashash, Y. M. A. (2009). Damping formulation for nonlinear 1D site response analyses. *Soil Dynamics and Earthquake Engineering*, *29*(7), 1143-1158. https://doi.org/10.1016/j.soildyn.2009.01.004

Ramírez-Guzmán, L., Boyd, O., Hartzell, S., Williams, R. (2012), “Seismic velocity model of the central United States (Version 1): Description and simulation of the 18 April 2008 Mt. Carmel, Illinois, Earthquake,” Bulletin of the Seismological Society of America, 2622-2645. <http://pubs.er.usgs.gov/publication/70045157>.

Rathje, E.M., Kottke, A.R., Trent, W.L. (2010) “Influence of Input Motion and Site Property Variabilities on Seismic Site Response Analysis,” Journal of Geotechnical and Geoenvironmental Engineering 136(4), 607-619.

Redpath, B.B. (1973). Seismic Refraction Exploration for Engineering Site Investigations, Explosive Excavation Research Laboratory, distributed by NTIS.

Redpath, Bruce B. Downhole Measurements of Shear- and Compression-Wave Velocities in Boreholes C4993, C4996, C4997 and C4998 at the Waste Treatment Plant DOE Hanford Site., report, April 27, 2007; Richland, Washington. (digital.library.unt.edu/ark:/67531/metadc891343/: accessed December 4, 2017), University of North Texas Libraries, Digital Library, digital.library.unt.edu; crediting UNT Libraries Government Documents Department.

Rix, G., Hebeler, G. L., and Orozco, M. C. (2002). Near-surface Vs profiling in the New Madrid seismic zone using surface-wave methods. Seismol. Res. Lett., 73(3), 380–392.

Rogers, D. J., Karadeniz, D., Kaibel, C.K. (2007) “Seismic Site Response Modeling for Three Missouri River Highway Bridges,” Journal of Earthquake Engineering 11, 400-424.

Romero, S.M., Rix, G.J. (2001) “Ground Motion Amplification of Soil in the Upper Mississippi Embayment,” National Science Foundation Mid America Center, GIT-CEE/GEO-01-1, Atlanta, Georgia.

Romero, S.M., Rix, G.J. (2005). Ground Motion Amplification of Soil in the Upper Mississippi Embayment. GIT-CEE/GEO-01-1, National Science Foundation Mid America Center, Atlanta.

Rosenblad, B. (2008). Deep shear wave velocity profiles of Mississippi Embayment sediments determined from surface wave measurements. U.S. Geol. Surv. Final Tech. Rept., USGS NEHRP Award No. 06HQGR0131, 23 pp.

Rosenblad, B., Goetz, R. (2009) “Study of the Horizontal-to-Vertical Spectral Ratio (HVSR) Method for Characterization of Deep Soils in the Mississippi Embayment,” Masters Thesis, University of Missouri-Columbia, 154.

Rosenblad, B., Li, J. (2009). Performance of Active and Passive Methods for Measuring Low-Frequency Surface Wave Dispersion Curves. Journal of Geotechnical and Geoenviornmental Engineering. Feb 14, 2009, 1419-1428.

Rosenblad, B., Bailey, J., Csontos, R. and Van Arsdale, R. (2010) “Shear Wave Velocities of Mississippi Embayment Soils from Low Frequency Surface Wave Measurements,” Soil Dynamics and Earthquake Engineering 30, 691 – 701.

Russell, E. E., D. M. Keady, E. A. Mancini, and C. E. Smith (1982). Upper Cretaceous in the lower Mississippi Embayment of Tennessee and Mississippi: lithostratigraphy and biostratigraphy. Field trip guidebook for the 1982 annual meeting of the Geol. Soc. Am., New Orleans, Louisiana, 40.

SESAME, (2004) “Guidelines for the implementation of the H/V spectral ratio technique on ambient vibrations: measurements, processing and interpretation,” <http://sesamefp5.obs.ujfgrenoble.fr/Delivrables/Del-D2>

Stewart, J.P., Kwok, A.O.-L., Hashash, Y.M.A., Matasovic, N., Pyke, R., Wang, Z., Yang, Z. (2008) “Benchmarking of Nonlinear Geotechnical Ground Response Analysis Procedures,” PEER Report 2008/04, Pacific Earthquake Engineering Research Center, University of California, Berkeley, 186 pp.

Street, R., E. W. Woolery, and J.-M. Chiu (2004). Shear-wave velocities of the post-Paleozoic sediments across the Upper Mississippi Embayment. Seismol. Res. Lett. 75, no. 3, 390–405.

Thomson, W. T. (1950) “Transmission of elastic waves through a stratified solid medium, Journal of Applied Physics,” 21, 89–93.

Tokimatsu, K., Shinzawa, K., and Kuwayama, S. (1992). “ Use“Use of short-period microtremors for Vs profiling.” Journal of Geotechnical Engineering, Vol. 118 (10): 1544-1558.

Tokimatsu K (1997) Geotechnical site characterization using surface waves. In: Ishihara (ed). Proc. 1st Intl. Conf. Earthquake Geotechnical Engineering vol 3. Balkema, pp 1333–1368.

Toro, G. (1995). “Probabilistic models of the site velocity profiles for generic and site–specific ground–motion amplification studies.” Technical Rep. No. 779574, Brookhaven National Laboratory, Upton, NY.

Tran, K.T. and Hiltunen D.R. (2008). A comparison of shear wave velocity profiles from SASW, MASW, and ReMi techniques. Proc., Geotechnical Earthquake Engineering and Soil Dynamics, Geotechnical Special Publication 181 (CD-ROM), ASCE, Reston, VA.

Tuttle, M.P., Schweig, E.S., Sims, J.D., Lafferty, R.H., Wolf, L.W., and Haynes, M.L. (2002). “The earthquake potential of the New Madrid seismic zone,” Bulletin of the Seismological Society of America, 92, 2080-2089.

U.S. Geological Survey (1960). Ground-Water Potential of Mississippi County, Arkansas. Water Resources Circular No. 7. Little Rock, AR. 1960.

USGS National Earthquake Information Center (2011). M7.7 New Madrid Earthquake Scenario of 16 May 2011. May 16, 2011. <http://earthquake.usgs.gov/eqcenter/eqarchives/poster/>.

Van Arsdale, R.B., TenBrink, R.K. (2000) "Late Cretaceous and Cenozoic Geology of the New Madrid Seismic Zone," Bulletin of the Seismological Society of America 90, 345–356.

Van Arsdale, R.B., R.A. Williams, E.S. Schweig, K.M. Shedlock, J.K. Odum, and K.W. King. (1995). The Origin of Crowley's Ridge, Northeastern Arkansas: Erosional Remnant or Tectonic Uplift? Bulletin of the Seismological Society of America, Vol. 85, No. 4, pp. 963-985.

Wang, Z. Zeng, X., Woolery, E., Street, R., Ni, B. (1996) "A Comprehensive Geological and Geotechnical Study on Site Response At Selected Sites in the New Madrid Seismic Zone," Eleventh World Conference on Earthquake Engineering. Paper No. 1631.

Wathelet, M., Jongmans, D., Ohrnberger, M., Bonnefoy-Claudet, S. (2008), "Array performances for ambient vibrations on a shallow structure and consequences over V_s inversion," Journal of Seismology 12, 1-19.

WINSEISAB (v5.0.8) (2009). Computer software. Rancho Cordova, CA: TRC Companies,Inc.

Woolery, E. W., Wang, Z., Carpenter, N. S., Street, R., Brengman, C., 2016. The Central United States Seismic Observatory: Site Characterization, Instrumentation, and Recordings. *Seismological Research Letters* 87 (1), 215–228. https://doi.org/10.1785/0220150169

Wood. C., Ellis, T., Teague, D., & Cox, B. (2014) "Analyst I: Comprehensive Analysis of the UTexas1 Surface Wave Dataset, ASCE Geo-Congress 2014: Geo-Characterization and Modeling for Sustainability," Atlanta, GA, 23-26 February 2014.

Yoon, S., and Rix, G. (2004). "Combined active-passive surface wave measurements for near-surface site characterization. Proc., Symposium on the Applications of Geophsics to Engineering and Environmental Problems, Vol. 17, Denver, CO: 1556-1564.

Youd, T. L., Idriss, I. M., Andrus, R. D., Arango, I., Castro, G., Christian, J. T., Dobry, R., Finn, W. D. L., Harder, L. F., Hynes, M. E., Ishihara, K., Koester, J. P., Liao, S. S. C., Marcuson, W. F., Martin, G. R., Mitchell, J. K., Moriwaki, Y., Power, M. S., Robertson, P. K., Seed, R. B., Stokoe, K. H. (2001) "Liquefaction resistance of soils: summary report from the 1996 NCEER and 1998 NCEER/NSF workshops on evaluation of liquefaction resistance of soils," Journal of Geotechnical and Geoenvironmental Engineering 127(10), 817–833.

Zheng, W., Hashash, Y., Petersen, M.M., Whittaker, A.S. (2010) "Site-Specific Response Analysis in the New Madrid Seismic Zone," International Conferences on Recent Advances in Geotechnical Earthquake Engineering and Soil Dynamics. 13 pp.

Zywicki, D.J. (1999) "Advanced signal processing methods applied to engineering analysis of seismic surface waves," Ph.D. Dissertation, School of Civil and Environmental Engineering, Georgia Institute of Technology, Atlanta, GA.

Zywicki, D.J. (2007). "The impact of seismic wavefield and source properties on ReMi estimates." Proc., Geo-Denver 2007, Innovative Applications of Geophysics in Civil Engineering, Geotechnical Special Publication 164 (CD-ROM), ASCE, Reston, VA.